STABILITY ASSESSMENT OF ENTRY ROOFS IN UNDERLYING MULTIPLE SEAM MINES

By

Muhammad Akram

Dissertation submitted to the Faculty of the
Virginia Polytechnic Institute and State University
in partial fulfillment of the requirements for the degree of
Doctor of Philosophy
in
Mining and Minerals Engineering

APPROVED

Dr. C. Haycocks, Chairman

Dr. M. Karmis, Department Head

Dr. M. Karfakis

Dr. G. Faulkner

Dr. G. Luttrell

June, 1993

Blacksburg, Virginia

STABILITY ASSESSMENT OF ENTRY ROOFS IN UNDERLYING MULTIPLE SEAM MINES

By

Muhammad Akram

Committee Chairman: Dr. Christopher Haycocks

Mining and Minerals Engineering

(ABSTRACT)

Entry roofs in underlying multiple seam mines are vulnerable to failure under the influence of stress transferred from the upper seam workings. Overburden depth, innerburden thickness, percentage of hard rock in the innerburden and relative location of pillars in the two seams are some of the factors known to influence stress transfer and ensuing instability in the lower seam. This study was undertaken to quantify the effects of these factors and to develop a comprehensive roof stability assessment model capable of predicting any instability in the lower seam entry roofs under given conditions of geology and loading.

The finite element analysis technique was used to model a range of loading conditions and innerburden lithology. The innerburden thickness was varied from 50 to 20 feet. The innerburden lithology was varied in terms of percentage of sandstone and its location in the innerburden. Various loading conditions were simulated by changing the relative location of pillars in the two seams and by varying overburden depths from 300 feet to 1500 feet. Excessive horizontal stresses and unsymmetric loading were also simulated. The effects of these factors were quantified in terms of safety factors across the entry span.

The finite element results were used to obtain curve-fitted equations for computing safety factors at roof corner and midspan for given conditions of innerburden thickness, percentage of sandstone in specified location, overburden depth and pillar arrangement. These results were verified by back analysis of case studies and then incorporated into a comprehensive roof stability assessment model.

Acknowledgments

I would like to thank Dr. Christopher Haycocks, my committee chairman, for his valuable help, guidance and support throughout this investigation; Dr. Michael Karmis, Dr. Gavin Faulkner, Dr. Mario Karfakis, and Dr. Gerald Luttrell, my committee members, for their review and criticism of this dissertation; and other staff members of the department for their help.

I would also like to extend special thanks to Mr. Richard Fraher, fellow graduate student, for the valuable help and suggestions received during the course of this study and to Margaret Radcliffe for the final editing of this dissertation.

Finally, I am indebted to my family for their tremendous support which enabled me to complete this study.

Table of Contents

List of Figures

List of Plates

List of Tables

Chapter 1

Introduction

A coal mine roof can fail in a number of ways depending on such factors as geology, span, floor and pillar response and loading conditions. In spite of the great body of literature that exists on roof control, the exact mechanisms of failure for specified conditions remain largely unknown. Stability assessment of entry roofs is an essential precursor to all underground design. Otherwise stable openings may be subject to radical changes in the stress field surrounding them as a result of multi-seam interaction. Such loading changes frequently produce instability and failure in the roof, floor and pillars.

Examination of a considerable number of coal mine roofs has shown that the mechanisms of failure can differ widely. Discounting both geologically-controlled and body-loaded failures, the remainder are primarily caused by changing stress environments. Radical changes in the stress field around a

mine opening are a common result of a number of mining situations, but especially of interaction between seams and in longwall gate entries.

Analysis of roof failure modes has a number of potential benefits. It can yield information on loading conditions and therefore suggest design changes and improved methods of support. It also may allow prediction of ground control effects where future changes in stress field and geological conditions are known. Stable roof design is essential for optimizing productivity and reserve recovery and therefore is of critical importance in mine design. Previous research has identified factors that control stress interaction in multi-seam mining. These factors include innerburden thickness, innerburden lithology, overburden depth, pillar sizes and their relative location in the two seams.

The main objective of this study is to develop a comprehensive roof stability assessment model for the lower seam entries incorporating the effect of these factors. The specific goals include:

- To determine the effect of innerburden lithology on lower seam entry roof stability
- To quantify the effects of various loading conditions expected in undermining cases
- To investigate the influence of excessive lateral stresses on entry stability

- To identify the modes and mechanisms of roof failure under specified conditions of geology and loading.

Chapter 2

Review of Literature

2.1 Introduction

The design of stable coal mine entries has been achieved with only partial success over the long history of mining. Modern numerical methods now offer a mechanism with which to study and evaluate alternate underground layouts in a systematic manner. But any design must commence with *where and when* failure could occur in terms of geology and loading conditions. Determining how and under what conditions roof failure can occur for either single or multi-seam conditions is the beginning of true ground control. The roles of geology and loading conditions in different types of roof failures observed in underground coal mines are reviewed in this chapter. The available alternatives for the stability assessment of entry roofs are also reviewed, including a brief summary of the roof rating systems.

2.2 *Loading Conditions*

Defining loading conditions is the first step in stability assessment of underground coal mine openings. In addition to gravity loading, entry roofs can be subjected to high stress levels due to load transfer from any adjacent mining areas. Both in longwall mining and in multi-seam situations, high stress concentrations are produced which are capable of causing potential instability in entry roof, floor and pillars. These conditions often result in unsymmetric loading of the entries and cause serious ground control problems in terms of roof and rib failures. Also, the tectonic horizontal stress prevalent in many mining areas is an important factor in the creation of unstable roof conditions. The types of stress field encountered in the major U. S. coal fields and their reported effects on the stability of coal mine entries are discussed in this section.

2.2.1 *Horizontal Stress*

Rocks at depth are loaded by the weight of overlying material. Under the influence of this load the strata tends to expand laterally which leads to the development of horizontal stress (σ_h). For plane strain conditions and assuming elastic behavior of rocks, horizontal stress induced due to this effect is computed by the following equation:

$$\sigma_h = \nu / (1-\nu)\, \sigma_v \qquad 2.1$$

where σ_v is the vertical stress due to the weight of the overburden and ν is the Poisson's ratio of the rocks.

The horizontal stress at many locations in the world, however, is much higher than predicted by the above equation (Hoek and Brown, 1982). The ratio of the average of the two horizontal stresses to the vertical stress varies widely, from 0.5 to greater than 3.5 near the surface and from 0.3 to 1.0 at higher depths (Figure 2.1).

The orientation of horizontal stresses in conjunction with their magnitude is important in determining their effect on the stability of underground openings. The available data concerning the orientation of horizontal stress field in north-eastern North America is shown in Figure 2.2. This data suggests a persistent east-northeast stress field, with some rotation towards east -west in the Illinois basin.

The horizontal stress data for U. S. are shown in Figure 2.3. The magnitude and orientation of the major and minor axes of each ellipse shown in this figure represent the excess maximum and minimum horizontal stresses at each site. The following observations summarize this data (Aggson, 1978):

- Near the eastern coast of the United States the maximum compressive component of the horizontal stress field tends to be parallel to the Appalachian Mountain chain;

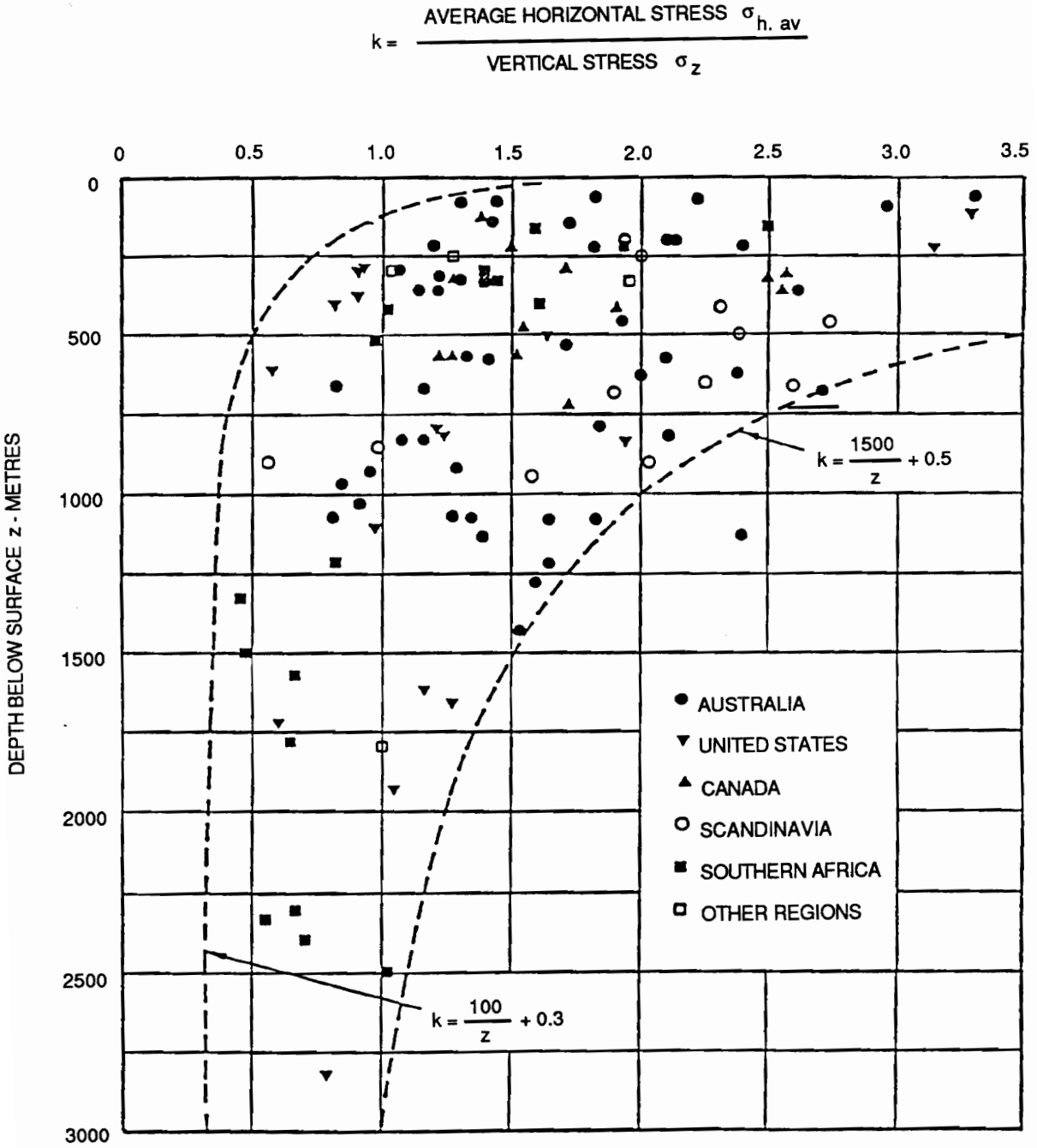

Figure 2.1 Depth vs. ratio of horizontal stress to vertical stress (After Hoek and Brown, 1982)

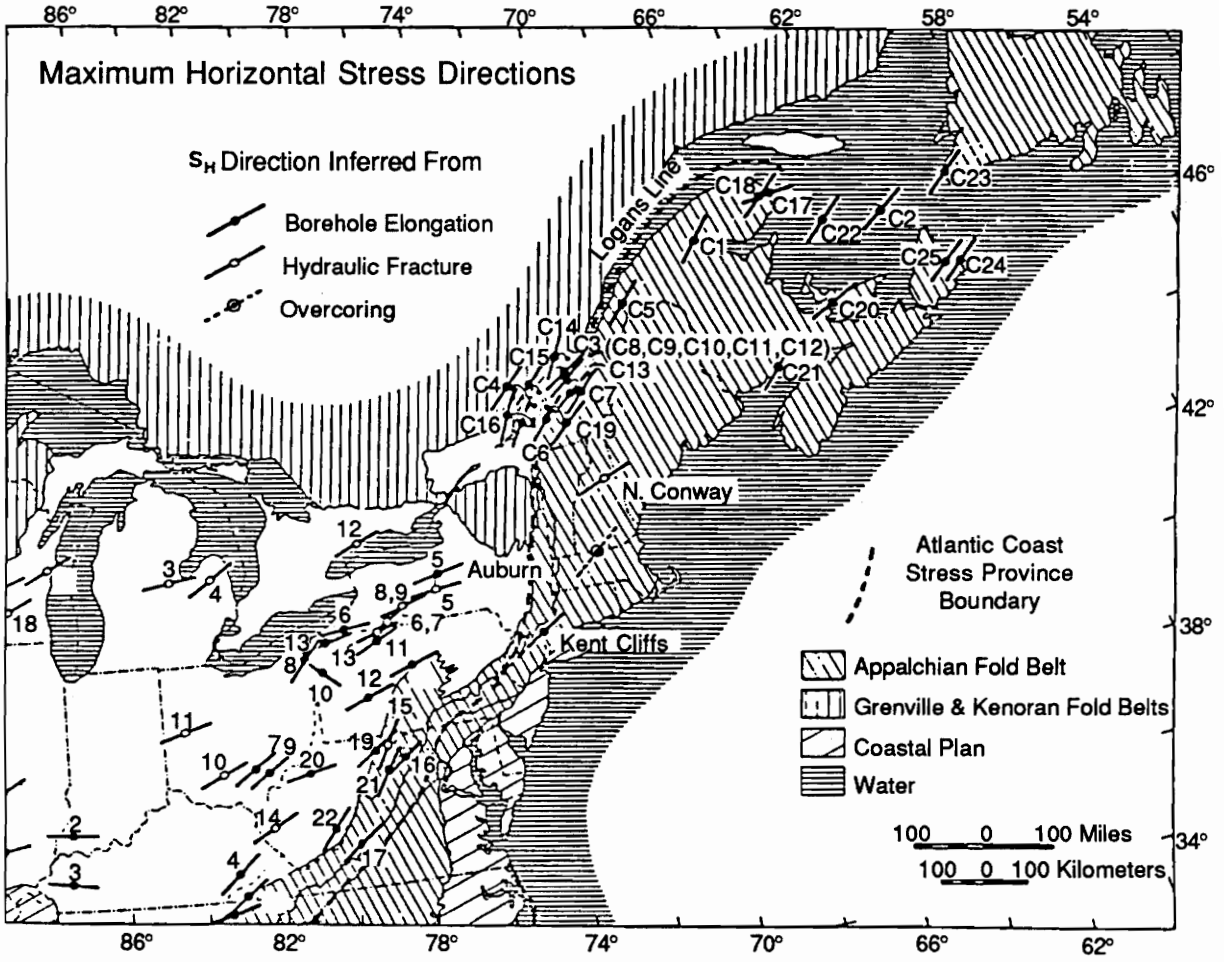

Figure 2.2 Orientation of the maximum horizontal stress in Northeastern North America (After Plumb and Cox, 1987)

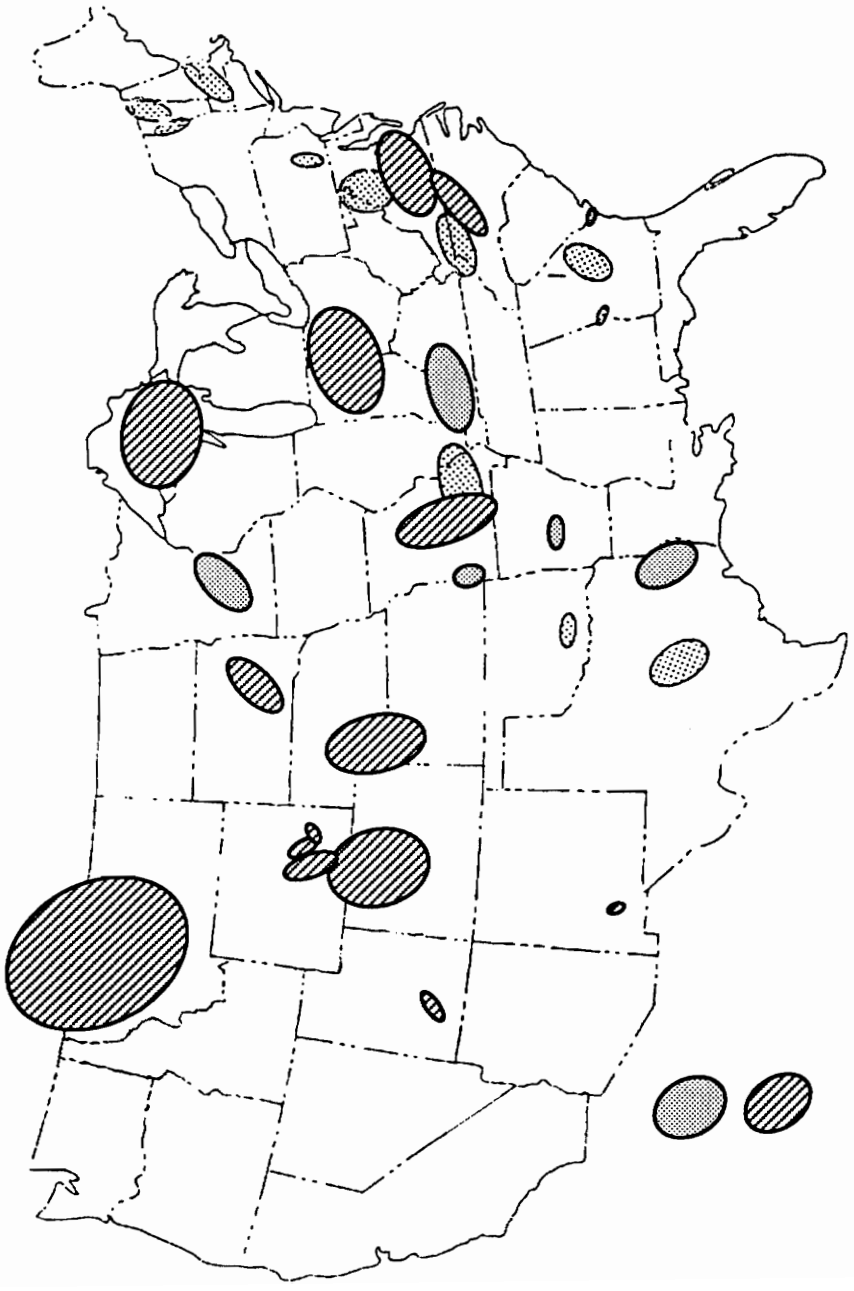

Figure 2.3 Orientation of horizontal stress for the U.S. (Aggson, 1978)

- Near the Great Lakes the maximum compressive stress tends to be tangential to the Michigan basin;
- In the Rocky Mountain states the maximum stress is parallel to the Rocky Mountains.

The horizontal stress data compiled from 25 mines in the eastern United States is shown in Figure 2.4. This data confirms the presence of an east-northeast stress field. Sixty-seven percent of the measurements from mines in the Appalachian and Warrior coal basins show the orientation of maximum horizontal stress between N80E and N50E. In the Illinois basin seventy percent of the measurements indicate that the stress field is rotated towards east-west by about fifteen percent. The magnitude of the maximum horizontal stress exceeds the vertical stress in more than 90 percent of the cases, mostly by a factor of two or more.

Many underground mines experience ground control problems that are attributed to the presence of high lateral stresses. Horizontal stress is considered to be one of the major causes of cutter roof problems encountered in many underground coal mines in the Eastern United States (Ahola et al., 1991; Bauer, 1990; Su and Peng, 1987; Mark, 1991; Agapito et al., 1980). This problem is common in mines with immediate roofs comprised of thin beds located in a high tectonic stress field. Cutter roof is a failure process that initially begins as a fracture plane in the roof rock parallel to and located at the roof-rib intersection. The fracture propagates upward in the

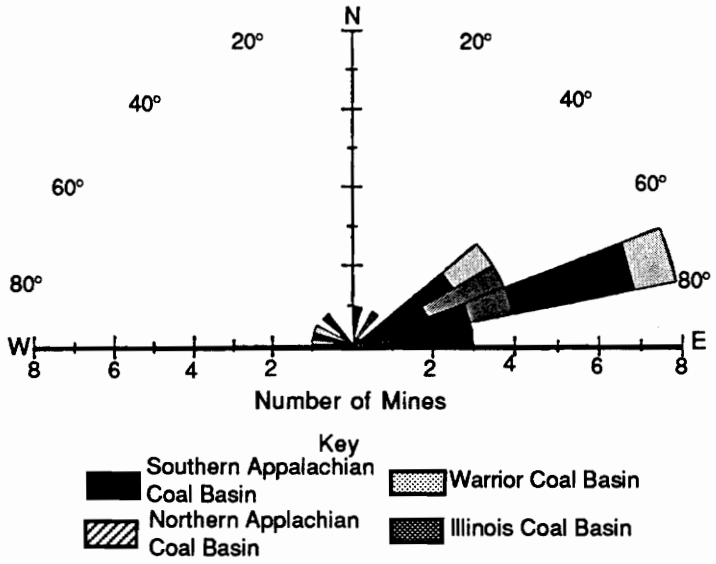

Figure 2.4 Orientation of maximum horizontal stress in Eastern U.S. coal mines (Mark, 1991)

roof over the mine opening at an angle usually steeper than 60 degrees from the horizontal (Hill, 1986).

The role of loading conditions in creating roof instability, such as the development of a cutter roof, was investigated for some West Virginia coal mines (Su and Peng, 1984; 1987). The immediate roof over most parts of the mines studied consists of a layer of gray shale 3-4 feet thick, overlain by a thick layer of sandstone. The thickness of the coal at the cutter roof area is about 4 feet and depth of cover is around 800 feet. No major geological structures are known to occur locally. The results of this study lead to the conclusion that excess horizontal stress contributes to the instability of the immediate roof. The differential stress, which is the difference in magnitude between the maximum and minimum excess horizontal stress, was found to have a less pronounced effect on softer immediate roofs. Under a given overburden, the differential horizontal stress had the least effect on the stability of immediate roof layer at the entry corners and the most effect at mid-span of the stiffer layer above the immediate roof layer (Su and Peng 1984). It was also found that the excess horizontal stress may have been the cause of low angle shear failure observed in some cases (Su and Peng, 1987).

Several mines in the Beckley coalfield of south-central West Virginia experience stress-related ground control problems (Aggson and Curran, 1978; Aggson and Mouyard, 1978; Agapito et al., 1980). The horizontal stress in this area is reported to be in the range of 3000 psi at a depth of approximately 700 feet. The common mode of failure found is low angle

shear failure of immediate roof layers. This type of failure is considered to be the result of prevalent high horizontal stresses (Agapito et al., 1980). The frequent floor heave observed in these mines is also attributed to the high horizontal stress field causing buckling of thin beds (Figure 2.5).

The direction of an excess horizontal stress field with reference to the direction of entries is also of critical importance in determining its effect on roof instability (Jeremic, 1985). When the roadways are perpendicular to lateral stress, the instability is most significant. Two modes of roof failure under different stress fields have been identified depending on rock types (Figure 2.6).

- Slip along bedding planes in thin bedded shales and siltstones.
- Shearing at low angles in thick bedded siltstones and sandstones.

In roadways parallel to lateral stress, roof failure is found to be less severe than in those oriented perpendicular to the lateral stress. The failure in this case is reported to be the result of sagging of thin roof layers and their ultimate failure in tension (Figure 2.7). Roadways aligned at an oblique angle to the lateral stress are found to be the most stable among the three cases considered (Jeremic, 1981).

The effect of magnitude and direction of lateral stresses on roof stability have been studied for some Illinois coal mines (Hanna et al., 1986; Ingram and Molinda, 1988; Blevins, 1982; Blevins and Dopp, 1985; Hanna and

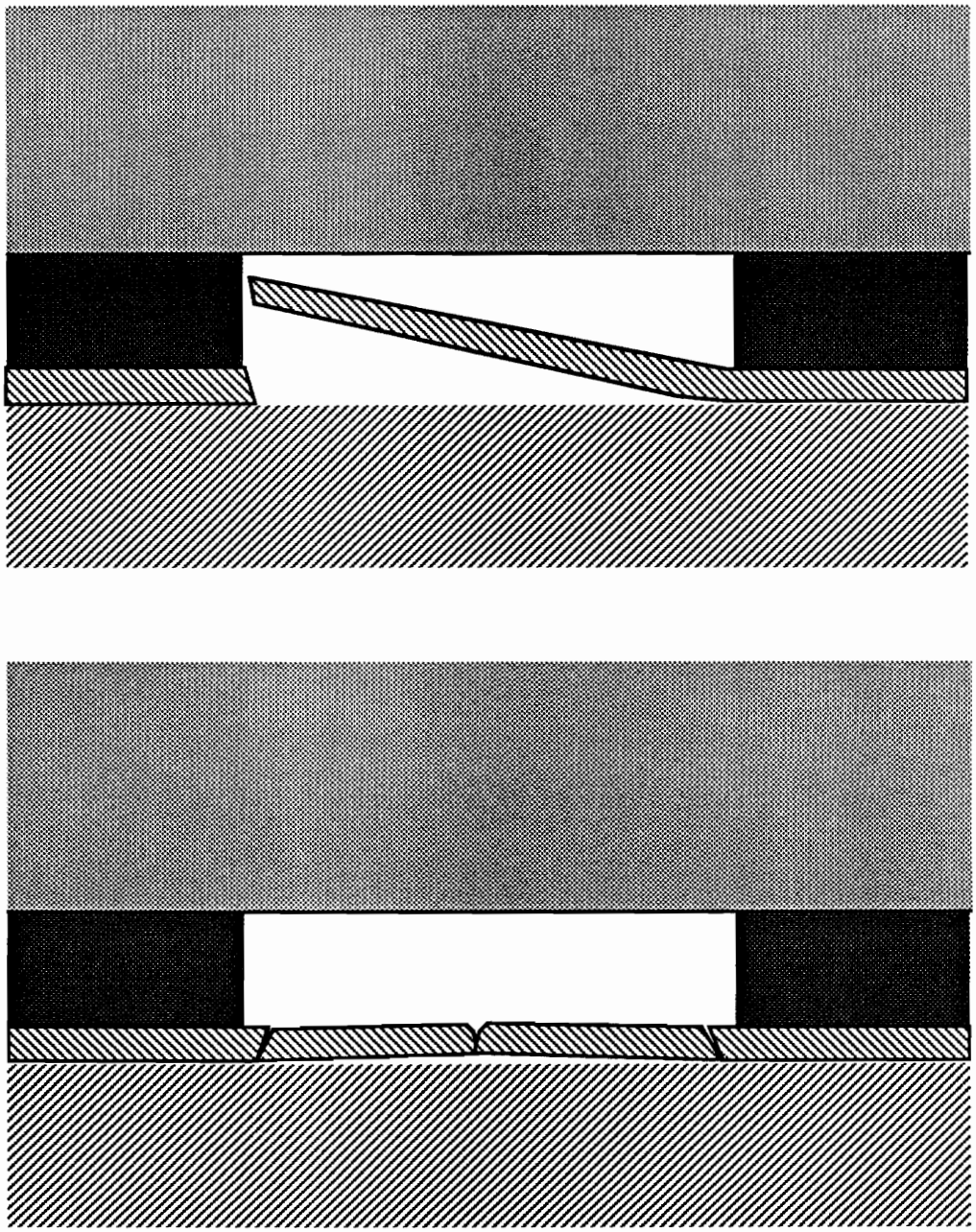

Figure 2.5 Various types of floor failures under the influence of high horizontal stress (After Aggson, 1978)

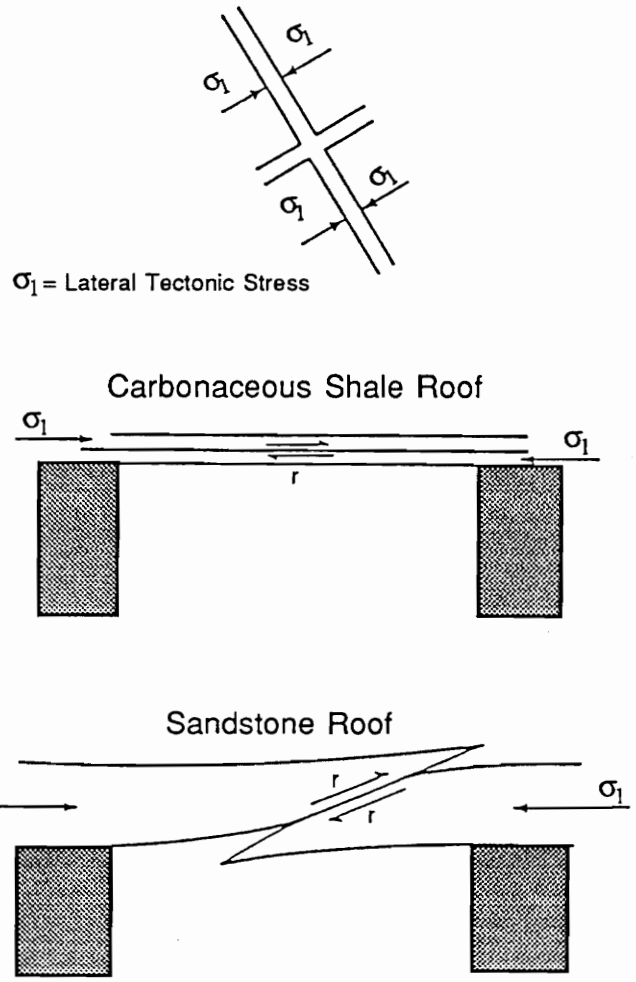

Figure 2.6 Type of failure expected under the influence of high lateral stress acting perpendicular to the roadways (After, Jermic, 1985)

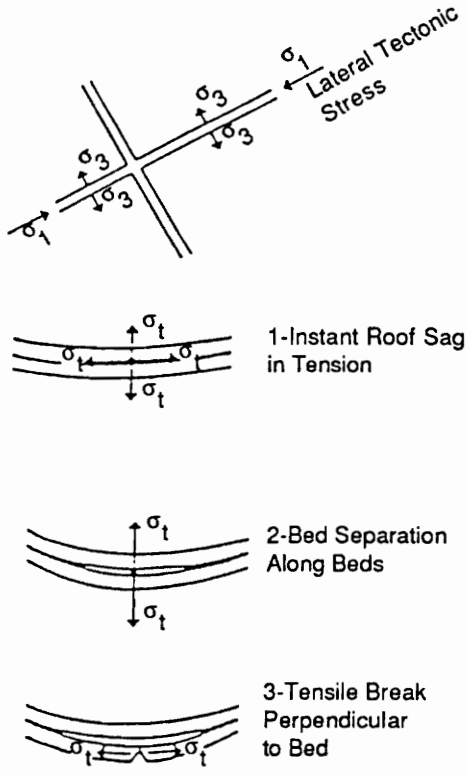

Figure 2.7 Type of failure expected under the influence of high lateral stress acting parallel to the roadways (After, Jermic, 1985)

Haramy,1985; Hanna, 1988). The typical depth of overburden for these mines is about 900 feet. The maximum and minimum horizontal stresses are reported to be of the magnitude of 2700 psi and 800 psi respectively. The seam height averages about 6.0 feet. The roof is of laminated medium gray shale. There are zones of slikensides, joints, rider coal, clay intrusions and rolls. The mines in this area experience severe roof fall problems in the entries driven north-south. The roof falls are steep sided, inclined up to 75 degrees from the horizontal. These falls are about 2 to 4 feet high and extend north-south parallel to the entry. Trends of roof falls observed with various entry orientations and the in-situ stress measurements indicate that this problem may have been the result of high differential lateral stress field. The worst possible mining direction is known to be N 6 W which is perpendicular to the average of various estimated stress directions. On the basis of this study the entry orientations were changed to N 45 E, which alleviated this problem to some extent (Blevens and Dopp, 1985; Hanna et al., 1986).

2.2.2 Vertical Stress

The complete state of stress in any underground mining situation can only be defined if both vertical load and horizontal confinement are known with reasonable accuracy. The vertical stresses encountered underground are categorized as:

- gravity induced - the stresses present due to the weight of overlying material;
- mining induced - the stresses transferred from the mined out areas to surrounding structures.

The vertical stress at depth h in an undisturbed strata due solely to the weight of overlying material is estimated by the following equation:

$$\sigma_v = \gamma h \qquad 2.2$$

where γ is the unit weight of the overlying rock material.

Excavation of underground openings disturbs the existing stress regime. Stresses are relieved in the immediate vicinity of the roof and floor whereas stress concentrations are created in other areas. Standard analytical solutions are available for calculating these stress changes for excavations of simple geometrical shapes in homogeneous and isotropic materials. In many real-life mining situations, however, the stress picture is much more complex and difficult to estimate. Longwall gate entries and mine openings in a multi-seam environment are two areas where radical changes in stress cause major stability problems. The assessment of these stress changes is the essential first step in the design of entries in such situations.

2.2.2.1 Load on Longwall Gate Entries

Before extraction of coal the vertical stress due to the weight of the overburden is uniformly distributed on the coal seam. As a result of development of gate entries and caving of the longwall panels this stress regime is completely disrupted. Part of the load from the gob is transferred to the gate entries and superimposed on the development-induced load. This load distribution is usually non-uniform across the openings and is in a continuous state of change with the changing position of the longwall face.

The distribution of vertical load around a longwall face has been studied by many researchers (Whittaker, 1974; Whittaker and Pye, 1975; Whittaker and Hodgkinson, 1971; Wilson, 1982; Adler, 1976; Peng and Chiang, 1984). The idealized picture of vertical stress around a retreating face is shown in Figure 2.8. The development component of this load (L_d) per foot of gate entry can be estimated using the tributary area concept:

$$L_d = (H)(w_t)(\gamma) \qquad 2.3$$

where

H = depth of cover (ft)

w_t = width of pillar system (ft)

$= \Sigma[(w)] + (n-1)w_e$

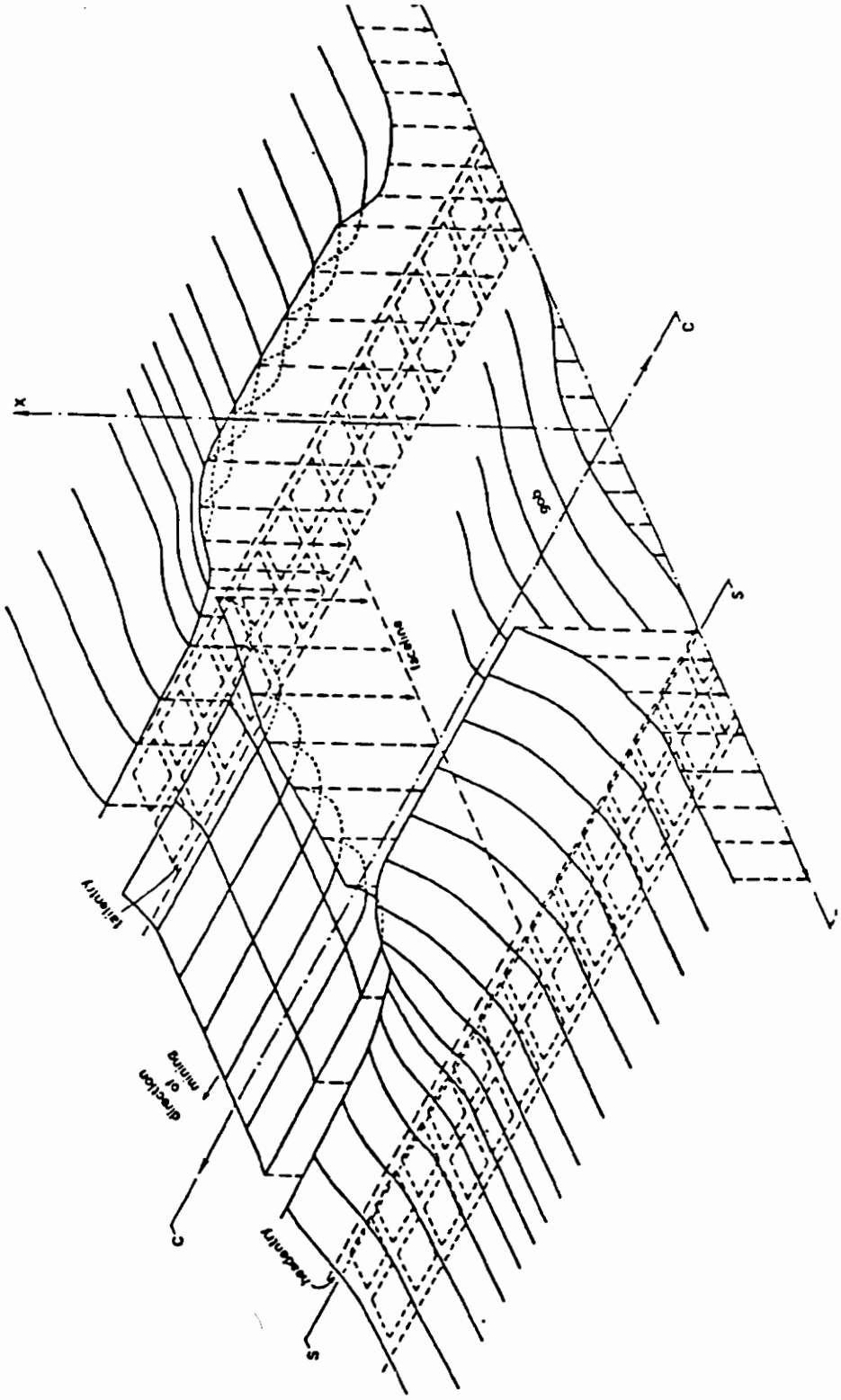

Figure 2.8 Distribution of vertical stress around a retreating longwall face (After, Peng and Chiang, 1984)

w = width of individual pillars (ft)

w_e = entry width (ft)

n = number of entries in the gate entry system

γ = unit weight of overburden (pcf).

The abutment load is the sum of side abutment load (L_s) and the front abutment load (L_f). This load has been characterized on the basis of location of face and the position of mined out panels (Mark, 1990). The most critical abutment load is that experienced by the system at the face ends or T-junctions.

Two similar empirical approaches are used for estimating the side abutment loads. In the first method the load is calculated on the assumption that the vertical stress in the gob increases linearly, from zero at the rib to the original overburden pressure at some point within the gob. It has been estimated that the distance required for the gob pressure to return to cover load is typically 0.3 times the depth cover (Wilson, 1982). The second technique for estimating the side abutment is based on the concept of a shear angle that determines the pillar loading (King and Whittaker, 1971). As shown in the upper part of Figure 2.9, the side abutment is represented as the wedge of strata defined by the shear angle β. Two equations are used for quantifying the side abutment per foot of gate entry, one for critical and super-critical panels, and the other for sub-critical panels.

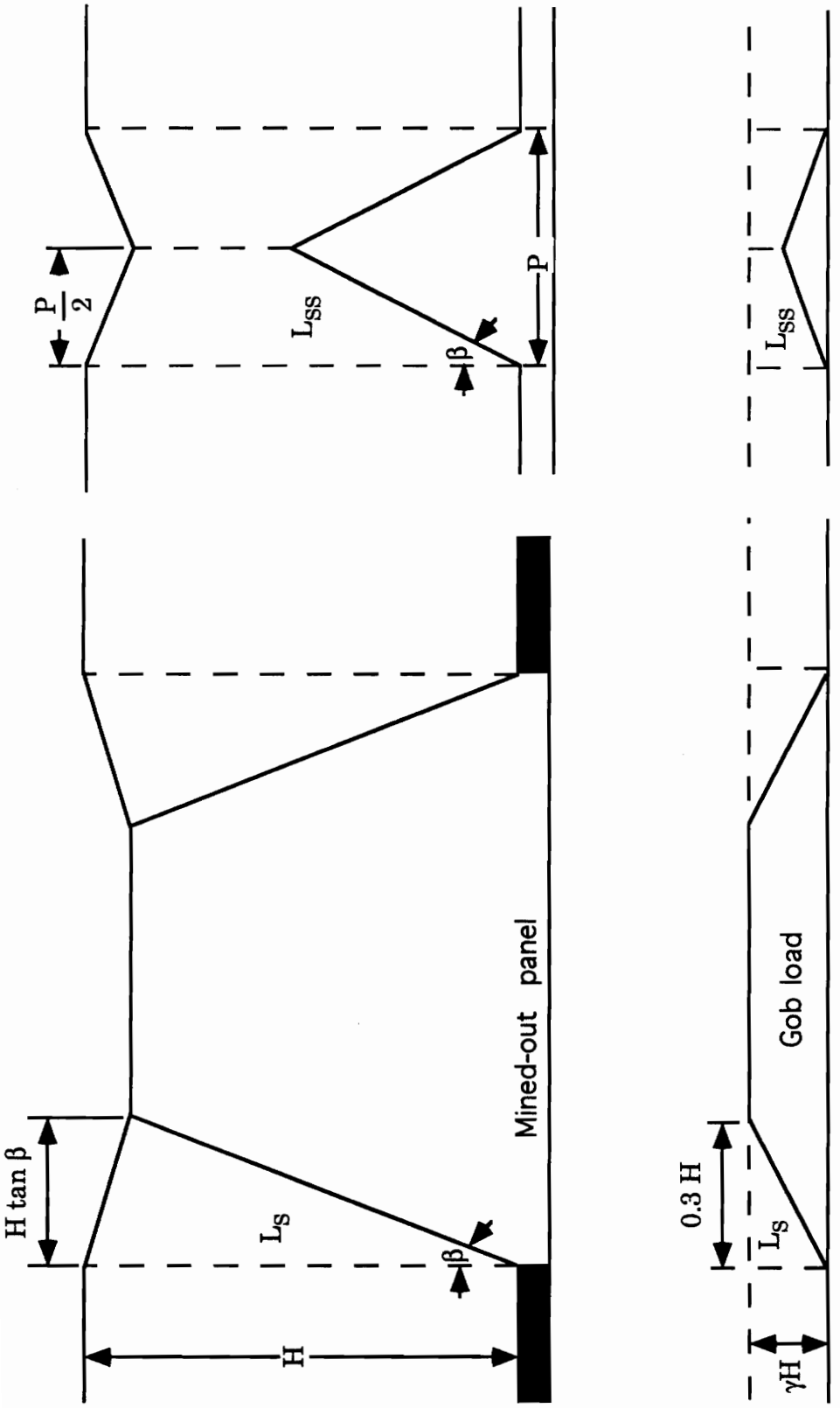

Figure 2.9 Estimation of side abutment load (After King and Whittaker, 1971; Wilson, 1973)

$$L_s = H^2(\tan\beta)(\gamma/2) \quad 2.4$$

$$L_{ss} = [(HP/2) - (P^2/8\tan\beta)]\gamma \quad 2.5$$

In the above equation it is assumed that the shear angle might be equal to the angle of draw used in subsidence analysis, which is estimated at 25 degrees for British conditions. This method was slightly modified for U.S. conditions on the basis of subsidence data for the Pittsburgh Seam (Choi and McCain, 1980).

The magnitudes of the front abutment is much more difficult to determine than that of the side abutment. Some researchers have used three-dimensional numerical modeling to analyze this problem (Hsuing, and Peng, 1985; Kripakov et al., 1988; Park et al., 1984). Others have developed procedures based on empirical results (Mark, 1990):

$$L_f = F(L_s), \quad 2.6$$

where F is the front abutment factor. This factor is assigned a value on the basis of field measurements. The maximum value assigned to F is 1. The final aspect of the abutment load prediction is assessment of its zone of influence and distribution across the entries. Field measurements were analyzed to determine the width of the abutment influence zone D, defined as the distance from the panel edge. The

following relationship was established on the basis of these observations (Peng and Chiang, 1984):

$$D = 9.3\,(H)^{0.5} \qquad 2.7$$

The stress within the abutment influence zone has been observed to decline as we move away from the ribline. The stress decays according to the inverse square of the distance from the panel edge. Once the quantity, zone of influence and distribution of abutment load is known, the total load on the system for a given location can be defined by the summation of development load and the appropriate value of abutment load for that location (Mark, 1990).

2.2.2.2 Load on Lower Seam Entries in Multi-Seam Conditions

Higher stresses encountered in multi-seam conditions are due to interaction phenomenon observed where more than one seam is mined in vertical proximity to another mine. The following major factors have been identified to control this type of interaction (Haycocks and Zhou, 1990):

Fixed Factors

- Overburden thickness and rock type
- Upper seam thickness
- Lower seam thickness
- Upper seam immediate roof thickness and rock type

- Lower seam immediate roof thickness and rock type
- Innerburden thickness and rock type
- Number of layers in the innerburden
- Existence of ground water

Controllable factors

- Sequence of mining
- Method of extraction
- Method of support
- Mine layouts and entry sizes
- Extraction percentage in both seams
- Location of mine in both seams
- Time delay between operations.

Of the controllable variables, sequence of mining is the most important in determining the type and magnitude of interaction. There are three basic sequences in which multi-seam mines can be worked (Haycocks and Karmis, 1983; King and Whittaker, 1972; Hladysz, 1985). These sequences are outlined below (Figure 2.10):

Undermining

- In this case the upper seam is mined out prior to the mining of the lower seam,

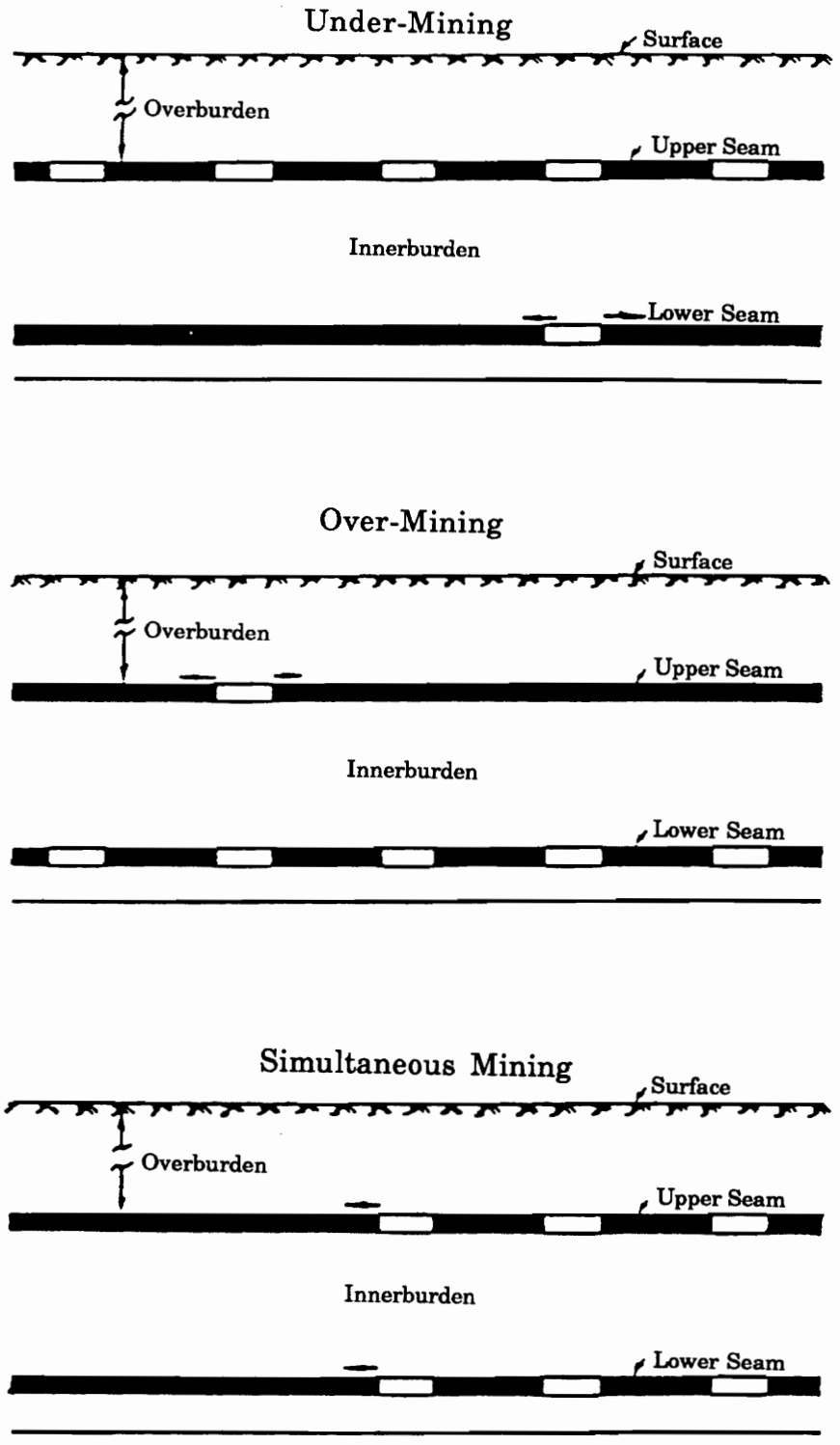

Figure 2.10 Various possible mining sequences in multi-seam mining (Haycocks and Karmis, 1984)

Overmining

- In this sequence the lower seam is mined prior to the mining of the upper seam,

Simultaneous Mining

- In this case mining in the lower and upper seams takes place simultaneously.

Each of these can produce a unique set of interactive conditions. Two major types of ground control problems occur in undermining cases: 1) roof, pillar and floor instability due to stress transfer from an upper seam remnant pillar or gob boundary, 2) massive failure of the innerburden (Stemple, 1956; Haycocks et al., 1982). Loads at the lower seam level may be either active, or passive. The passive condition is the most common case and occurs when a mine is developed within 110 feet of an abandoned upper seam operation for room and pillar mines and 700 feet for longwall mines (Haycocks et al., 1987). In this case otherwise stable openings are subjected to increasing loads depending upon the relative position of pillars in the two seams.

A major problem in terms of the stability of lower seam openings is the lack of symmetry that often occurs in the loading conditions. The unsymmetric loading on lower seam structures results from offset pillars in the upper seam. This condition is very common because perfectly columnized pillars are difficult to achieve in practical situations (Figure 2.11). This effect can significantly contribute to instability as the more heavily loaded pillar rib deforms, resulting in significant roof distortion across the opening. Offset

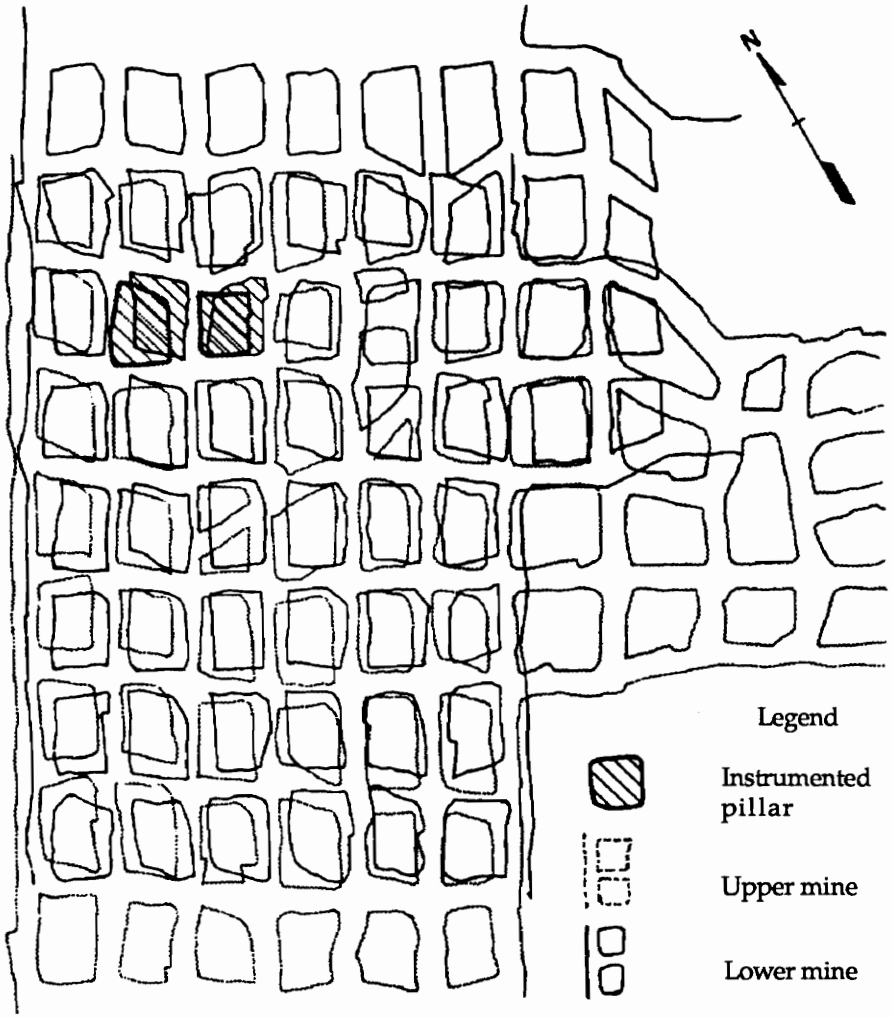

Figure 2.11 Superpositioning of pillars showing pillar offsetting (After Matetic and Chekan, 1988)

pillars have been shown to generate high shear stresses in underlying entries, particularly for very close mining conditions (Zhou and Haycocks, 1989; 1990). Loads on entries can be determined for multi-seam conditions once the geology and spatial conditions are determined. Defining geology and spatial distances between seams, however, is a major problem in many operations because of the large spacing between exploration boreholes (Fraher et al., 1992).

The lower seam stress concentrations typically occur under structures such as remnant pillars and gob edges. Stress increase may cause roof falls, floor heave and pillar failure in the lower seam depending on innerburden thickness , lithologic composition, and pillar geometry. The stress transfer from the upper seam working to the lower seam can be explained by the following mechanisms.

2.2.2.2a Pressure Arch Theory

When an entry is created in a coal seam, the coal removed is no longer available to support the overburden. The immediate roof strata is destressed and the load of the overlying rocks is transferred to the sides, thus creating a pressure arch. The formation of such an arch is shown in Figure 2.12 (Stefanko, 1983). If a number of entries are developed parallel to each other, pressure arches will be formed around each of these entries. The higher stress levels in the pillars will cause deformations, thus moving the stresses outwards creating concentrated stress abutments. These high stress zones,

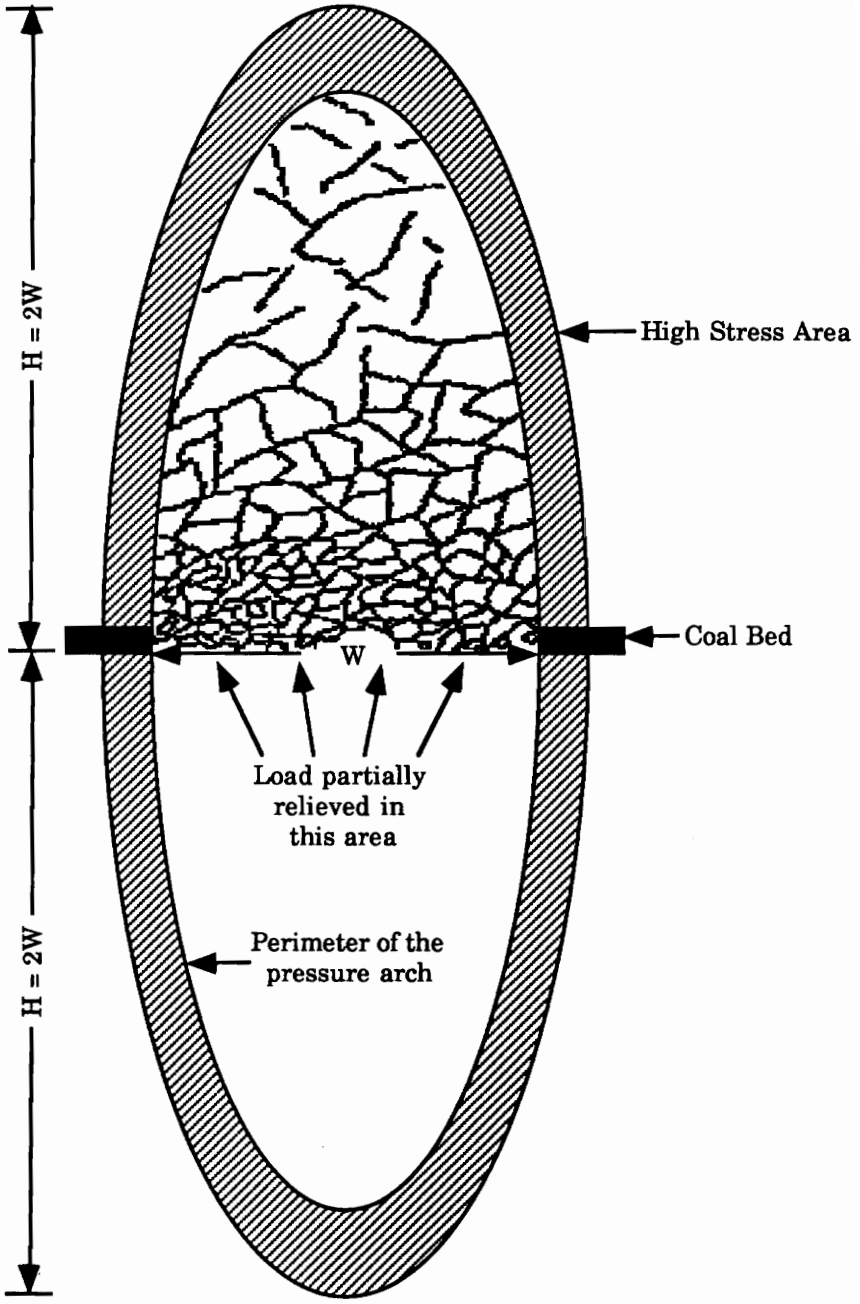

Figure 2.12 Idealized arching effect around a mine opening (After Stefanko, 1983)

also known as mining-induced abutment stresses, are dependent upon the mining sequence. These zones are known to shift with the progression of mining and are implicated in many roof instabilities (Karabin et al., 1982). The width of the arch can be estimated from the following empirical relationship (National Coal Board, 1954):

$$W = 0.15\,D + 60 \qquad 2.8$$

where;
W = maximum width of the pressure arch (ft)
D = depth of the arch below surface (ft)

It has been observed that if the width of the excavation exceeds the maximum width of the pressure arch, intense roof fracturing occurs. The height of the pressure arch is a function of the material properties, rate of extraction, span of the working area, and vertical to horizontal stress ratio. In cases where rock strength is low and horizontal stresses are small, the height of the pressure arch is relatively greater (Adler and Sun, 1976).

The concept of a negative pressure arch around upper entries has been applied in multi-seam research to determine whether the arch formed under an upper seam opening intersects with the lower seam and thus produces interaction. Finite element analysis and photoelastic modeling were used to evaluate the influence of thickness and location of sandstone layers in the innerburden and overburden on the size and shape of the pressure arch

around the upper opening. It was found that the modulus of the material has little effect on the arch dimensions or abutment pressures (Hudock, 1983). The significance of a high modulus layer above an excavation, however, has been recognized in other studies (Peng and Chandra, 1980).

2.2.2.2b Dome Theory

The three-dimensional extension of arch theory is known as dome theory. It is analogous to a pressure ring around the mine opening. The rock within the ring is separated from the rest due to horizontal shearing and vertical tension. This mass of rocks entirely rests on the roof supports. Static analysis of the forces acting on the dome indicates that the height of the dome is directly proportional to the vertical pressure (Dinsdale, 1935). The height of dome can be calculated as following (Figure 2.13):

$\Sigma F_y = 0$; leads to $R = P(2L + b)/2$ 2.9

$\Sigma M_B = 0$; leads to $M_B = P[(2L+b)/2][(2L+b)/4] + H\,h - R[(L+b)/2]$ 2.10

Therefore,

$h = (P/8H)\,(2Lb + b^2)$ 2.11

where,

P = vertical force (lbs)

H = horizontal force (lbs)

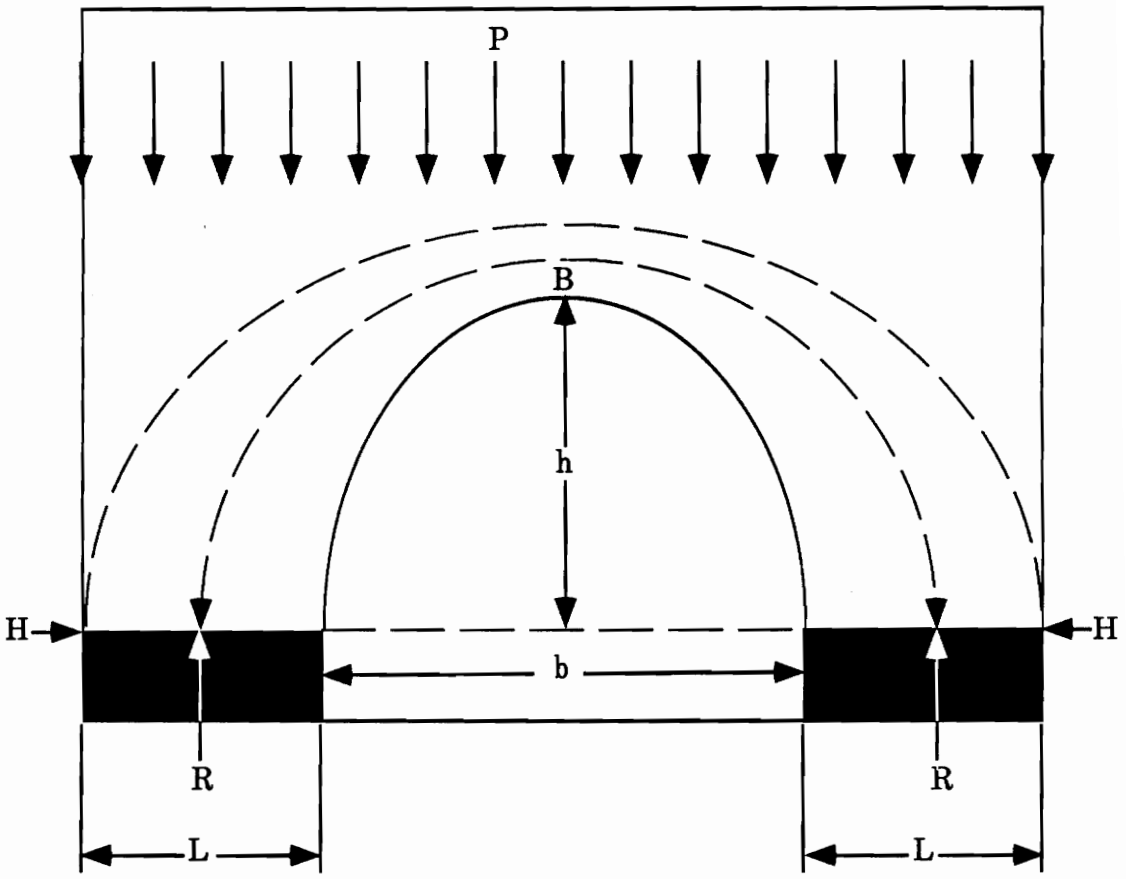

Figure 2.13 Forces acting on a pressure zone (Dinsdale, 1935).

h = height of dome

b = span of opening

L = width of abutments.

This analysis assumes that the value of L is given; the location of the vertical force (R) is at the center of the abutment; and the values of P and H are known.

The stress distribution for an elastic dome can also be calculated based on the equilibrium of forces at the dome boundary (Denkhaus, 1964). If the rock is not cohesive the core will separate from the dome boundary and the weight of the core will thus be taken by the supports. In this case the height of the dome and span are related as:

$$s = \sqrt{\frac{8\sigma_c d}{w}(1-\frac{h}{d})\log(1-\frac{h}{d})} \qquad 2.12$$

where,

s = span of the dome

h = height of the dome

d = depth of the opening

w = specific weight of the rock

σ_c = uniaxial compressive strength of the rock.

For cohesive rocks the core will not separate from the dome boundary. As a result the dome boundary will carry the weight of the core. In this case the

failure, if occurs, is sudden and catastrophic. The above relationship, for this case becomes:

$$s = \sqrt{\frac{8\sigma_c d}{w}(1-\frac{h}{d})} \qquad 2.13$$

A modified dome theory assumes that the rock inside the dome is fractured and the dome has an elliptical shape (Adler and Sun, 1976). The following equation is used to calculate the height of the dome (Figure 2.14):

$$h = \{[(1 + \sigma_c d / w)2K] - 0.5\} L/2 \qquad 2.14$$

where,

K = the ratio of lateral to vertical stress

σ_c = tensile strength of the rock.

2.2.2.2c Pressure Bulb Theory

The stress distribution in a homogeneous elastic foundation can be derived on the basis of this theory, provided the load distribution over the foundation is known (Timoshenko and Goodier, 1970; Peng and Chandra, 1980). For a uniformly distributed load, the stress trajectories form a series of bulb-shaped curves.

This concept has been used in multi-seam mining to estimate load transferred to the lower seam from remnant pillars in the upper seam

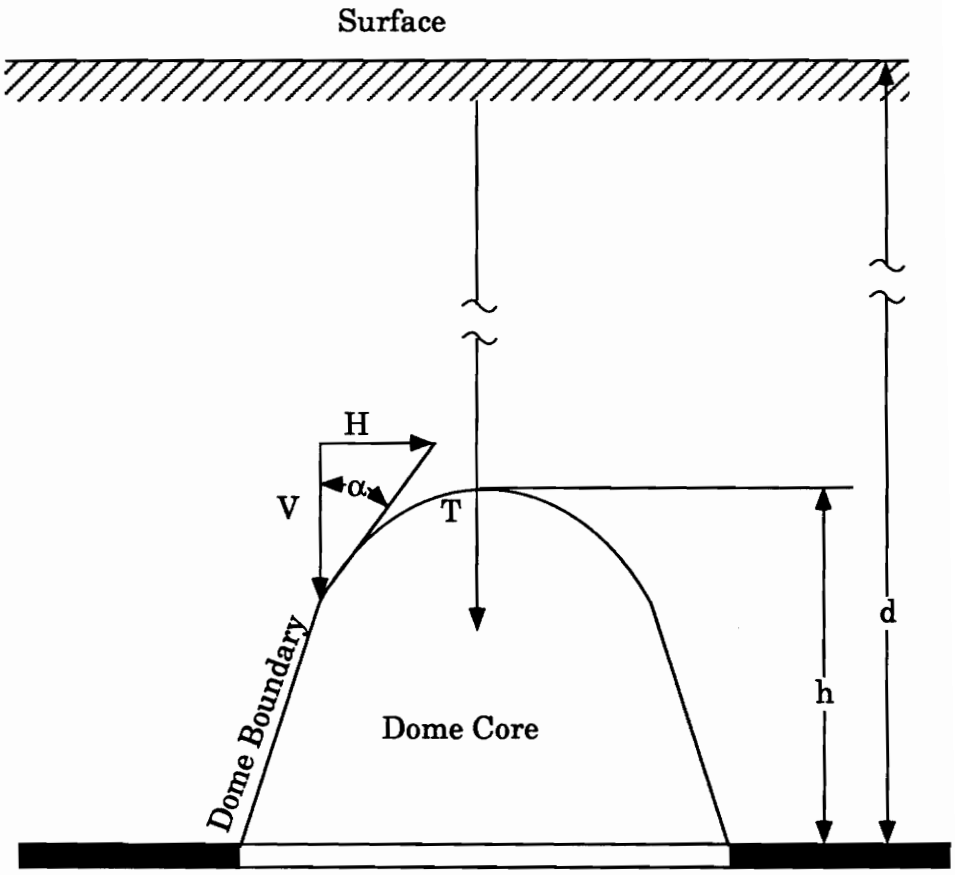

Figure 2.14 Forces at the dome boundary (After Denkhaus, 1964)

(Stemple, 1956; Stassen and Van Duyse, 1972; Spedding, 1976; Wilson et al., 1982). Finite element and photoelastic methods were used to analyze the pillar load transfer mechanisms. It was found that innerburden stratification affects the transfer of pillar stresses. Interaction effects due to pillar load transfer range from 52 feet for a monolithic innerburden to 120 feet or more when the innerburden is composed of 10 layers of modeling materials. A high modulus layer in the innerburden inhibits pressure bulb formation, while a low modulus layer increases both vertical and horizontal transfer distances of pillar loads (Ehgartner, 1982). In regard to other aspects, research has been conducted to determine the loading characteristics of a pillar, shape of loading, peak value, location of peak value, etc., which are of particular importance in the determination of the distance and magnitude of load transferable from upper seam structures (National Coal Board, 1972).

It has been estimated that the load transferred from the upper seam pillars approaches the normal background value at a distance of approximately four times the pillar width below the floor. If the innerburden is less than eight times the pillar width, the pressure contour lines at the bottom of a pillar in the upper seam superimpose on those at the top of the corresponding pillar in the lower seam. The pressure at any point in the strata between the two pillars is thus the sum of the two pressure contours. The smaller the interval the greater the net pressure. This net pressure will determine the stability of the strata in a given situation (Peng and Chandra, 1980).

The influence of rock type and its location in the innerburden on the load transfer was quantified on the basis of field data and photoelastic modeling (Ehgartner, 1982; Grenoble, 1985; Haycocks et al., 1987). The occurrence of interaction below an upper seam has been shown to depend on the percent of hard rock in the innerburden (Figure 2.15):

$$I = 110 - 0.65\,S \qquad 2.15$$

where,

I = Required safe innerburden for lower seam stability (ft)

S = Innerburden sandstone or hard rock percentage.

The safe innerburden thickness has been shown to be related to the number of rock layers in the innerburden (Figure 2.16):

$$I = 55 + 6.8\,N \qquad 2.16$$

where,

I = Required safe inner burden for lower seam stability (ft)

N = Number of layers in the innerburden.

If the above equations establish interaction, the stress at the lower seam horizon due to this interaction is calculated. First the stress in the upper seam remnant pillar or coal/gob interface is calculated by tributary area theory. The magnitude of stress under the remnant pillar at the lower seam

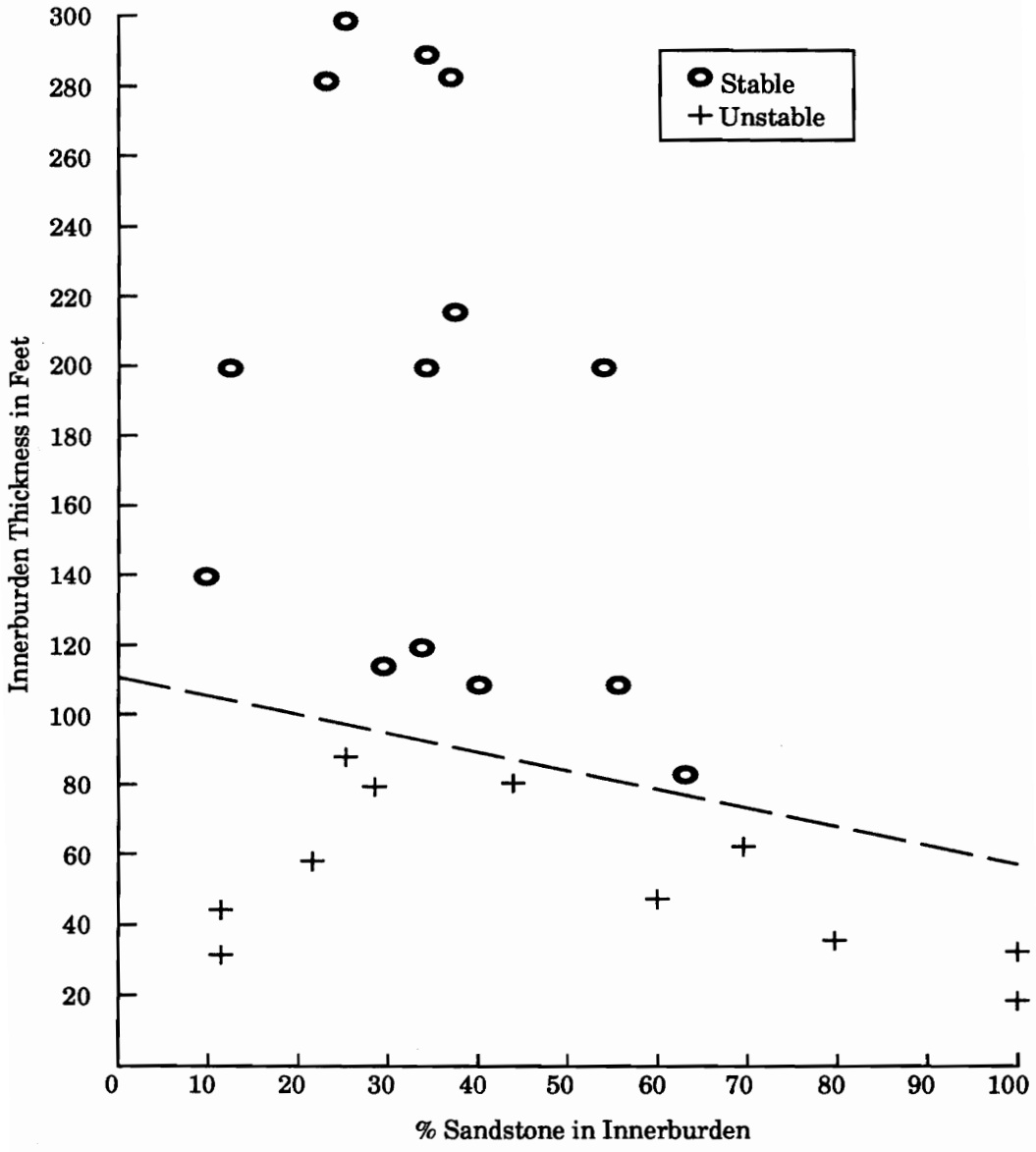

Figure 2.15 Innerburden thickness vs. sandstone percentage for stable/unstable lower seam conditions
(After Ehgartner, 1982)

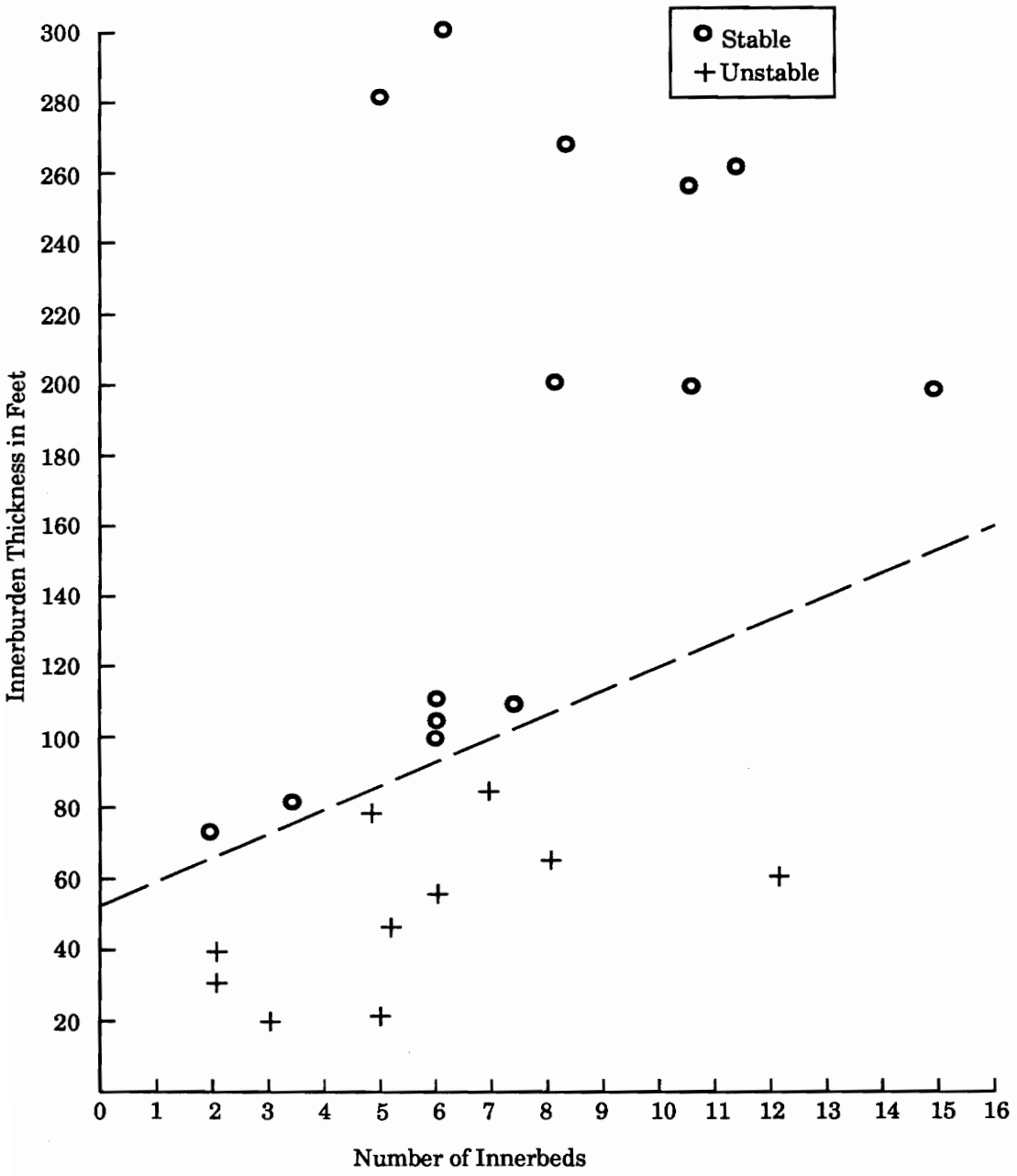

Figure 2.16 Innerburden thickness vs. number of beds in the innerburden for stable/unstable lower seam conditions (After Ehgartner, 1982)

horizon is then calculated using the pressure bulb theory. The pillar load transfer equations were developed using photoelastic models. The following two equations were obtained by curve fitting of experimental data (Ehgartner, 1982).

$$S = 0.0172D^2 - 0.284D + 1.03 \qquad 2.17$$

$$S = 0.00956D^2 - 0.1977D + 0.9889 \qquad 2.18$$

In the above equations S is the stress intensity factor defined as the percentage of the upper seam stress transferred to the lower seam. D is the ratio of the depth below the remnant pillar and width of the remnant pillar. The first equation corresponds to innerburden where layer thickness is greater than 5 feet whereas the second equation is for thin layered innerburden. The lower seam stress is then calculated by the following equation:

$$\sigma_l = \sigma_v S + Hg \qquad 2.19$$

where σ_l is the lower seam stress, σ_v is the upper seam pillar stress, H is the depth below surface, and g is the weight density of the rock layers. The stresses under the coal gob interface are obtained by computing the percentage of abutment stress transfered to the lower seam (National Coal Board, 1954; Wu, 1987).

These relationships have been verified in some recent field studies. The effects of pillar load transfer were studied at two mines sites in Raleigh County, West Virginia (Matetic et al., 1987). The upper mine is located in the Peerless Coalbed, which is approximately 72 inches thick. The lower mine is located in the No. 2 Gas Coalbed, which is approximately 48 inches thick. The mines are separated by 40 to 50 feet of innerburden. The overburden predominantly consists of sandstone interbedded with shale. The innerburden also mainly consists of sandstone with some shale beds. According to equations 2.15 and 2.16 (Haycocks et al., 1987), interaction was predicted for the given data. Extensive instrumentation was done to assess the amount of pressure transferred to the lower mine through upper seam pillars. The measured pressures were correlated with the theoretical pressures calculated according to the procedure outlined by Peng and Chandra (1980). The areas of pressure were found to be experiencing roof and floor problems. A number of other studies also relate the existence of high stresses at the lower seam to the pillar load transfer phenomena (Chekan and Listak, 1992; Chekan and Matetic, 1990; Matetic and Chekan, 1988; Matetic et al., 1987; Chekan et al., 1986).

2.3 Geologic Conditions

2.3.1 Geologic Structures

Lithology and structure of coal mine strata can drastically affect the stability of entries. The rock type and stratification, along with other factors,

influence the roof behavior. The entries with soft, low strength roof rock are naturally more susceptible to roof failures than those with stronger roof beds. Typical low strength rocks include clay stone and underclay. These rocks are very sensitive to moisture present in the mine air. The moisture causes their progressive slaking and disintegration. Entries where the roof is highly laminated are prone to roof failures compared to massive roof rock conditions. This is because a bedding plane in laminated roof strata constitutes a potential plane of separation. The combination of weak bonding and thin laminations of claystone/shale makes this type of roof difficult to support by bolts. Minor geologic structures are responsible for many of the roof falls in underground coal mines. These structures include virtually any geological feature other layering of the roof strata. Slickensides, paleochannels, kettle bottoms, clay dikes, joints, pinchouts, concretions and localized faults are some of such structures. Most minor structures constitute a discontinuity in the normal beam-like structure of a mine roof and therefore have a weakening effect (Moebs and Stateham, 1986).

Slickensides are perhaps the most dangerous of all geologic structures encountered in underground coal mines. This type of structure is most common in argillaceous rocks such as shales and claystones. Slickensides are described as smooth, polished and sometimes striated surfaces resulting from relative movement due to differential compaction of sediments at the time of formation of these rocks (Moebs and Ellenberger, 1982). The slickensided surface is usually curved and convexed toward the coalbed. Slickensided surfaces create low shear strength conditions susceptible to roof

failures due to slippage of the rocks along these planes (Milici et al., 1982; Moebs, 1986). Many of the geology related roof falls in the coal mines of Appalachia are attributed to this condition (Moebs, 1984; Moebs and Bauer, 1989).

Paleochannels are structures formed by stream channels cut into older rocks such as roof shale/coal bed and later filled with younger sediments. These are trough-like masses of cross-bedded sandstone recognized by their horse-belly appearance and slickensided margins. The weak bond between such a sandstone body and the surrounding rock mass poses a great hazard from the point of view of roof stability (Moebs, 1984; Moebs and Ellenberger, 1982)

Clay veins are wedge-shaped masses of mudstone or claystone filled in the crevices of a coal bed. The pattern and character of clay veins found in the coal mines of West Virginia and Illinois suggest that they were formed as a result of filling of the tension cracks in the peat with argillacious material (Moebs, 1984, 1986; Moebs and Ellenberger, 1982). Slickensides accompanying clay veins further contribute to the roof fall hazard (McCable and Pascoe, 1978).

Crevasse splays refer to a particular lithologic unit, consisting of sandstone thinly interbedded with shale or thin bedded micaceous sandstone. These structures are considered to be formed as a result of flooding of a stream channel and consequent deposition of sand over the mud flats. Roof failures in such environments occur due to separation along a bedding plane at or

above the bolt anchors. The weakness of splay-type deposits is attributed to the lack of cohesion between the mica and shale layers. This problem is made worse by plant remains and carbonaceous layers on the bedding planes (Moebs, 1984; Chase and Sames, 1983).

A pinch-out is defined as the abrupt termination of a stratum. These structures are often found on the boundaries of the channels. These are considered to be the result of the same cutting action that formed paleochannels. The effect of pinch-out in a thick competent roof strata is weakening of the roof beam action due to discontinuity (Moebs and Ellenberger,1982).

Kettle-bottom is the term used to describe the fossil casts of trees in the rock layers above coal beds. These are a common occurrence in the Appalachian coal fields. These vary in size from 6 inches to 6 feet in diameter and extend up to 8 feet into the roof. Kettle-bottom surfaces are highly slickensided which makes them a roof hazard (Chase and Sames, 1983).

2.3.2 Geological Factors in Multi-Seam Interaction

Geology of the innerburden is an important factor in determining the stability of lower seam structures (Szwilski, 1979; Johnson, 1973; Haycocks, 1991). In previous research to quantify geologic data and to provide initial guidelines for assessment of roof and innerburden conditions, two geologic characterization systems were developed, one for roof strata, the other for

innerburden (Wu, 1987; Haycocks, 1990). Of primary concern in the innerburden characterization are the major types of rocks present. Structural strengths, resistance to weathering and inherent structural characteristics, particularly layering are of special concern (Moebs and Ellenberger, 1982; Haycocks and Zhou, 1990).

In practice it has been found that, in unjointed roof rocks, the number of layers in the innerburden have a significant effect on stress transfer in both case studies and physical modeling (Ehgartner, 1982; Haycocks et al., 1982; Wu, 1987). In terms of load transfer, innerburden layering affects both the size and shape of the pressure bulb (Matetic and Chekan, 1988).

2.4 Stability Assessment Alternatives

2.4.1 Analytical Approach

Almost all physical phenomena can be represented by partial differential equations. Although the derivation of such equations for real life problems is generally simple, finding their solutions is a real challenge. These solutions, commonly termed as analytical solutions or close form solutions, are possible to obtain if the problem geometry is relatively simple and the boundary conditions are well defined. The solutions for beam and plate problems are the two examples of close form solutions commonly applied in mining. Entry roof in underground coal mines is treated as a beam whereas the entry intersection is represented by a plate. Both of these analogies have their

limitations in realistic representation of the prevailing complex geology and stress conditions

2.4.2 Empirical Roof Ratings

These systems are developed on the basis of past experience in the excavation and support of tunnels. Most of the roof rating schemes developed over the past thirty years are meant to evaluate the roof conditions in terms of rock quality, spacing of discontinuities and ground water conditions. In each of these schemes a numerical value is assigned to a particular set of conditions. This value is then used as a measure of rock quality for support requirements and standup time.

2.4.2.1 Rock Load Classification

This classification is designed to estimate rock loads on tunnel supports. The concept on the basis of which these loads are calculated is illustrated in Figure 2.17. It is assumed that, as a result of the excavation, the rock within the dotted region is loosened and tends to move towards the excavated area. This movement is resisted by friction forces along the lateral boundaries, thus transferring a major portion of the overburden weight on the sides of the tunnel. The roof and sides of the tunnel are therefore required to support only the load equivalent to height H_p. The classification gives the range of rock loads in terms of tunnel dimensions for various rock types as shown in Table 2.1 (Terzaghi, 1946). This classification, though widely used in the

Table 2.1 -- Terzaghi's Rock Load Classification for Steel Arch-Supported Tunnels

Rock condition	*Rock load H_p in feet*	*Remarks*
1. Hard and intact.	zero	Light lining required only if spalling or popping occurs.
2. Hard stratified or schistose.	0 to 0.5 B	Light support, mainly for protection against spalls.
3. Massive, moderately jointed.	0 to 0.25 B	Load may change erratically from point to point.
4. Moderately blocky and seamy.	0.25B to 0.35(B + H_t)	No side pressure.
5. Very blocky and seamy.	(0.35 to 1.10)(B + H_t)	Little or no side pressure.
6. Completely crushed but chemically intact.	1.10(B + H_t)	Considerable side pressure. Softening effects of seepage towards bottom of tunnel requires either continuous support for lower ends of ribs or circular ribs.
7. Squeezing rock, moderate depth.	(1.10 to 2.10) (B + H_t)	Heavy side pressure, invert struts required. Circular ribs are recommended.
8.Squeezing rock, great depth.	(2.10 to 4.50) (B + H_t)	
9. Swelling rock.	Up to 250 feet, irrespective of the value of (B + H_t).	Circular ribs are required. In extreme cases use yielding support.

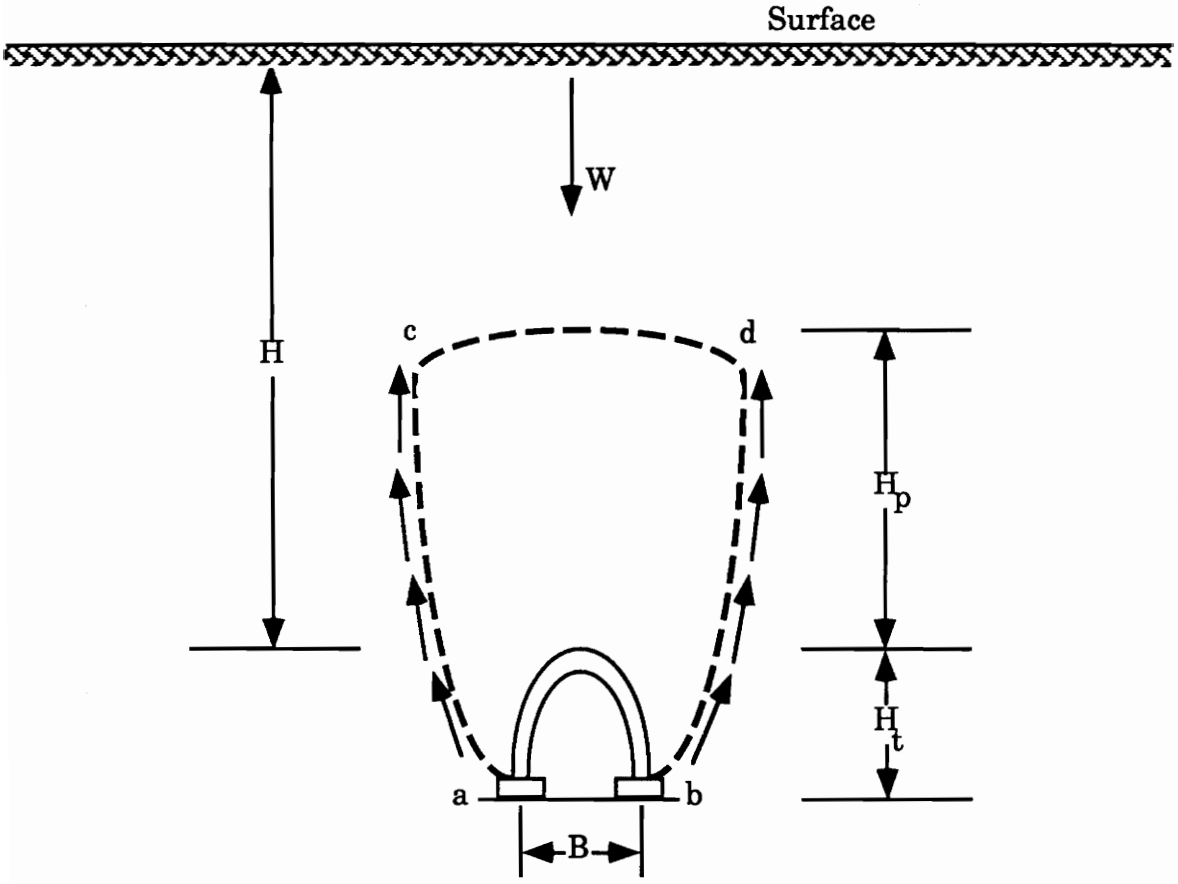

Figure 2.17 Simplified diagram representing rock load on tunnel supports (After Terzaghi, 1946)

past, is too general to allow an objective evaluation of rock quality without providing any quantitative information on the properties of rock mass.

2.4.2.2 Rock Quality Designation (RQD)

RQD is defined as the percentage of core recovered in intact pieces four inches or more in length in the total length of a borehole (Deere, 1964). The RQD and engineering quality of rock masses are related as follows (Deere, 1968):

RQD(%)	*Rock Quality*
<25	Very poor
25-50	Poor
50-75	Fair
75-90	Good
90-100	Excellent

The application of RQD in tunnel support estimation is illustrated in Figure 2.18. Although RQD is considered to be a good measure of classifying rock masses for tunnel support purposes (Wickham et al., 1972), it has limitations where rock joints contain clay fillings and weathered materials (Merrit, 1972).

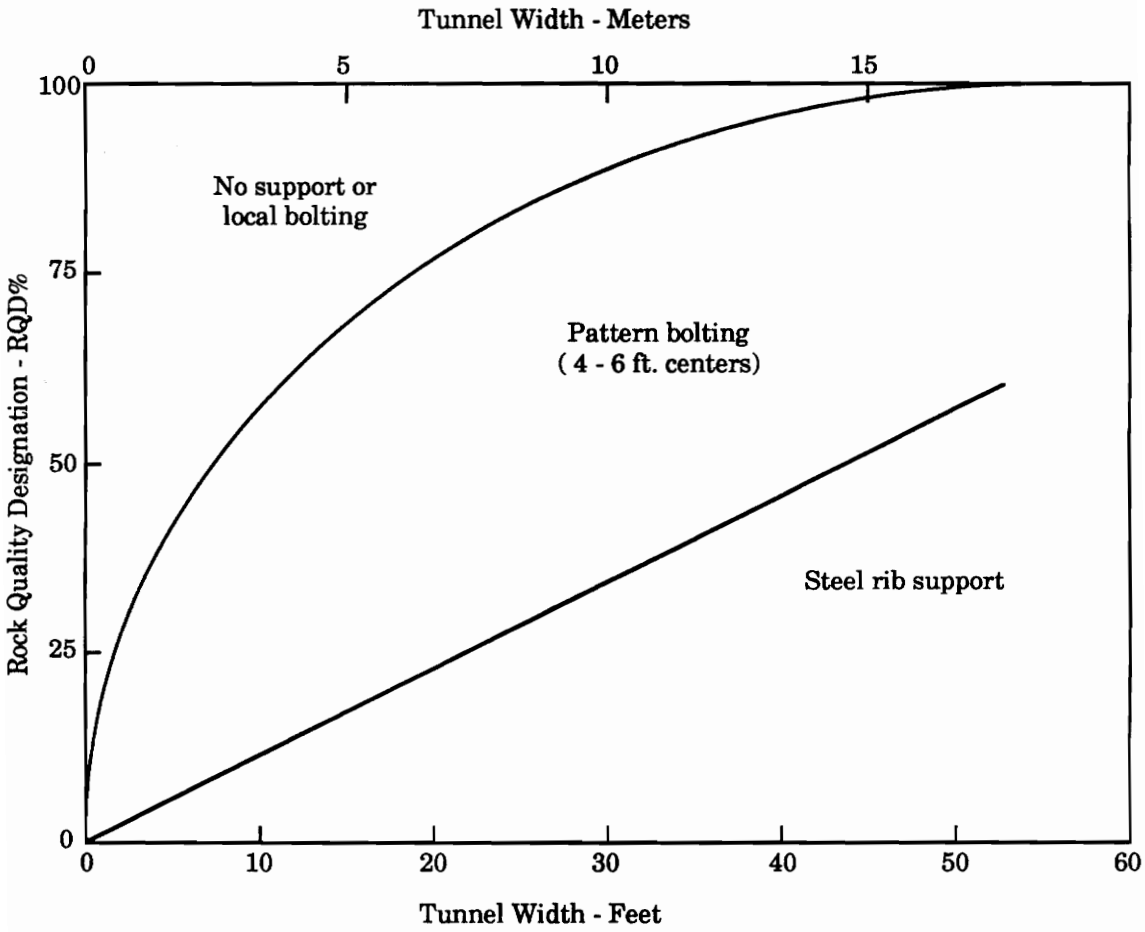

Figure 2.18 Rock support assessment from RQD values
(After Merrit, 1972)

2.4.2.3 Rock Mass Rating (RMR)

It is difficult to use any one indicator of rock quality such as RQD to represent the complex behavior of rock mass in many practical situations. More comprehensive schemes have therefore been developed incorporating other important parameters along with the RQD index. One such scheme, proposed by Bieniawski, has been well received by the industry (Bieniawski, 1974, 1976). In this scheme the following six parameters are used to classify a rock mass:

- Uniaxial compressive strength of rock material;
- Rock Quality Designation;
- Spacing of discontinuities;
- Condition of discontinuities;
- Groundwater conditions;
- Orientation of discontinuities.

The RMR scheme is presented in Table 2.2 (Bieniawski, 1989). Each of the six parameters used in this classification do not necessarily contribute equally to the behavior of rock mass. Therefore a rating is assigned to each parameter from a range of values for that parameter. The overall rating for the rock mass is achieved by adding the ratings for the six individual parameters. This overall rating is then related to support requirements and standup time as shown in Figure 2.19.

Table 2.2 – Rock Mass Rating System (RMR)

Parameters		Range of Values				
Strength of intact rock material	**Point-load strength index (MPa)**	> 10	4-10	2-4	1-2	For this low range, uniaxial test is preferred
	Unixial compressive strength (Mpa)	> 250	100 - 250	50 - 100	25 - 50	5-25 1-5 < 1
	Rating	**15**	**12**	**7**	**4**	**2 1 0**
	Drill Core Quality RQD (%)	90 - 100	75 - 90	50 - 75	25 - 50	< 25
	Rating	**20**	**17**	**13**	**8**	**3**
	Spacing of discontinuities	> 2 m	0.6 - 2 m	200 - 600 mm	60 - 200 mm	< 60 mm
	Rating	**20**	**15**	**10**	**8**	**5**
	Condition of discontinuities	Very rough surfaces Not continuous No separation Unweathered wall rock	Slightly rough surfaces Separation < 1 mm Slightly weathered walls	Slightly rough surfaces Separation < 1 mm Hightly weathered walls	Slickensided surfaces or Gouge < 5 mm thick or Separation 1-5 mm Continuous	Soft gouge > 5 mm thick or Separation > 5 mm Continous
	Rating	**30**	**25**	**20**	**10**	**0**
Ground-water	**Inflow per 10 m tunnel length (L/min)**	None	< 10	10 - 25	25 - 125	> 125
	Ratio $\frac{\text{Joint water pressure}}{\text{Major principal stress}}$	0	< 0.1	0.1 - 0.2	0.2 - 0.5	> 0.5
	General conditions	Completely dry	Damp	Wet	Dripping	Flowing
	Rating	**15**	**10**	**7**	**4**	**0**
	Adjustments for Strike and Dip Orientations of Discontinuities	Very Favorable	Favorable	Fair	Unfavorable	Very Unfavorable
	Ratings	**0**	**-2**	**-5**	**-10**	**-12**

(Bieniawski ,1989)

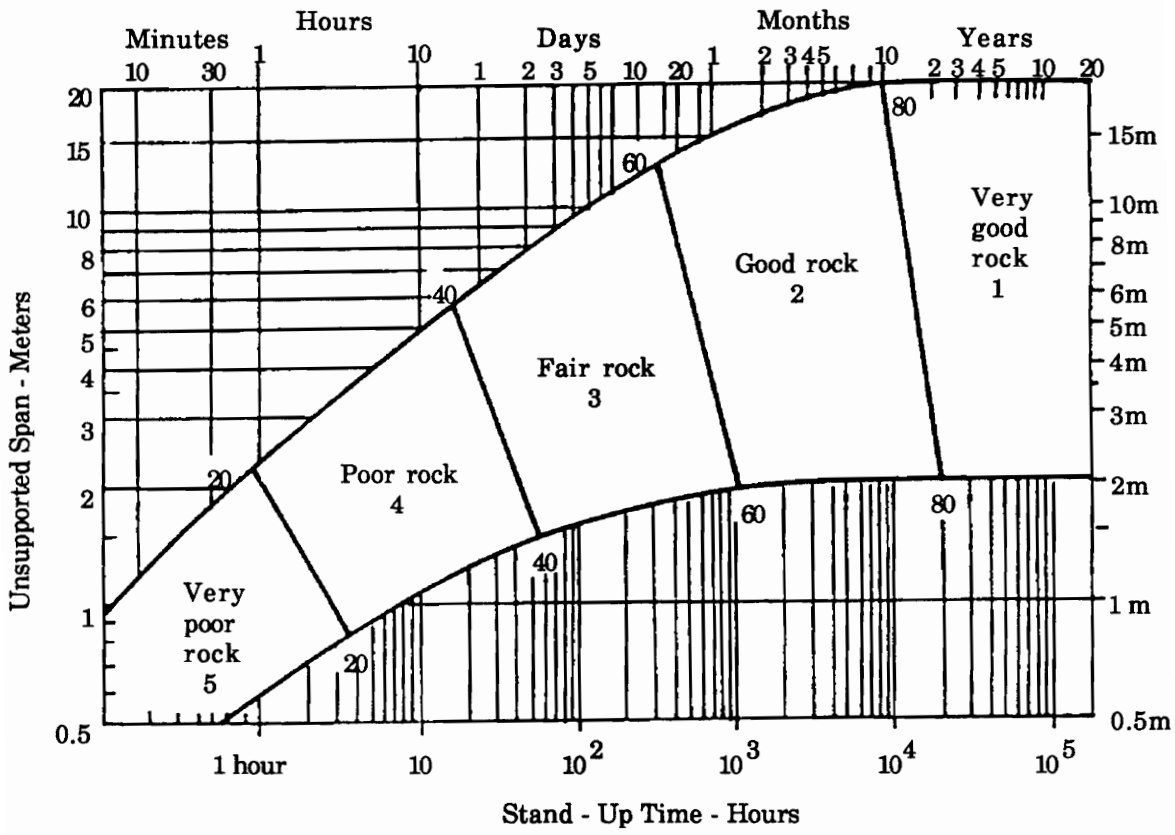

Figure 2.19 Realtionship between the stand-up time of an unsupported span and the RMR (After Bieniawski, 1976)

2.4.2.4 Q-System

This system was developed at the Norwegian Geotechnical Institute to assign a numerical index for the determination of rock mass quality in tunneling (Barton, 1976). The value of this index is defined by:

$$Q = (RQD / J_n) \times (J_r / J_a) \times (J_w / SRF) \qquad 2.20$$

where;

J_n - joint set number

J_r - joint roughness number

J_a - joint alteration number

J_w - joint water reduction number

SRF - stress reduction factor.

These six parameters are separately classified for the purpose of assigning particular values. The Q-index obtained from the above equation is related to an equivalent dimension D_e indicative of the support requirements in a given set of conditions (Figure 2.20).

2.4.3 Numerical Modeling

The application of numerical methods to analyze and design underground structures is gaining popularity with the availability of powerful personal computers.

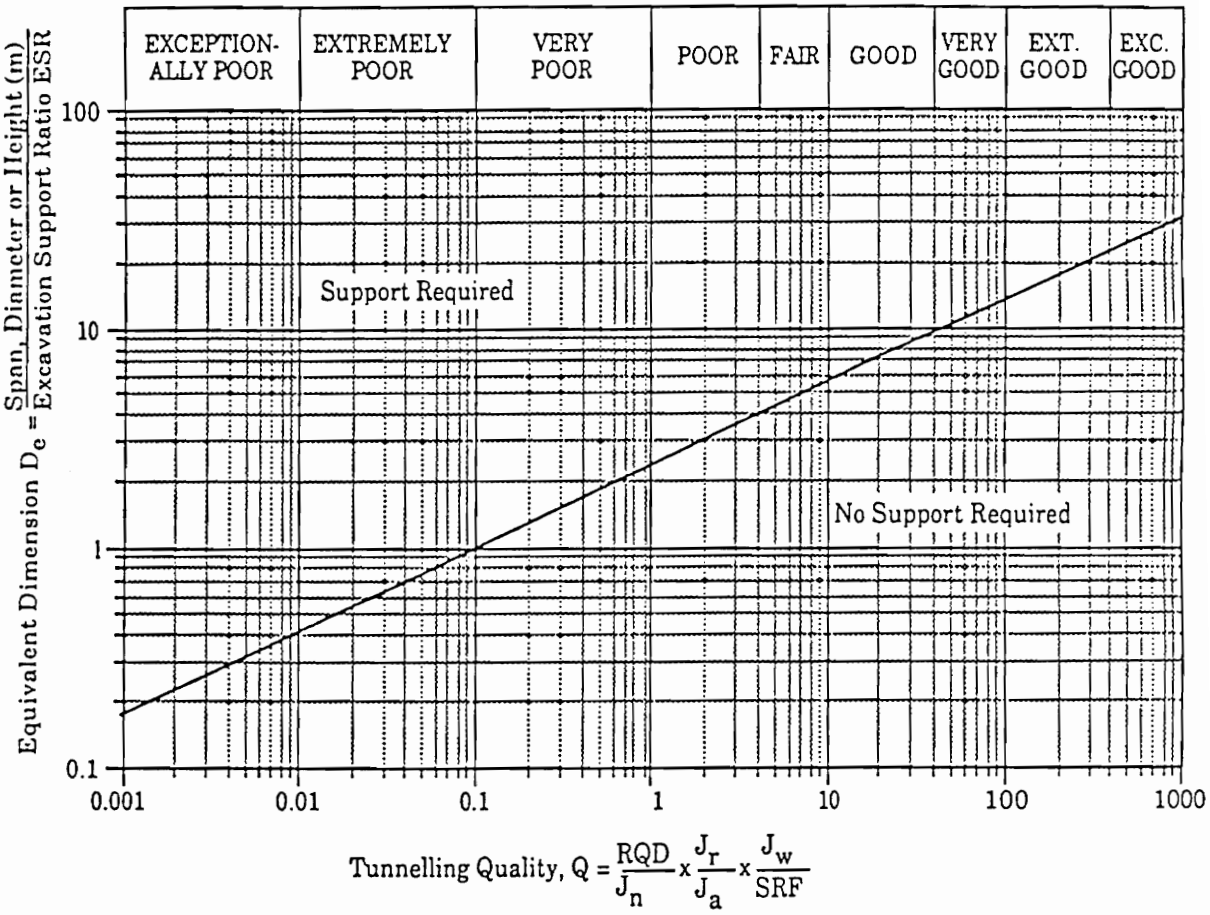

Figure 2.20 Relationship between equivalent dimension of an underground excavation and the tunnelling quality index Q (After Barten et al., 1976)

The basic principle involved in these methods is to transform differential equations into equivalent algebraic equations. The obvious advantage of numerical methods is that virtually any layout can be analyzed in the conditions of geology and stress fields prevalent underground

Chapter 3

Numerical Stress Analysis Techniques

3.1 General

The stress and displacement field in a body of specified geometry and loading conditions can be determined by a close-form solution. This is possible when the differential equations of equilibrium, constitutive relations for the material, strain compatibility equations and boundary conditions of the problem are defined. The boundary conditions are defined by the imposed state of traction or displacement at the excavation surface and the far field stresses. The remaining conditions are generally combined analytically to establish a governing equation for the medium under consideration. A particular function is then obtained which satisfies both the governing equation and the boundary conditions (Brady and Brown, 1985).

In practice, a problem arises due to the fact that, even for a simple excavation geometry and homogeneous isotropic material, great mathematical skills and

time are required to obtain close-form solutions. This fact limits the scope and practicality of these solutions in mining where the excavation geometry and constitutive relations are often complex. The alternative approach is to seek approximate solutions by numerical computational techniques. These techniques are gaining popularity, especially, because of the availability of fast and powerful personal computers.

3.2 Numerical Methods

The common approach adopted in all numerical methods is to divide the problem into smaller physical and mathematical components and then to sum the influence of the components to approximate the behavior of the whole system. The problem is generally formulated as a set of simultaneous equations which are assembled in the matrix form. The solution of these equations is then obtained by a variety of techniques for solving matrices (Hoek et al., 1991).

The numerical methods used in rock mechanics can be placed in two broad categories -- differential methods and integral methods. In differential methods the domain of interest is divided into simple geometrical shapes (discretization), whereas in integral methods only the domain boundary is discretized (Zienkiewicz, 1985). Finite element and finite difference methods are examples of the differential methods, whereas boundary-element is an integral method of numerical computation. The differences in problem formulation between differential and integral methods lead to

various fundamental and operational advantages and disadvantages for each. The basic concepts and limitations of the boundary element and finite element method are summarized below.

3.2.1 Boundary Element Method

The boundary element method is based on the concept that the stress and displacement distribution in the medium is uniquely determined by the conditions on the surface. Thus if some method is established for inducing a traction distribution on the boundary identical to the imposed distribution, the problem is solved. Two different methods are used to achieve this goal:

- In the indirect or fictitious stress method, the stresses on the boundary are found first and separate relations are subsequently applied to find boundary displacements.
- In the direct method, the solution for the unknown stresses and / or displacements is found directly from the boundary conditions.

The main advantage of the boundary element method lies in its ability to discretize the problem geometry with fewer elements and thus less computing time. It also has the advantage of accurately simulating the far field stresses because no approximations are involved, as is the case with the finite element analysis. The boundary element method, however, cannot handle different material types in the domain of interest as efficiently as the finite element method.

3.2.2 Finite Element Method

The finite element method is a powerful numerical technique that uses variational methods and interpolation theory for solving differential equations of initial and boundary value problems (Desai and Abel, 1972). In this method the region of interest is divided into a collection of smaller regions called finite elements. The elements are connected at joints called nodes or nodal points. The distribution of displacements over an individual element is represented by simple displacement functions. Linear equations are developed for each element. The equilibrium condition is obtained by combining the equations of the individual elements in such a way that continuity of displacements is preserved at the nodes. Boundary conditions are imposed and the final solution of this system of equations is obtained by matrix algebra. The solution obtained yields the unknown displacements at desired locations in the body. These displacements are converted to stresses in the post processing stage (Wang and Sun, 1970). The major steps involved in this method are summarized as follows (Reddy, 1984):

- *Discretization.* This is the process of dividing a given domain into simple sub-domains, called *finite elements.* The domain represents a physical region over which the governing equations are to be solved. The collection of elements is called the *finite element mesh* (Figure 3.1). The following steps are required in the discretization of a given domain:

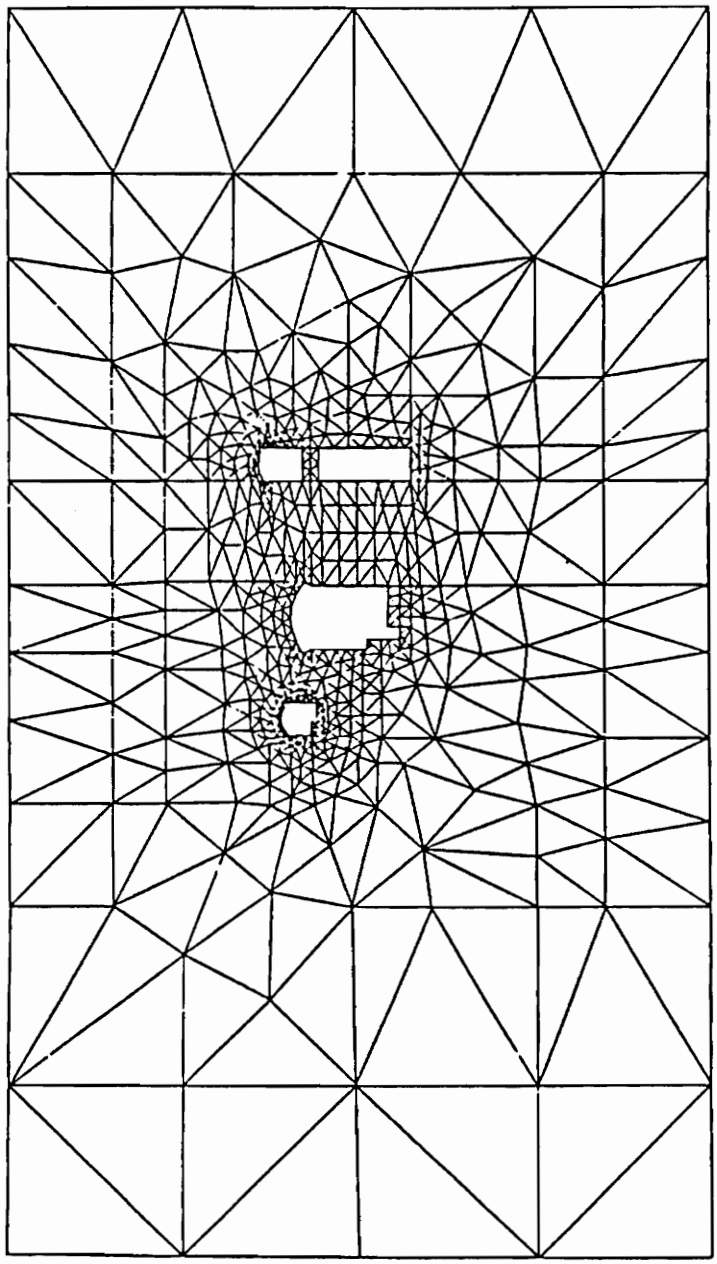

Figure 3.1 Typical finite element mesh (Zienkiewicz, 1985)

- Construct the finite element mesh of pre-selected elements.
- Number the nodes and elements.
- Generate the geometrical properties of the mesh, i.e., coordinates, cross-sections etc.

- *Finite Element Formulation.* This is the derivation of element equations for a typical element in the mesh. The theoretical formulation consists of the following distinct steps:

  - Construct the variational formulation of the given differential equation over the typical element.
  - Assume that the dependent variable, the displacement u, is of the form

    $u = \Sigma u_i \psi_i$

    and substitute it into the above step to obtain element equations in the form

    $[K^e]\{u^e\} = \{F^e\}$
  - Select element interpolation functions ψ_i and compute the element matrices.

- *Assembly.* This is the assembly of element equations to obtain the equations of the whole system. The procedure followed to assemble the equations of whole system is as follows:

- Identify the inter-element continuity conditions among the primary variables, i.e., displacements.
- Identify the equilibrium conditions among the secondary variables, i.e., forces.
- Assemble element equations.

- *Solution.* It involves the imposition of boundary conditions and then solving the matrices. The solution for a given system is obtained as the following procedure:

  - Identify the specified primary degrees of freedom.
  - Identify the specified secondary degrees of freedom.
  - Solve the assembled equations.

- *Postprocessing*. It is the process of calculating stresses from the displacement values. Graphical representation of the results is the final step in postprocessing.

The finite element method has an advantage over boundary element methods, while modeling problems that involve heterogeneous and non-linear material properties, since each element models the response of its contained material. One difficulty with finite element modeling, when dealing with underground excavations, is that it cannot accurately simulate the far off boundaries. The practice is to discretize beyond the zone of

influence of the excavation and to apply appropriate boundary conditions to the outer edges (Hoek et al., 1991).

This method of numerical computation has been used to model underground mining conditions with respect to stress around entries (Hsiung and Peng, 1985; Park et al., 1992; Serata, 1986). The method has also been used to simulate longwall conditions (Kripakov, 1991; Donato, 1992; Ahola et al., 1991).

3.3 Material Models and Failure Criterion

If a test specimen of rock is loaded to the elastic limit under various combinations of confining stresses, the resulting locus of points plotted in stress space defines the strength of the material (Pariseau, 1992). This locus of points is represented by a function $F(\sigma_1, \sigma_2, \sigma_3)$. It serves as a criterion of failure and its form may be suggested according to some empirical rule (Jaeger, 1969; Hoek and Brown, 1982). Any such function should be consistent with the experimental data and have a simple mathematical form. The failure criteria commonly used in rock mechanics analyses include:

- Mohr-Coulomb criteria;
- Drucker-Prager criteria;
- Nonlinear forms of the these two criteria.

In the following sections a brief description of each of these criteria is included. Their application to rock mechanics analyses as well as their limitations are also discussed.

3.3.1 Mohr-Coulomb Criteria

According to Mohr-Coulomb theory, failure is hypothesized to occur on a given plane in a material when a critical combination of shearing and normal stresses acts on that plane. This critical combination of shear and normal stresses is mathematically represented by the following equation:

$$\tau = c + \sigma \tan(\phi) \qquad 3.1$$

where τ and σ are the stresses acting on the failure plane. The quantities c and ϕ are the material constants known as cohesion and angle of internal friction respectively. These constants are determined graphically by the straight line envelope of Mohr's stress circles drawn in the τ-σ plane from the conventional test results (Figure 3.2). Since τ and σ are functions of the principal stresses, the above equation can be expressed as:

$$\tau_m = c \cos(\phi) + \sigma_m \sin(\phi) \qquad 3.2$$

where

$$\tau_m = (1/2)(\sigma_1 - \sigma_3) \qquad 3.3$$

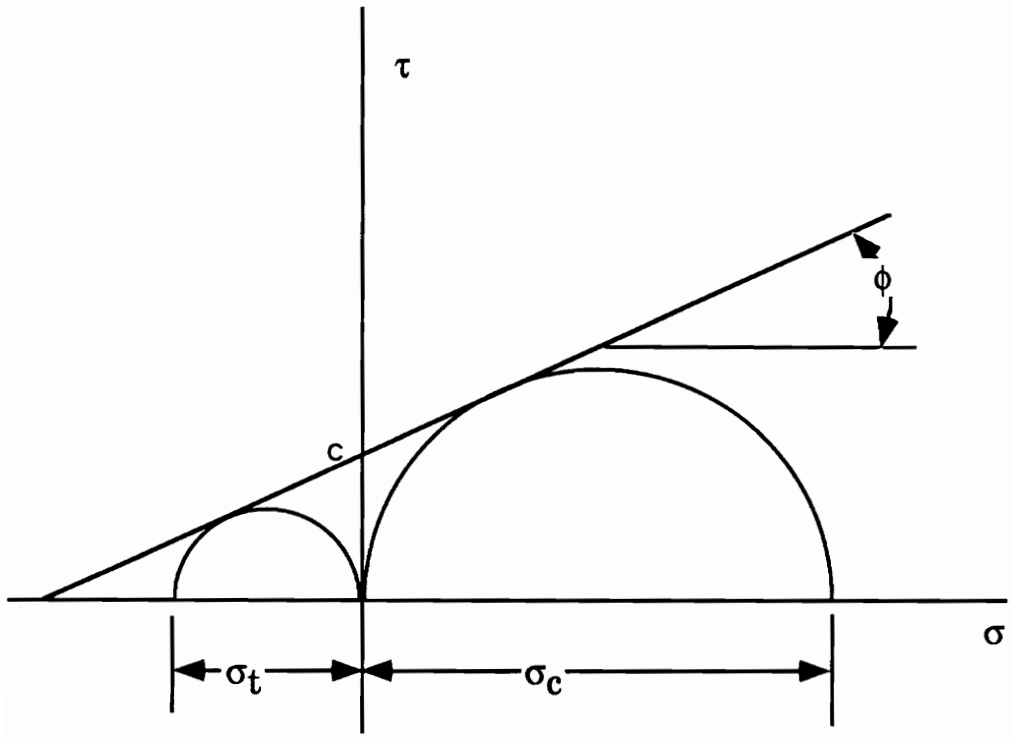

Figure 3.2 Mohr failure criteria in graphical form

$$\sigma_m = (1/2)\ (\sigma_1 + \sigma_3) \qquad 3.4$$

For a given set of applied stresses, the failure condition is checked by seeing whether the Mohr's circle corresponding to these stresses touches the envelope described by the above equation. If the circle does not touch this envelope, a factor of safety greater than unity exists. Equation 3.2 can be rearranged as:

$$\sigma_1 = 2c \cos(\phi)/[1 - \sin(\phi)] + \sigma_3\ [1 + \sin(\phi)]/\ [1 - \sin(\phi)] \qquad 3.5$$

This equation expresses the failure condition in terms of σ_1 as a function of σ_3. This criteria tacitly assumes that the intermediate principal stress has no influence on failure. A criteria that lacks one of the principal stresses, if plotted in principal stress space of σ_1, σ_2, and σ_3, leads to the edges on the failure surface in the form an irregular shaped pyramid (Figure 3.3). The failure surface (with tension cutoff) on the plane $\sigma_3 = 0$, representing the biaxial state of stress, is also an irregular hexagon (Figure 3.4).

The Mohr-Coulomb criteria also has shortcomings due to the linear approximation of failure conditions. Experimental data for high confining pressures has shown disagreements with the linear envelope (Tandanand and Thill, 1987). The non-linear trend of the failure envelope at high confining pressures has been approximated with a parabola for rocks such as shales and mudstones. Because of the corners of the failure surface, a

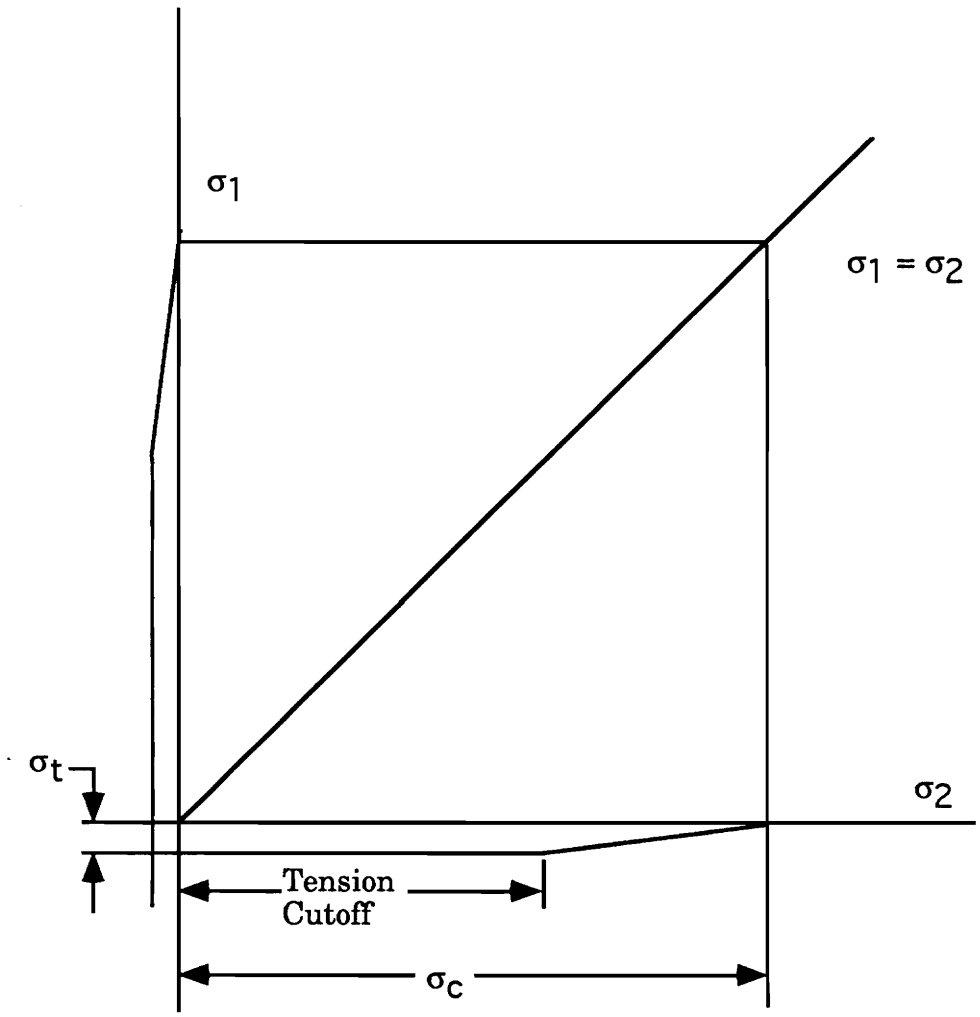

Figure 3.3 Mohr-Coulomb surface in the biaxial stress space

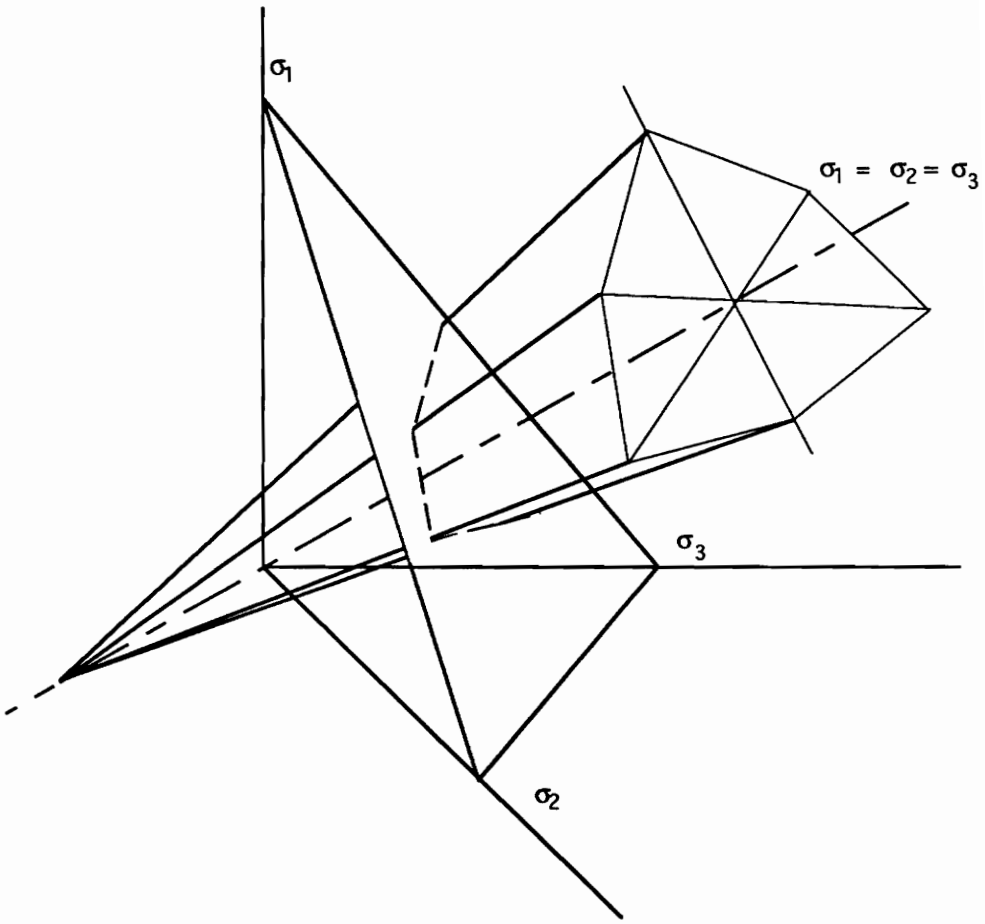

Figure 3.4 Mohr-Coulomb surface in the principal stress space

mathematical difficulty is encountered in the numerical analysis. This difficulty is overcome in the Drucker-Prager criteria where the yield surface is assumed to be a smooth conical surface.

3.3.2 Drucker-Prager Criteria

This is a failure criteria which accounts for the effect of hydrostatic stress on the yield condition of geologic materials. The yield surface of this criteria is a right circular cone that has its apex at the hydrostatic stress axis in the tension octant (Figure 3.5). Mathematically it is expressed as:

$$(J_2)^{1/2} = A\, I_1 + B \qquad 3.6$$

where A and B are material constants which are related to the uniaxial tensile and compressive strengths. The values of the constants can be found from Table 3.1 (Pariseau, 1968). I_1 is the first invariant of total stress tensor, whereas J_2 is the second invariant of deviatoric stress.

$$I_1 = \sigma_1 + \sigma_2 + \sigma_3 \qquad 3.7$$

$$J_2 = (1/6)[(\sigma_1 - \sigma_2)^2 + (\sigma_2 - \sigma_3)^2 + (\sigma_3 - \sigma_1)^2] \qquad 3.8$$

The quantity $(J_2)^{1/2}$ is similar to a root-mean-square measure of shear stress and is analogous to the maximum shear stress τ_m, while I_1, is a true mean normal stress analogous to the average of normal stress σ_m.

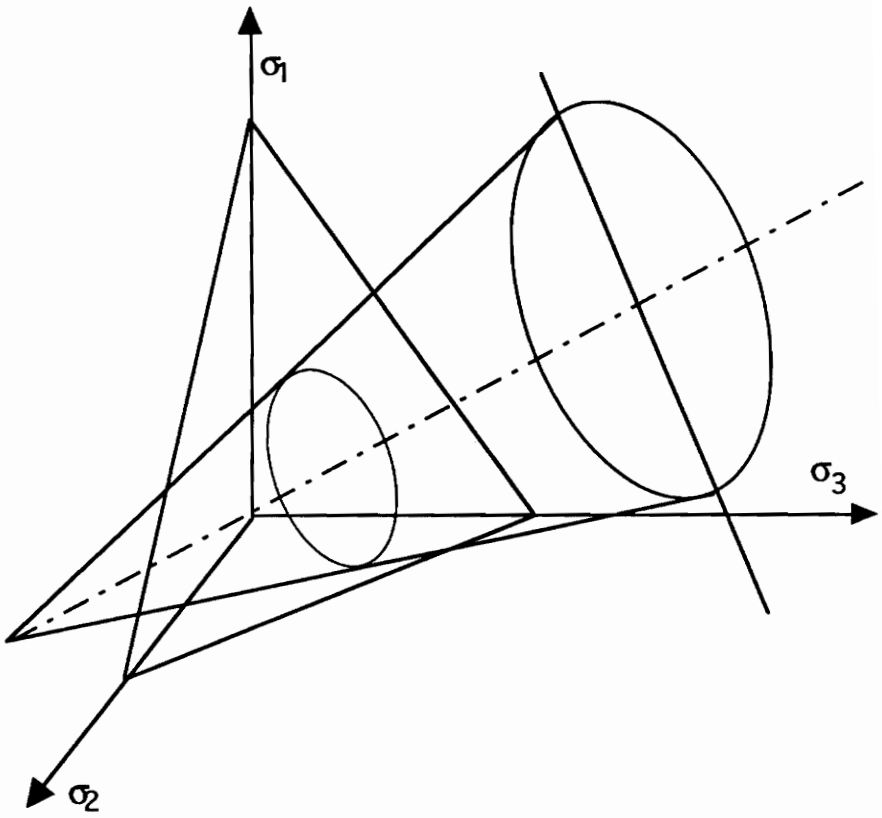

Figure 3.5 Drucker-Prager yield surface

Table 3.1 - Methods of calculation of constants, A & B for common yield conditions (Pariseau, 1968)

Yield Condition	Tresca (constant)	Coulomb (linear)	Torre (parabola)	Griffith		Modified Griffith		General "n" type	Tension "Cutoffs"
constant				$2\sigma_m \leq \tau_m$	$2\sigma_m \geq \tau_m$	$2\sigma_m \leq \tau_m$	$2\sigma_m \geq \tau_m$		
n =	1	1	2	1	2	1	1	n	$n \rightarrow \infty$
A =	0	$(C\text{-}T)/C+T)$	$\frac{1}{2}(C - T)$	1	$\frac{1}{2}C$ or $4T$	1	$(C\text{-}2T)\backslash C$	$\frac{(\frac{1}{2}C)^n - (\frac{1}{2}T)^n}{\frac{1}{2}C + \frac{1}{2}T}$	A
B=	$\frac{1}{2}C$ or $\frac{1}{2}T$	$CT/(C+T)$	$\frac{1}{4}CT$	T	0	T	T	$\frac{T(\frac{1}{2}C)^n - C(\frac{1}{2}T)^n}{C+T}$	0
$\sin\phi$	0	A	$\frac{A}{2\lvert\tau_m\rvert}$	1	$\frac{A}{2\lvert\tau_m\rvert}$	1	A	$\frac{A}{n\lvert\tau_m\rvert^{n-1}}$	0

In a deviatoric plane of the principal stress space in which σ_1, σ_2, σ_3 are the coordinate axes, the trace of the Drucker-Prager yield surface is represented by a circle. Since the stress condition at failure in compression, for most cases in rocks follows the Mohr-Coulomb criteria at moderate confining pressures, the Mohr-Coulomb hexagonal surface and the Drucker-Prager conical surface partially coincide at the corners (Figure 3.6).

The application of modified Drucker-Prager criteria for the analysis of various mining problems has been demonstrated recently (Jones and Pariseau, 1990; McMahon and Pariseau, 1989; Pariseau, 1978; Pariseau, 1968).

3.3.3 Non-Linear Failure Criterion

3.3.3.1 Non-Linear Forms of Mohr-Coulomb Criteria

The non-linearity of the failure envelope of the Mohr's circle is represented by several approximations. All of these criteria have special properties and contain tacit assumptions regarding the material behavior. Quadratic criterion is the most common approximation and is considered suitable in describing the failure of rocks .

Hoek and Brown criteria, being the most widely accepted, will be briefly reviewed here. This is an empirically based criterion which relates the

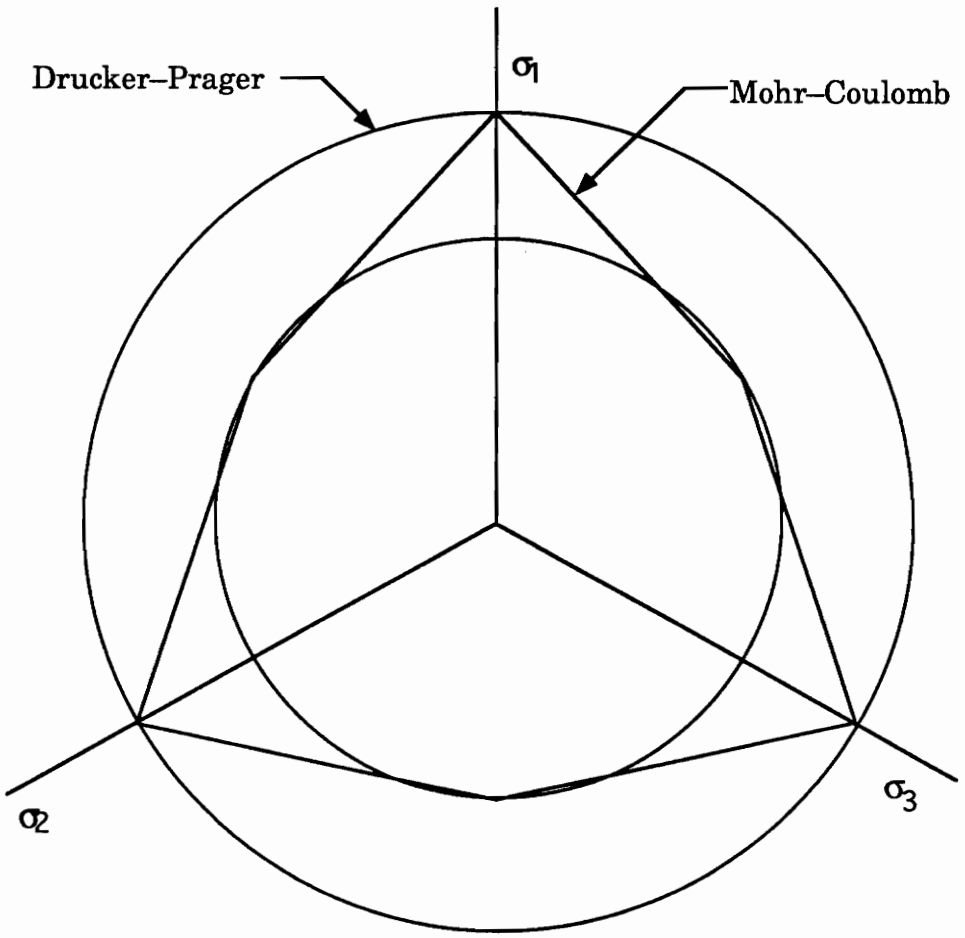

Figure 3.6 Traces of Mohr-Coulomb and Drucker-Prager surfaces in deviatoric plane

principal stresses at failure for brittle rock containing random discontinuities (Figure 3.7). It is expressed in the following equation:

$$\sigma_1 = \sigma_3 + (m\,\sigma_c\,\sigma_3 + s\sigma_c^2)^{1/2} \qquad 3.9$$

where,

σ_1 is the major principal stress at failure

σ_3 is the minor principal stress applied to the test specimen

σ_c is the uniaxial compressive strength of the intact rock material

m and s are material constants representing the tensile strength degree of fracturing of the rock.

The values of the material constants are determined from test results (Hoek and Brown, 1982). The value of s is always 1 (for intact rock) or less than 1 (for previously broken rocks).

3.3.3.2 Non-linear Forms of Drucker-Prager Criteria

The quadratic and n-type forms of J_2 -I_1 yield functions have been reported. These are the modified forms of Drucker-Prager criteria. Their general form is represented as under:

$$(J_2)^{n/2} = A\,I_1 + B \qquad 3.10$$

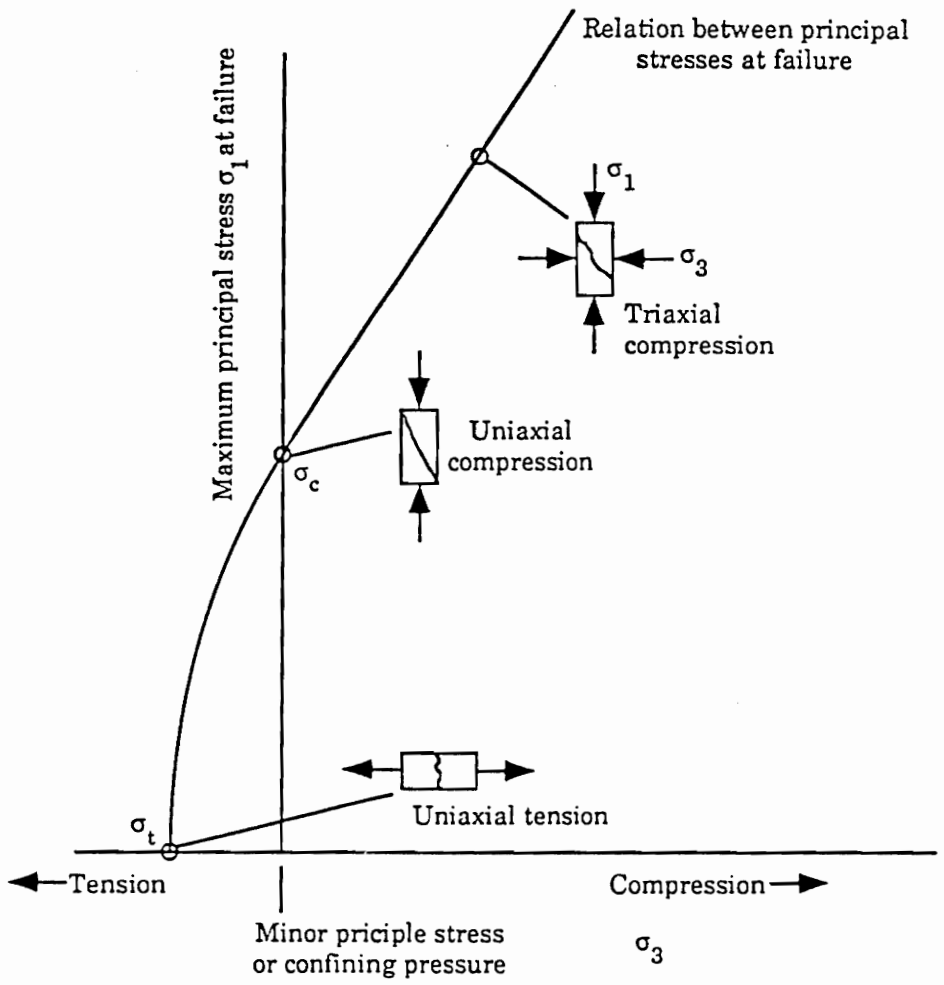

Figure 3.7 Graphical representation of stress conditions for failure of intact rock (After Hoek and Brown, 1982)

Anisotropic forms that take into account the directional properties of certain rocks are also available. In the finite element code UTAH2 (which was used for the purpose of stress analysis in this study), a modified Drucker-Prager criteria is used for plane stress and plane strain analysis (Pariseau, 1978).

In this criteria, the safety factor against failure is calculated according to the following equation:

$$FS = \frac{\sqrt{J_{2_{max}}}}{\sqrt{J_{2_{act}}}} \qquad 3.11$$

where

$$\sqrt{J_{2_{max}}} = (1 - I_1)^{1/n} \qquad 3.12$$

$$\sqrt{J_{2_{act}}} = \{F(\sigma_{yy} - \sigma_{zz})^2 + G(\sigma_{zz} - \sigma_{xx})^2 + H(\sigma_{xx} - \sigma_{yy})^2 + L\tau_{yz}^2 + M\tau_{zx}^2 + N\tau_{xy}^2\}^{1/2} \qquad 3.13$$

$$I_1 = U\sigma_{xx} + V\sigma_{yy} + W\sigma_{zz} \qquad 3.14$$

In these equations *F, G, H. L, M, N, U, V,* and *W* are the material constants related to the tensile, compressive and shear strength of rock (C_1, C_2, C_3, T_1, T_2, T_3, R_1, R_2, R_3). The subscripts used above refer to the anisotropy direction. The quantity (3.11) is an anisotropic extension of the second invariant of deviatoric stress and is a measure of the intensity of the shear stress in three-dimensional anisotropic stress space. The term (3.12) is an

anisotropic form of the first invariant of total stress. The equations to calculate the nine material constants from the input strength properties are given in Table 3.2.

3.4 Summary

The finite element method is considered to be the best choice if multi-layer, heterogeneous, anisotropic materials are to be modeled for stress analysis. The stress analysis for multi-seam conditions modeled in this study was, therefore, performed using this techinique. The computer code selected for this purpose was a package developed by the University of Utah in collaboration with the U. S. Bureau of Mines. This program has been used to model room and pillar as well as longwall mining conditions. It uses the modified version of Drucker-Prager criteria for calculating safety factors. This code was selected because it has features capable of handling non-linear, heterogeneous, anisotropic materials.

Table 3.2 Description of the procedure used to calculate constants from material properties (Pariseau, 1993)

$$F = \frac{1}{2}(p(6) - p(4) + p(5))$$

$$G = \frac{1}{2}(p(4) - p(5) + p(5))$$

$$H = \frac{1}{2}(p(5) - p(6) + p(4))$$

$$L = \frac{1}{R_1(j)^2}$$

$$M = \frac{1}{R_2(j)^2}$$

$$N = \frac{1}{R_3(j)^2}$$

T = tensile strength
C = compressive strength
R = shear strength
p_n = 1 for linear yield conditions
2 for parabolic yield case

$$U = \frac{(C_1(j))^{p_n} - (T_1(j))^{p_n}}{p(1)}$$

$$V = \frac{(C_2(j))^{p_n} - (T_2(j))^{p_n}}{p(2)}$$

$$W = \frac{(C_3(j))^{p_n} - (T_3(j))^{p_n}}{p(3)}$$

$$p(1) = (T_1(j))(C_1(j))^{p_n} + (C_1(j))\left(T_1^{p_n}\right)$$

$$p(2) = (T_2(j))(C_2(j))^{p_n} + (C_2(j))\left(T_2^{p_n}\right)$$

$$p(3) = (T_3(j))(C_3(j))^{p_n} + (C_3(j))\left(T_3^{p_n}\right)$$

$$p(4) = \frac{(C_1(j))(T_1(j))}{p(1)}$$

$$p(5) = \frac{(C_2(j))(T_2(j))}{p(2)}$$

$$p(6) = \frac{(C_3(j))(T_3(j))}{p(3)}$$

$$p_n = \frac{2}{p_n}$$

$$p(4) = p(4)^{p_n}$$

$$p(5) = p(5)^{p_n}$$

$$p(5) = p(5)^{p_n}$$

Chapter 4

Modeling of Multi-Seam Conditions

4.1 General

Previous research into multi-seam mining predicts interaction occurs if the offending seam lies within 50 ft of the seam to be mined (Haycocks et al., 1987; Wu, 1987). To quantify this interaction, roof lithology and overburden depth were modeled, in this study, for a wide variety of conditions. Roof lithology was defined in terms of percentage of hard rock (primarily sandstone) in the innerburden. The effect of percentage and distribution of sandstone in the innerburden on lower seam entry roof stability was studied for overburden depths ranging from 300 ft to 1500 ft.

The effect of unsymmetric loading, as encountered in multi-seam conditions and longwall gate entries, was modeled. The effect of excess horizontal stress on roof stability was also studied. A description of the representative model analyzed in this study is given in the next section.

4.2 Description of the Model

To investigate entry roof stability an extensive selection of underlying multi-seam situations was analyzed by finite element modeling. The numerical modeling was carried by evaluating the stability of the lower seam entry in terms of depth and roof safety factors. Initial model entry stability analysis consisted of determining the effect of:

1 - Percentage of sandstone in the innerburden
2 - Distribution of the sandstone
3 - Innerburden thickness
4 - Depth
5 - Loading conditions

To convert predicted effects into specific ground control effects, plain strain conditions were assumed which represent conditions between the pillars. Intersections must be viewed three-dimensionally; however, this has not been included in this analysis.

Figures 4.1 and 4.2 outline the range of conditions modeled in this investigation. The innerburden thickness was varied from 20 to 50 feet for an overburden of 300 to 1500 ft. Opening widths were set at 20 feet, which best represents field conditions. To evaluate the effect of different roof lithologies, a number of differing combinations were examined. Both pure

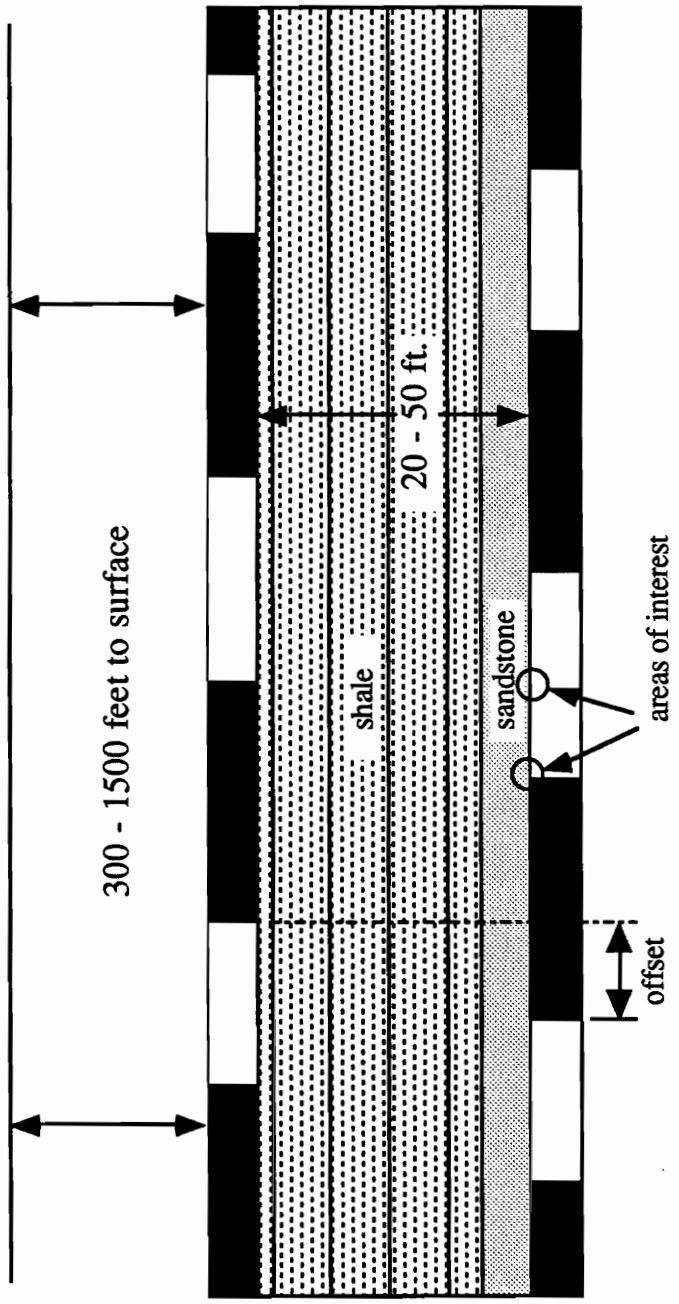

Figure 4.1 A general representation of the model with sandstone in the immediate roof of lower seam entries

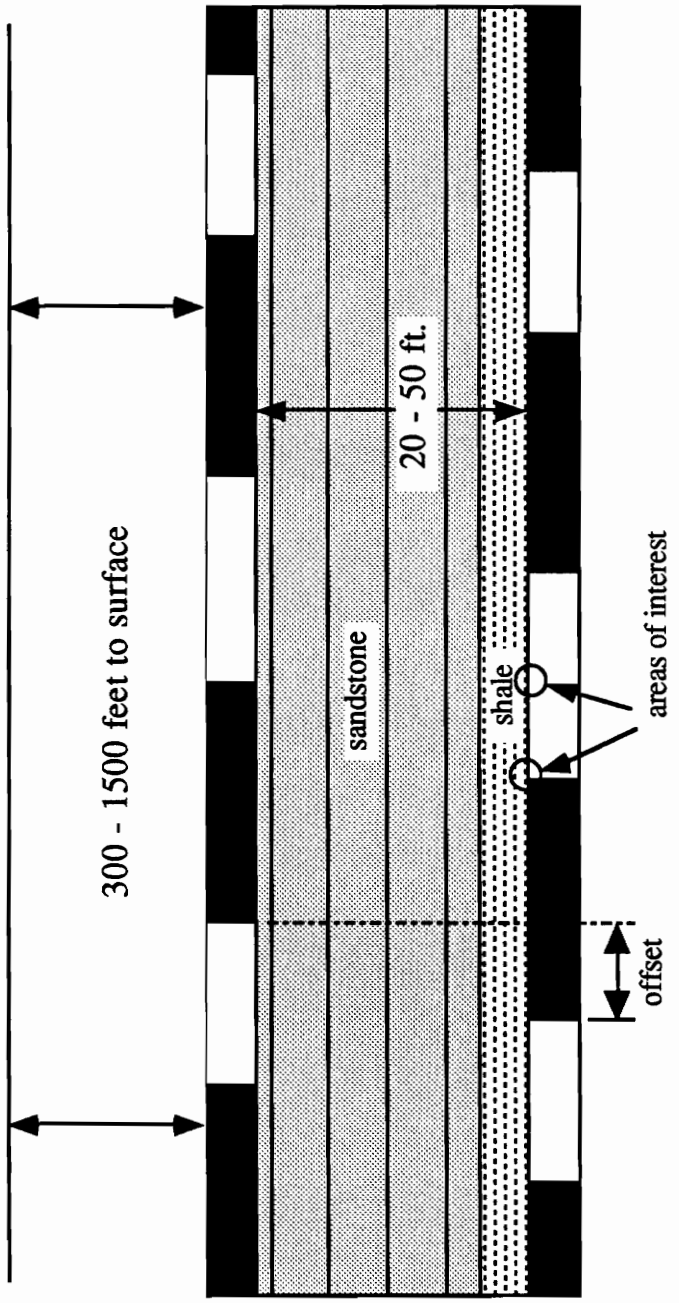

Figure 4.2 A general representation of the model with shale in the immediate roof of lower seam entries

sandstone and pure shale roofs were modeled first, then a sandstone roof grading to shale and a shale roof grading to sandstone was studied. The effect of unsymmetric loading due to offset pillars in the upper seam was also investigated. Three configurations were evaluated to determine the effect of unsymmetric loading due to pillar offsetting. These were the cases with perfectly columnized pillars, partially offset pillars and completely offset pillars. The influence of excessive horizontal stress on entry stability was also investigated. A whole range of values representing the reported stress levels in the field were simulated.

The effect of the factors outlined above on entry stability was studied by finite element modeling. The use of the finite element method in mining has been demonstrated in a variety of conditions ranging from room and pillar to longwall mining (Grenoble and Haycocks, 1985; Su and Peng, 1987; Park et al., 1992; Kripakov, 1988; Pariseau, 1978; Ahola et al., 1991; Wen and Peng, 1986). The finite element modeling required certain assumptions regarding the material around openings. The first assumption was that there is no roof bed separation as could be expected under many conditions. This assumption leads to conditions similar to a bolted roof. The second assumption was that the average values of material properties were adequate for the analysis. The representative set of properties used in the analysis is given in Table 4.1. The discontinuities in the vicinity of the opening were not included in the model because the analysis was limited to the stress related failures.

Table 4.1 - Representative set of properties used in the finite element analysis

Rock type	Specific Gravity	Poisson's Ratio	Compressive Strength (psi)	Tensile Strength (psi)	Shear Strength (psi)	Young's Modulus (psi)	Shear Modulus (psi)
Coal	1.40	0.30	3000	300	548	500000	192307
Sandstone	2.65	0.17	6000	600	2738	1800000	769230
Siltstone	2.60	0.20	5000	500	913	1500000	625000
Shale	2.70	0.25	3500	350	639	940000	376000

The finite element program used in this analysis was the U. S. Bureau of Mines code UTAH2PC. This is a 2-D program having the option of plane stress and plane strain analyses. It uses the modified Drucker-Prager failure criteria as described in Chapter 3. This criteria is suitable for the modeling of non-linear, anisotropic behavior of stratified rocks (Pariseau, 1978; 1969; Dahl, 1968). A brief description of the program input and output is given in the following section.

4.3 Input for UTAH2PC

The input needed for the program is contained in nine files. They are:

Master runstream file
Material properties file
Element connection file
Node coordinate file
Boundary condition file
Screen output file
Cut or fill element file
Initial stress file
Cut node file.

The master runstream file contains the file names and the parameter specifications necessary for the analysis. The material property file lists the rock type, its elastic constants (E, G and ν), specific gravity, compressive

strength, tensile strength and shear strength. This sequence is repeated as needed for the number of materials being modeled. The program can handle any number of materials. The element connection file contains the element number, the numbers of the connecting nodes and the material type for each element. The node coordinate file contains the node numbers and their coordinates. All this information is required in a given format for the use of UTAH2PC (Pariseau et al., 1992).

The preparation of these files becomes increasingly difficult and time consuming as the size of the problem becomes bigger. In this study more than 200 situations were modeled with the mesh size in the range of about 2000 elements for each case. This situation necessitated the automation of the input data. Three separate computer programs, MESH, BOUNDARY, and CUTELEM, were developed for this purpose. The code for these programs is given in Appendix A. A brief description of the programs is provided in the following sections.

4.3.1 Mesh Generation

An AutoLisp program UTAH2CAD comes with the code UTAH2PC. The program can plot the mesh in AUTOCAD if the node coordinate information and element connectivity data is arranged in two separate files in specified formats. The program MESH was written for the creation of these files. It creates two separate files containing required information on the node coordinates, element connectivity and material type in the required format

for UTAH2CAD.

The input data required for this program is very simple and format free. This data, in the following sequence, include the number of horizontal layers to be simulated, the number of vertical divisions, thickness of each layer, its material type, and the width of each vertical division. The program can handle any number of four nodal quadrilateral elements in a rectangular domain. UTAH2CAD, however, had difficulty reading files for meshes having more than 2500 elements. The plotted mesh is a multi-layer drawing with the option of displaying black and white layers with nodes and element numbers or the colored mesh showing different material layers with separate colors. Figure 4.3 shows a typical black and white mesh plotted by AUTOCAD.

4.3.2 Defining Boundary Conditions

All the nodes on the outer boundary of the mesh must be specified in a separate file, specifying nodal forces and displacement prevalent over these nodes, before loading the mesh. For a fairly large mesh, such as those modeled in this analysis, specifying the constraints and nodal forces and / or displacements is time consuming and the possibility of making an error in entering these numbers is difficult to eliminate. To deal with this problem the program BOUNDARY was written.

This program reads the information regarding the boundary nodes from the

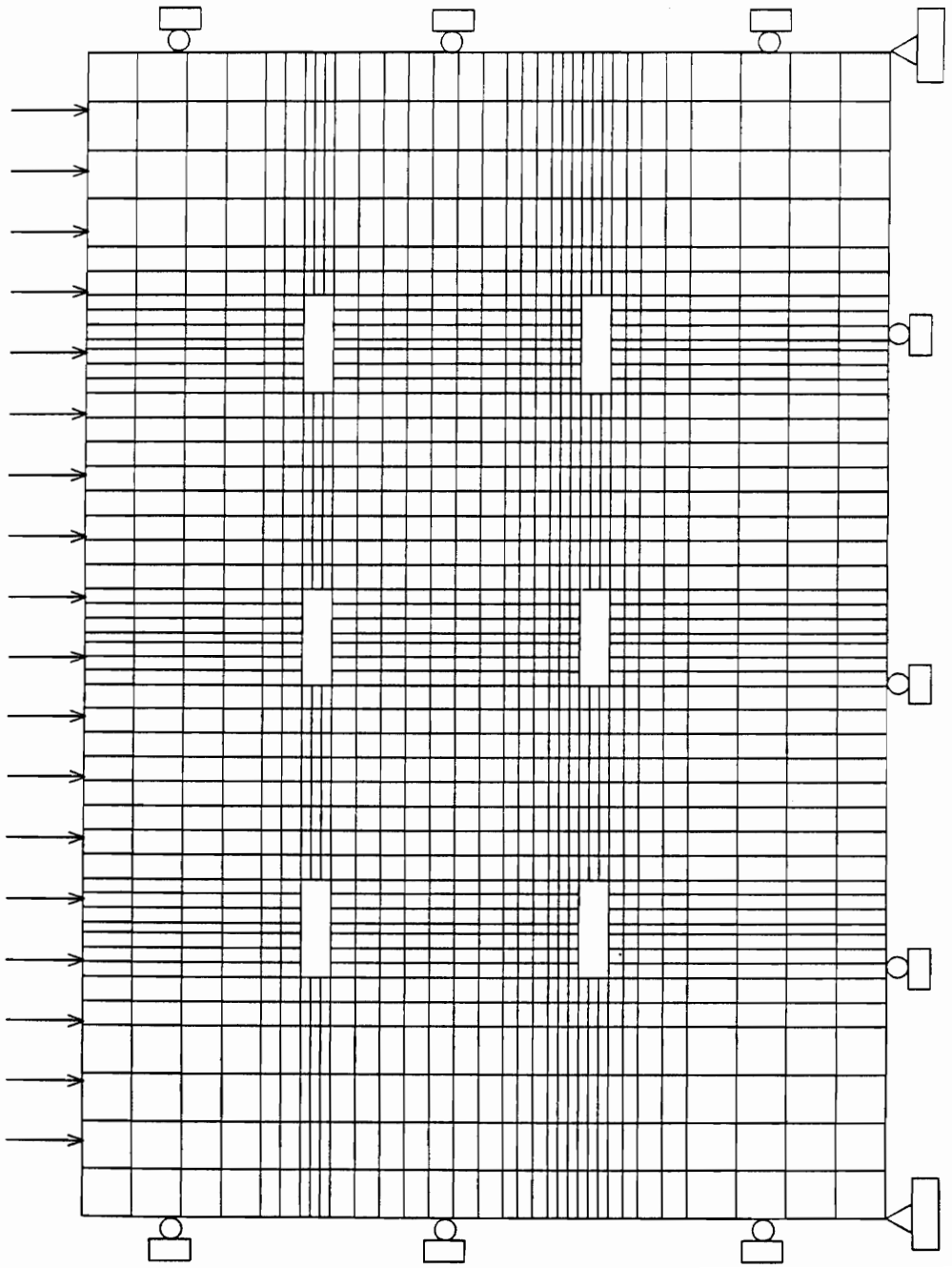

Figure 4.3 A typical finite element grid showing loading conditions and constraints

existing mesh generation file and asks the user to specify the type of constraints to be put on the side and top of the mesh. The two lower corner nodes are kept fixed whereas the rest of the nodes on the lower boundary are restricted in the vertical direction but allowed to move in the horizontal direction. From this input the program creates the necessary file containing the specified nodal displacement and / or forces on the outer boundary of the mesh. The program includes the option of specifying additional vertical stress on top of the mesh and excess horizontal stress on the sides. The vertical stress can be specified as a uniform load, a ramp load, a step load or a combination of any of these. With these options almost any loading condition can be modeled.

4.3.3 Simulating Mine Entries

There are two ways to simulate entries or any other mined-out area. The first is to model the mined-out area as a cavity (hole) and consider the nodes surrounding this surface as boundary nodes. The second approach is to model the whole area of interest as a solid area. The mesh is gravity loaded and then the mined-out area is specified in terms of cut elements. The finite element program reads the stress output from the gravity load run as initial stress and computes the new stresses and displacements as a result of mining specified by the cut elements. The second approach is preferred and used in this analysis because it allows any sequence of mining to be simulated with more flexibility.

If the area to be simulated is large, it can contain a fairly large number of elements, thus making the preparation of input information cumbersome and susceptible to error during data entery. To overcome this difficulty the program CUTELEM was written which generates a file containing the element numbers in the simulated cut. The input for this program includes the left top element number of the opening and the number of elements in the x and y directions in that opening. Any number of openings can be specified in a single run by repeating the above sequence.

4.4 FEM Output

The output from UTAH2PC is in the form of three separate files. One of these files contains the stress values (σ_x, σ_y σ_z τ_{xy}) and safety factors for each element. Another file contains the coordinates and forces for each node in the mesh. The third file contains the values of principal stresses for each element. These files along with the runstream file, node coordinate file, and element connectivity file (required to run UTAH2PC), are then used by an AutoLisp program to graphically plot the output in an AUTOCAD environment. AUTOCAD plots the modeled mesh showing a variety of information in different layers of the same drawing. These drawing layers include the mesh showing various material layers in different colors, the nodal displacements in the vector form, the element stress trajectories, and the safety factors. The safety factors can be viewed as numbers or in solid color codes. Figures 4.4 and 4.5 show three different layers of a typical AUTOCAD drawing prepared from one of the UTAH2 runs from this study.

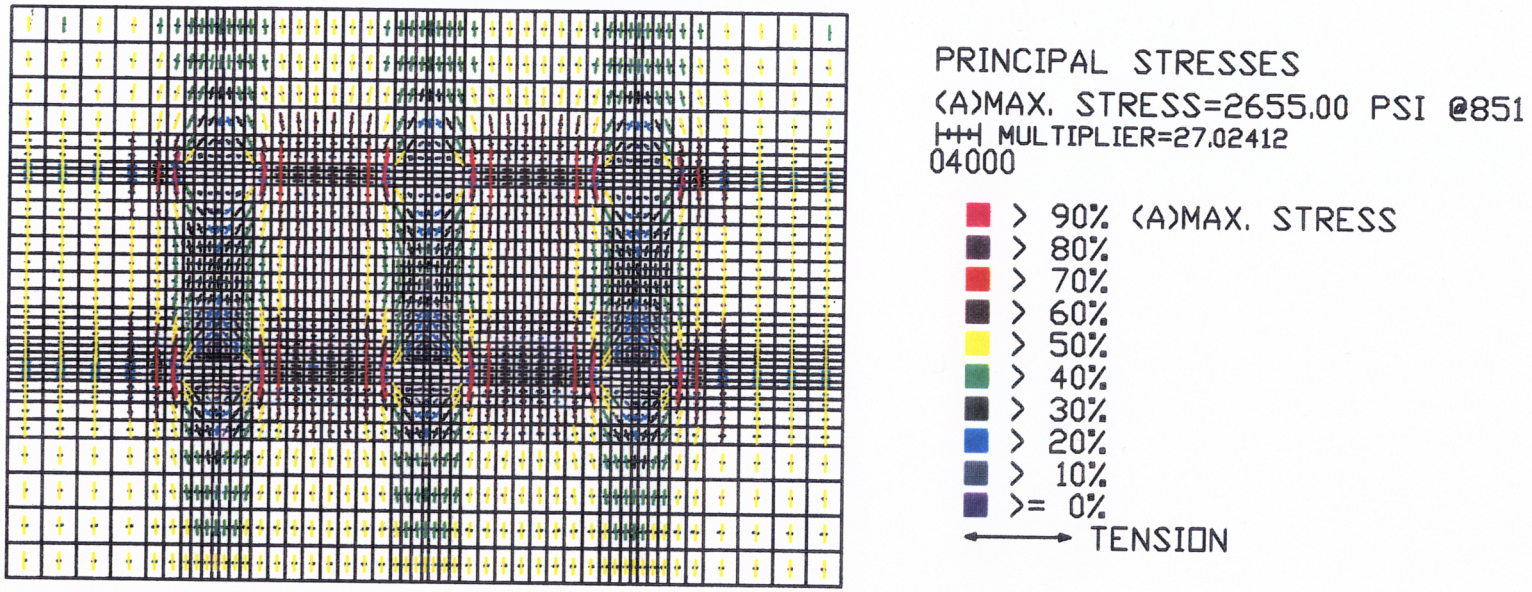

Figure 4.4 A typical plot showing stress trajectories

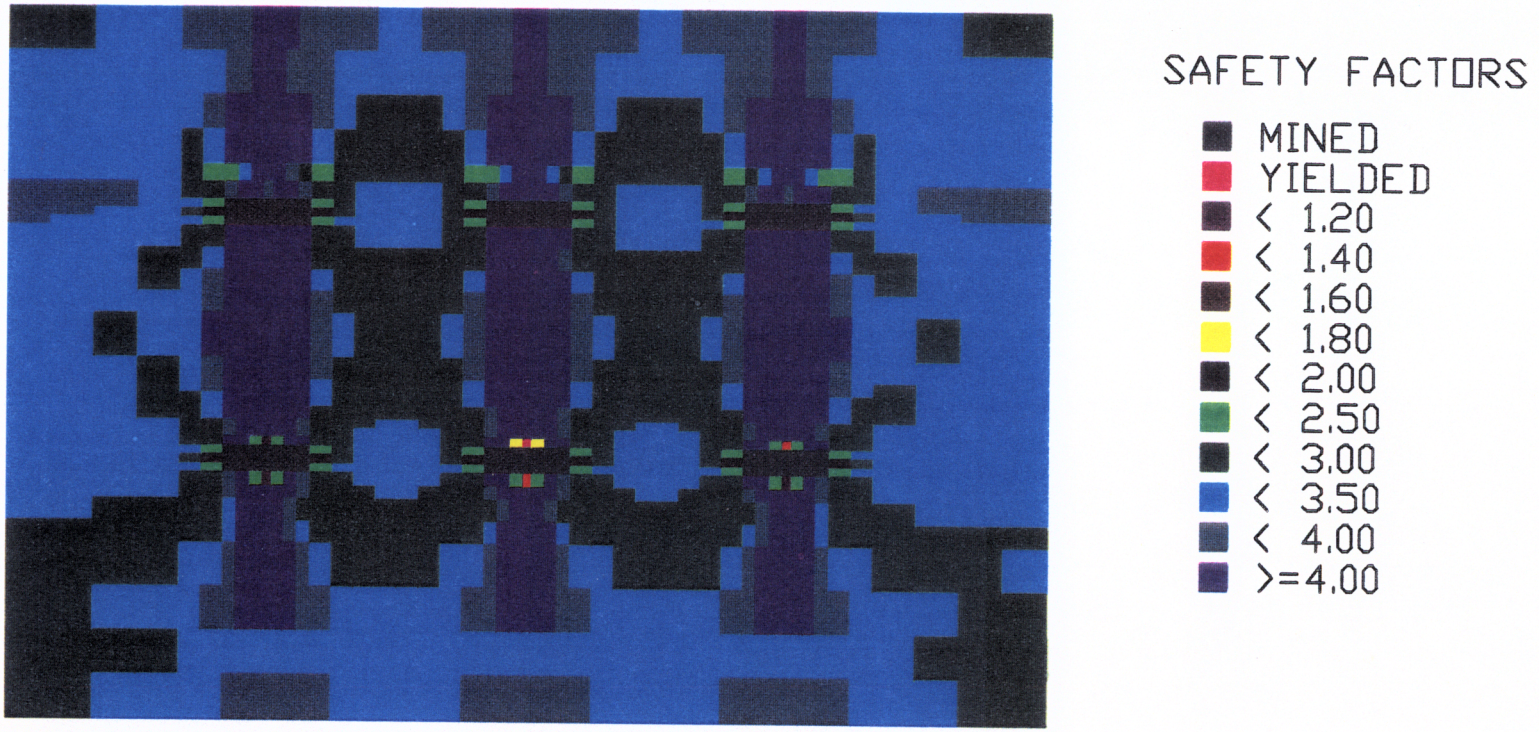

Figure 4.5 An AUTOCAD plot showing safety factors in solid colors

Although the graphic output from AUTOCAD in the form of stress trajectories, displacement vectors and safety factors looks impressive, it became evident at the early stages of this study that it is difficult to quantify the observed ground control effects by viewing a series of stress trajectories or displacements. The alternate was to plot the contours of the desired parameters using a contouring package such as SURFER. Figure 4.6 shows one such plot obtained from one of the Finite Element Modeling (FEM) runs. In this case also, it became clear that it would not be possible to develop any quantitative relationships from a series of contour plots obtained from different FEM runs. It was therefore decided to selectively extract the data only for those elements which are in the immediate roof of the entry of interest, as indicated previously in Figure 4.1.

This data extraction from the UTAH2PC output files was done using EXCEL, a WINDOWS spreadsheet. The results were then plotted using graphing software. Although the output from UTAH2PC runs contains information regarding stresses, displacements and safety factors, it was decided to use safety factor values as an index of stability because they reflect the state of stress and the material behavior in one number.

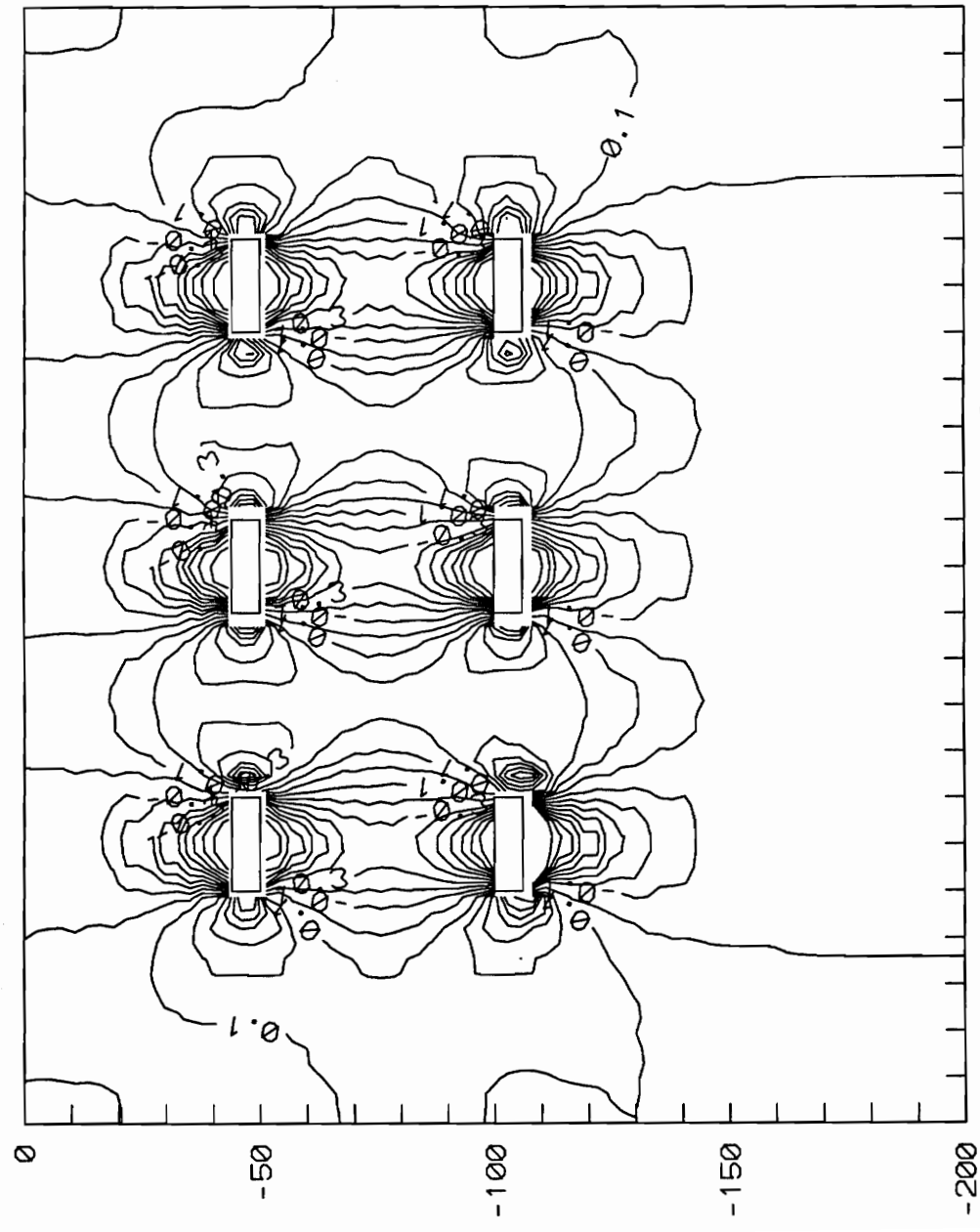

Figure 4.6 A SURFER plot showing percent stress change due to mining in two seams

Chapter 5

FEM Results and Stability Assessment

5.1 General

A range of loading conditions and innerburden lithology was modeled to evaluate their effects on the stability of lower seam entry roofs. The conditions modeled in the finite element analysis are explained in Section 4.2 (Figures 4.1 and 4.2). External loading conditions were simulated by incorporating different overburden depths as additional load on the top boundary of finite element mesh. The horizontal stress due to the prevalent vertical load and lateral confinement is calculated by the program based on the input values of Poisson's ratio, modulus of elasticity and overburden depth. The excess horizontal stress, if any, was specified as additional lateral load on the side boundaries of the mesh. The non-uniform load due to changing topography was simulated in the form of a variable load on the top boundary. The effect of unsymmetric loading encountered in multi-seam conditions was evaluated by changing the relative position of pillars in the two interacting seams. The influence of innerburden lithology was studied in terms of sandstone percentage and its location in the immediate roof. To

compare the finite element analyses results with the field conditions, data from 20 multi-seam cases were collected and analyzed to establish a correlation between the stress levels at the lower seam horizon with the observed entry roof conditions. Based on FEM results and the case study data, a comprehensive model was developed for the stability assessment of entry roofs for any given set of conditions for underlying multiple seam mines. This chapter describes FEM results, case study data, and the roof stability assessment model developed from these results.

5.2 Geologic Conditions

The influence of innerburden geology and depth was investigated in terms of lower seam entry roof stability for a number of combinations of sandstone and shale. Ten distinct innerburden lithologic conditions were evaluated, each for seven overburden depths. The lithologic sequences analyzed in this study were:

1) 100 percent shale in the innerburden
2) 40 percent of the innerburden is sandstone located in the top portion, the immediate roof of lower seam entries is of shale
3) 60 percent of the innerburden is sandstone located in the top portion, the immediate roof of lower seam entries is of shale
4) 80 percent of the innerburden is sandstone located in the top portion, the immediate roof of lower seam entries is of shale
5) 90 percent of the innerburden is sandstone in the top portion, the immediate roof of lower seam entries is of shale
6) 100 percent sandstone in the innerburden

7) 10 percent of the innerburden is sandstone, located in the immediate roof of lower seam entry
8) 20 percent of the innerburden is sandstone, located in the immediate roof of lower seam entry
9) 40 percent of the innerburden is sandstone, located in the immediate roof of lower seam entry
10) 60 percent of the innerburden is sandstone, located in the immediate roof of lower seam entry.

Each of these ten cases was analyzed for overburden depths of 300, 500, 700, 900, 1100, 1300, and 1500 feet. For each of these 70 combinations, at least three finite element analyses were required. First the mesh was gravity loaded (no cuts), this provided the input stresses for the subsequent run. The second run simulated mining in the upper seam thus providing stresses for the third run which simulated entries in the lower seam. The output from the final FEM run for each case was used to quantify the effects of geology and overburden depths. These effects were plotted in terms of safety factors across the lower seam entry roof. The critical location across the entry roof in a given set of conditions was either the entry corner or center of the span. The safety plots showed the dependence of this location on overburden depth and roof lithology. To see which one is the controlling location for a given set of conditions, the safety factors were plotted for various depths for each of the modeled roof lithologies.

Figures 5.1 through 5.5 show the safety factors for the cases where the immediate roof is of shale overlain by sandstone beds. As is evident from these plots, the change in safety factors is negligible when the sandstone

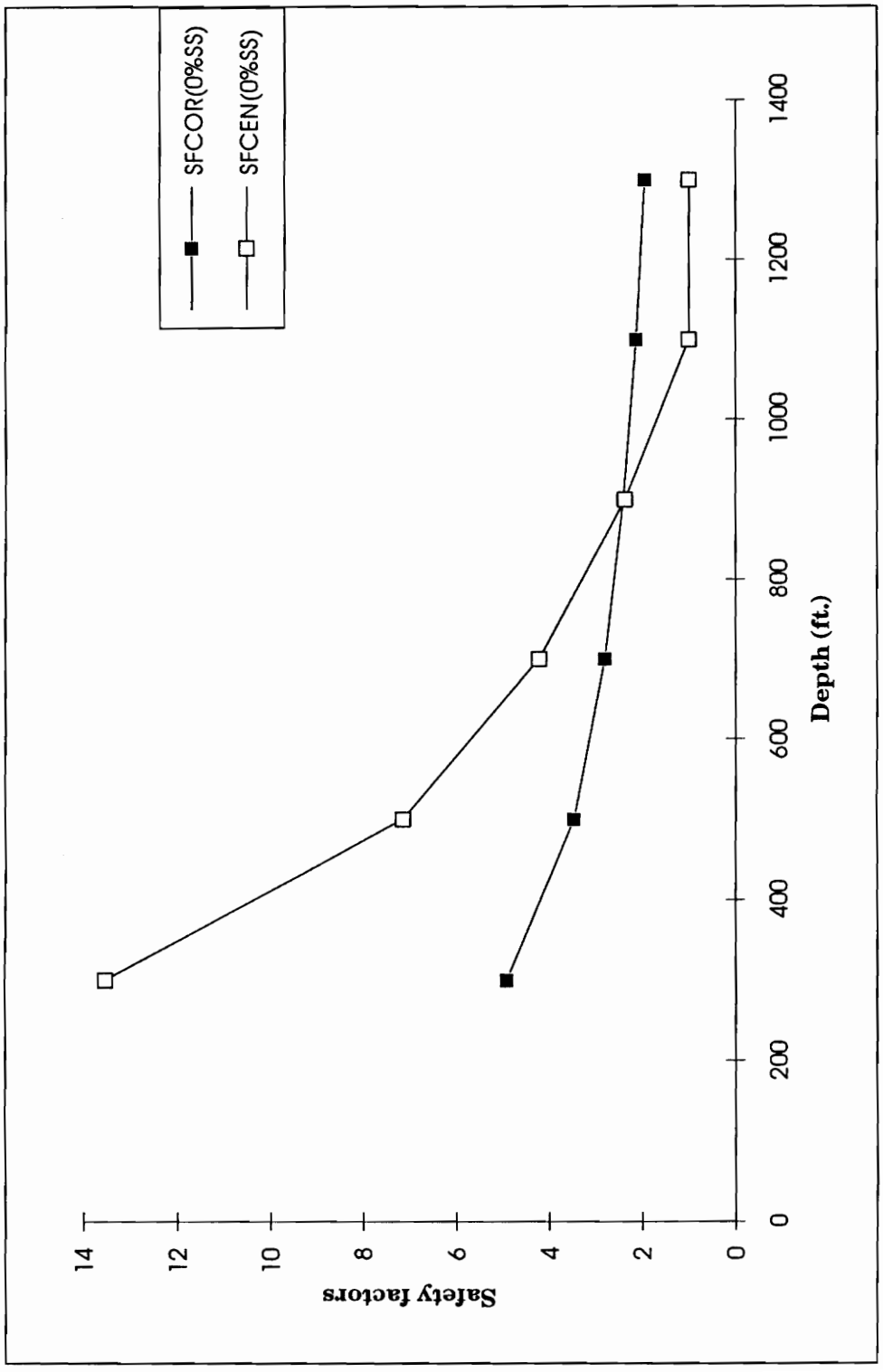

Figure 5.1 Effect of depth on entry stability for shale roof

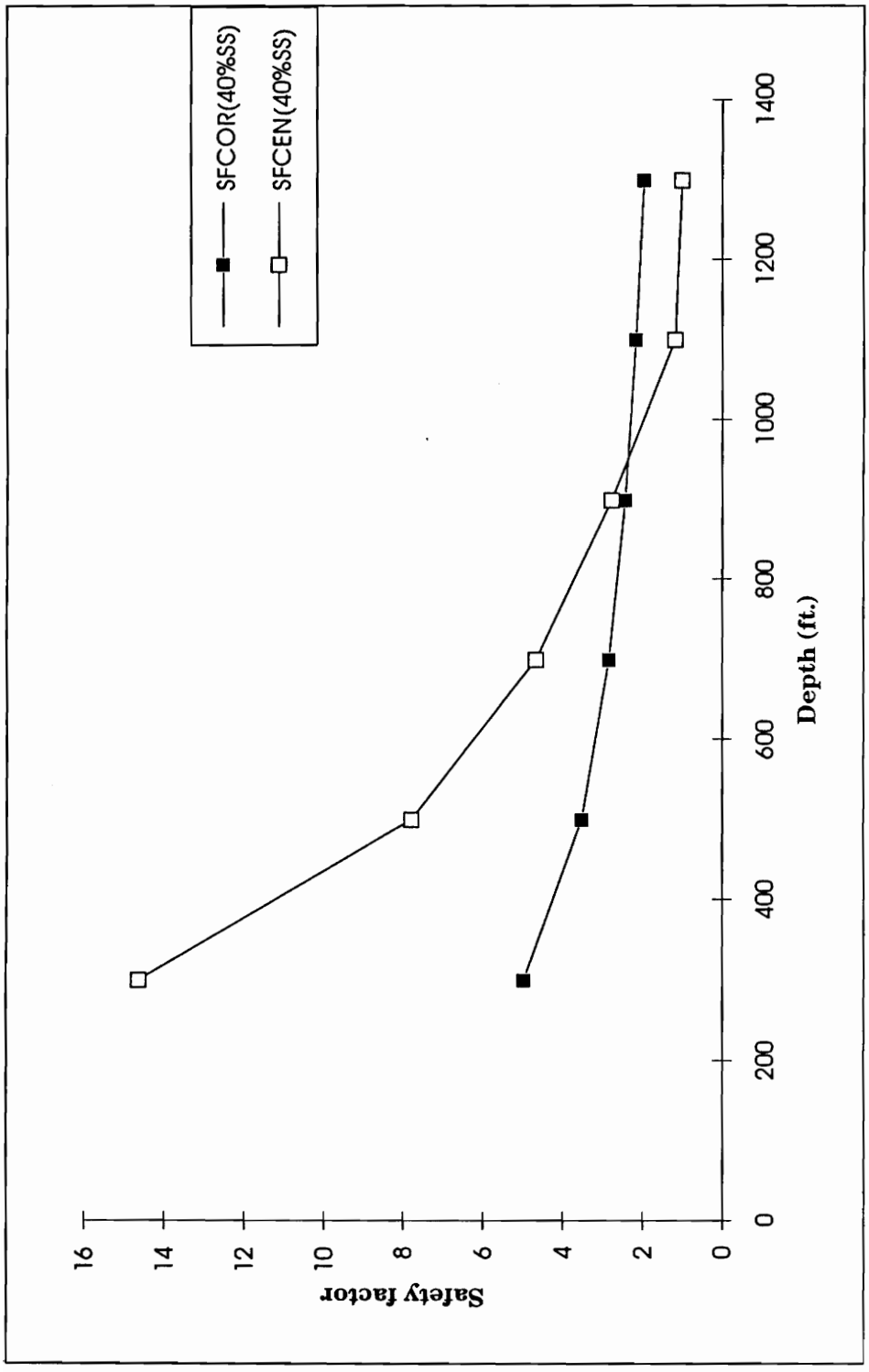

Figure 5.2 Effect of depth on entry stability for 40 percent sandstone in the top of innerburden

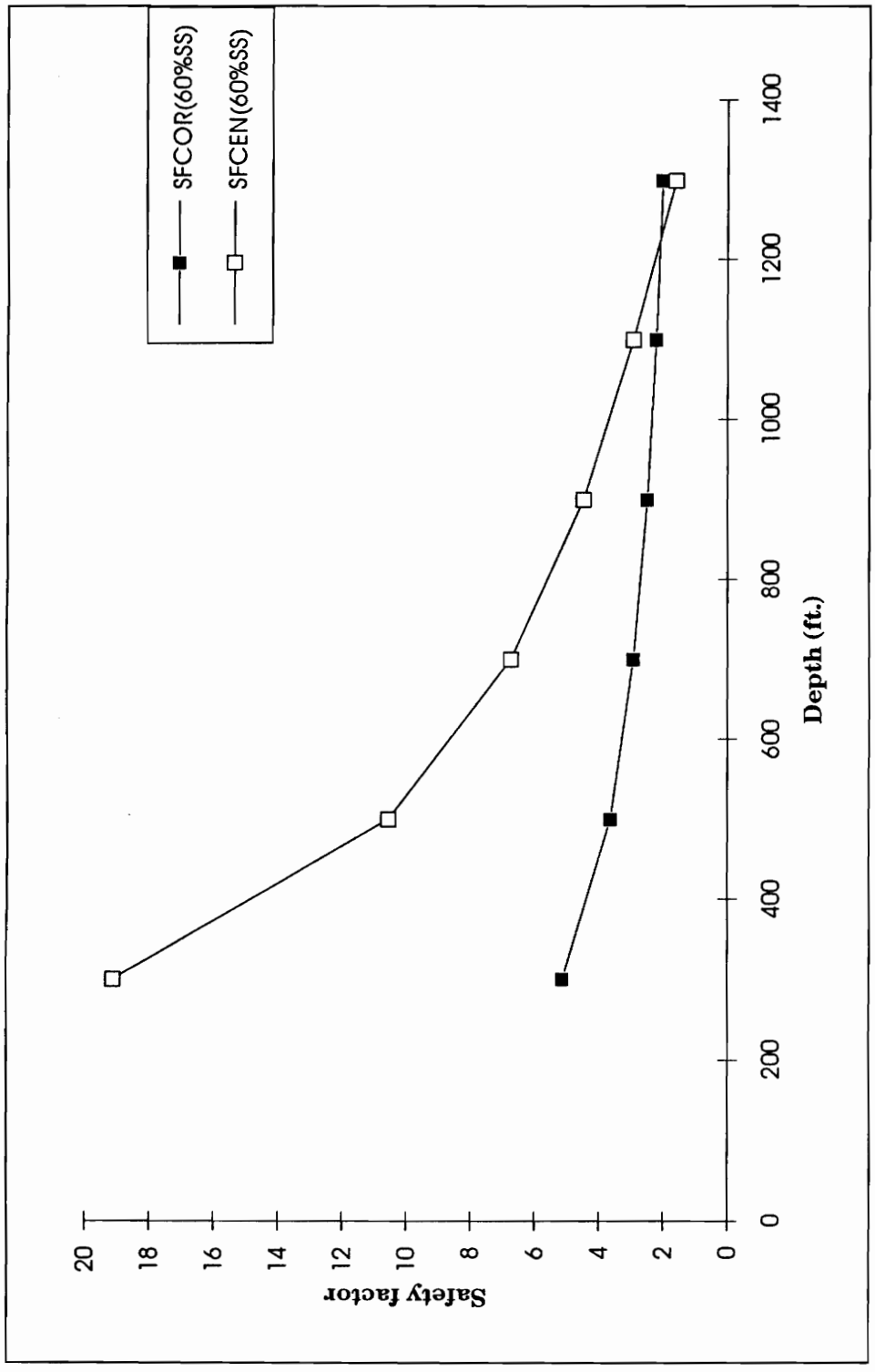

Figure 5.3 Effect of depth on entry stability for 60 percent sandstone at the top of innerburden

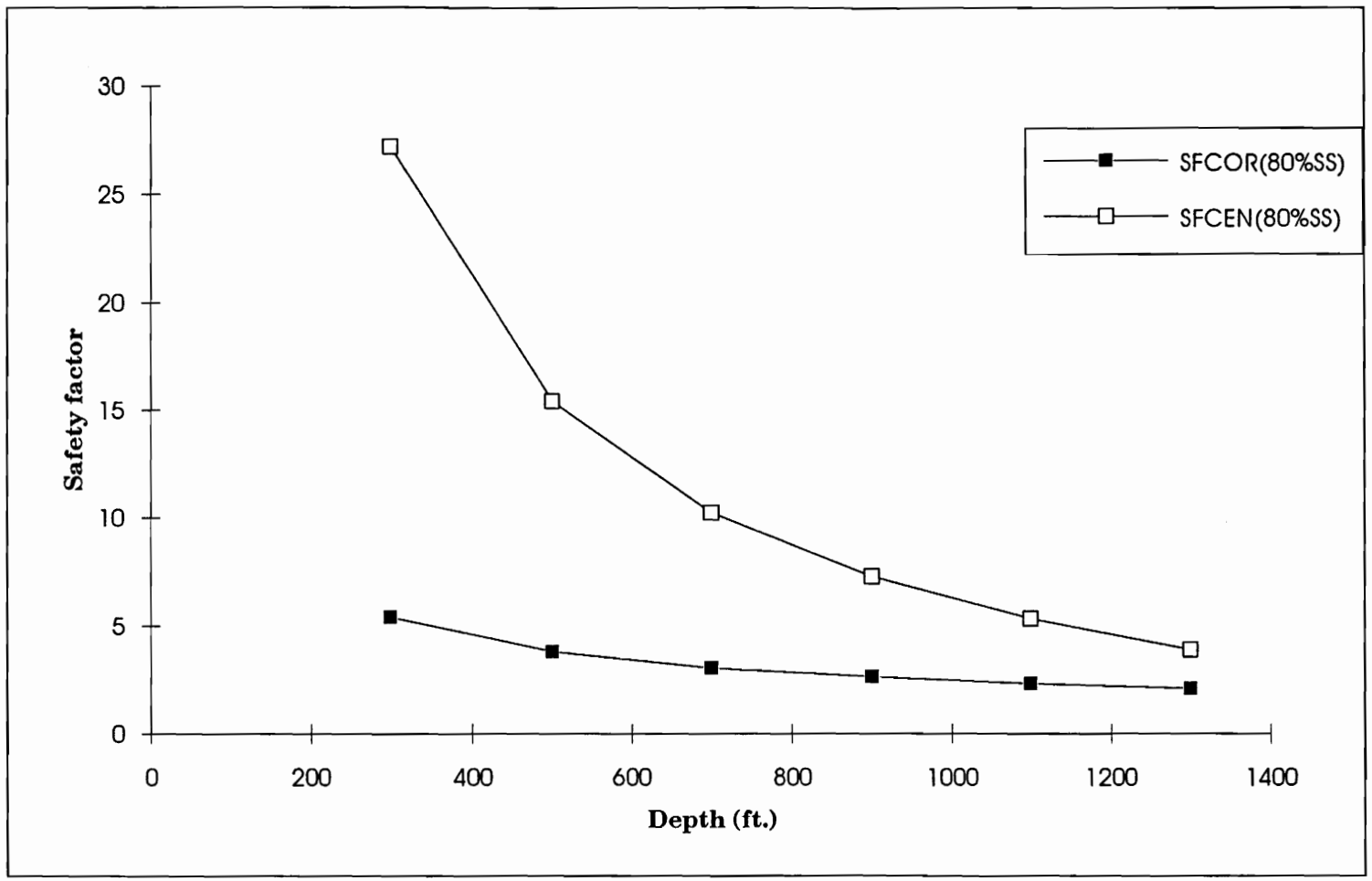

Figure 5.4 Effect of depth on entry stability for 80 percent sandstone in the top portion of innerburden

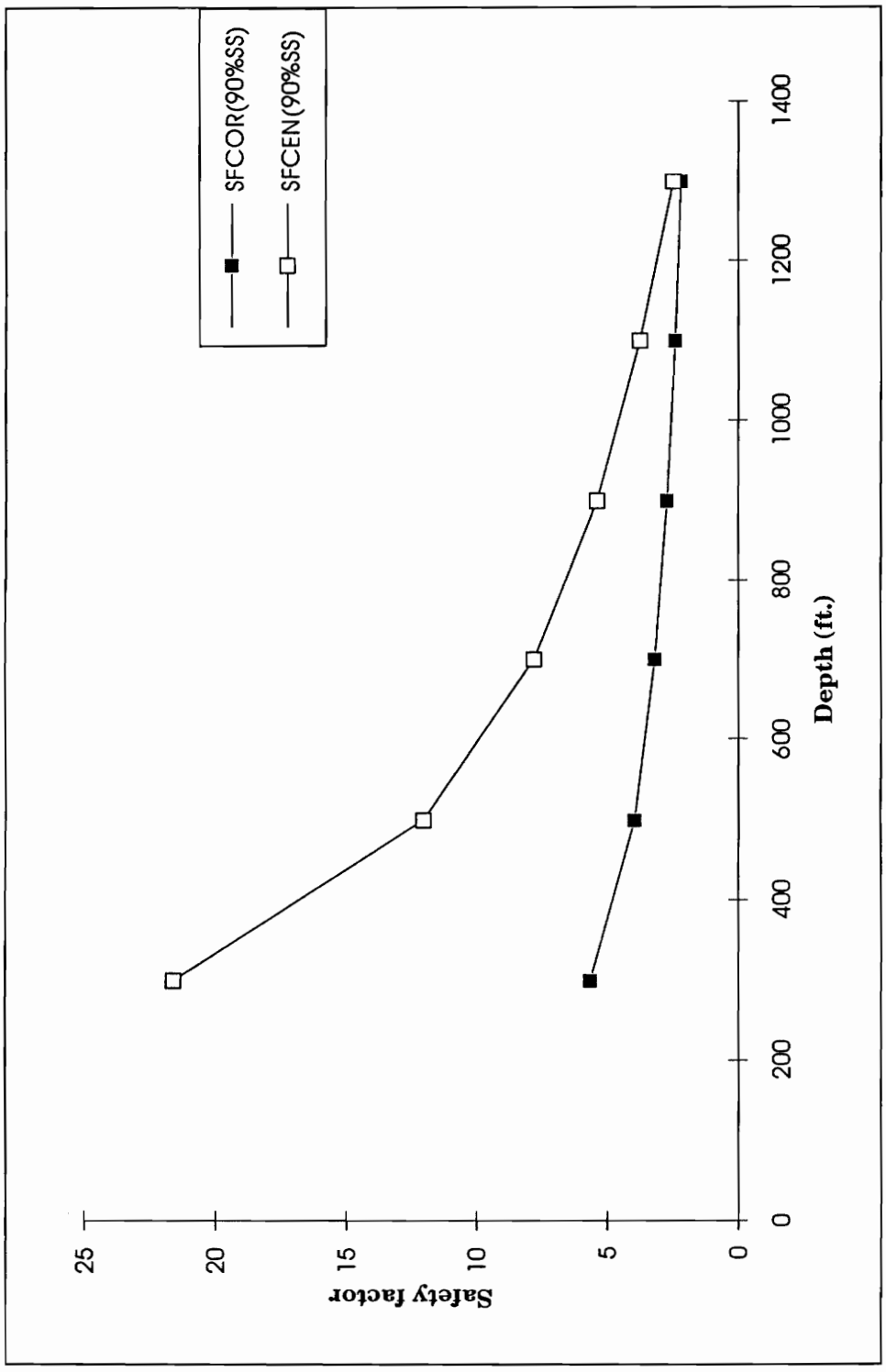

Figure 5.5 Effect of depth on entry stability for 90 percent sandstone in the top portion of innerburden

thickness is increased from 0 to 40 percent. For these two cases, shear at entry corner is the controlling failure mechanism up to an overburden depth of 900 feet, beyond which tensile failure at mid-span becomes the controlling mechanism. Further increase in the thickness of sandstone (60, 80 and 90 percent) greatly improves the entry stability against tensile failure at the mid-span. The entry corner, however, becomes the critical location for these cases for the whole range of overburden depth. The improvement in stability against shear failure, with the increase in sandstone percentage in this sequence, is not substantial when compared to improvement in stability against tensile failure.

To quantify the effect of roof lithology and overburden depths on entry roofs, a curve fitting routine in DELTAGRAPH, a WINDOWS program, was used to obtain empirical equations for each of the curves described above. The following ten equations correspond to curves shown in Figures 5.1 through 5.5. The first set of five equations computes the corner safety factors for lower seam entry roofs, while the second set of equations is for mid-span safety factors.

$$f(x) = 180.0470\ [x^{-0.6338}] \qquad 5.1$$

$$f(x) = 183.6946\ [x^{-0.6349}] \qquad 5.2$$

$$f(x) = 190.3334\ [x^{-0.6354}] \qquad 5.3$$

$$f(x) = 210.2677\ [x^{-0.6641}] \qquad 5.4$$

$$f(x) = 228.3955\ [x^{-0.6505}] \qquad 5.5$$

The variable x in the above equations is overburden depth expressed in feet, f(x) is the corner safety factor of lower seam entry roof. Equations 5.1, 5.2, 5.3, 5.4 and 5.5 correspond to 0 %, 40 %, 60 %, 80 % and 90 % innerburden sandstone respectively.

$$f(x) = 29.3030\ [e^{-0.00279}] \qquad 5.6$$

$$f(x) = 32.7350\ [e^{-0.00281}] \qquad 5.7$$

$$f(x) = 36.8587\ [e^{-0.00237}] \qquad 5.8$$

$$f(x) = 40.3728\ [e^{-0.00189}] \qquad 5.9$$

$$f(x) = 36.6910\ [e^{-0.00210}] \qquad 5.10$$

f(x) in these equations is the safety factor at midspan of the lower seam entry roofs, corresponding to the five innerburden lithologies (0 %, 40 %, 60 %, 80 % and 90 % innerburden sandstone).

Figures 5.6 through 5.10 are safety factor plots for the cases where the immediate roof is sandstone, its thickness being different in each case. For the cases where the sandstone is 10 and 20 percent of the innerburden in the immediate roof, tensile failure is the dominant mode of failure. No noticeable improvement in stability is achieved when sandstone is increased from 10 to 20 percent. However, further increase in sandstone percentage (20 to 40 to

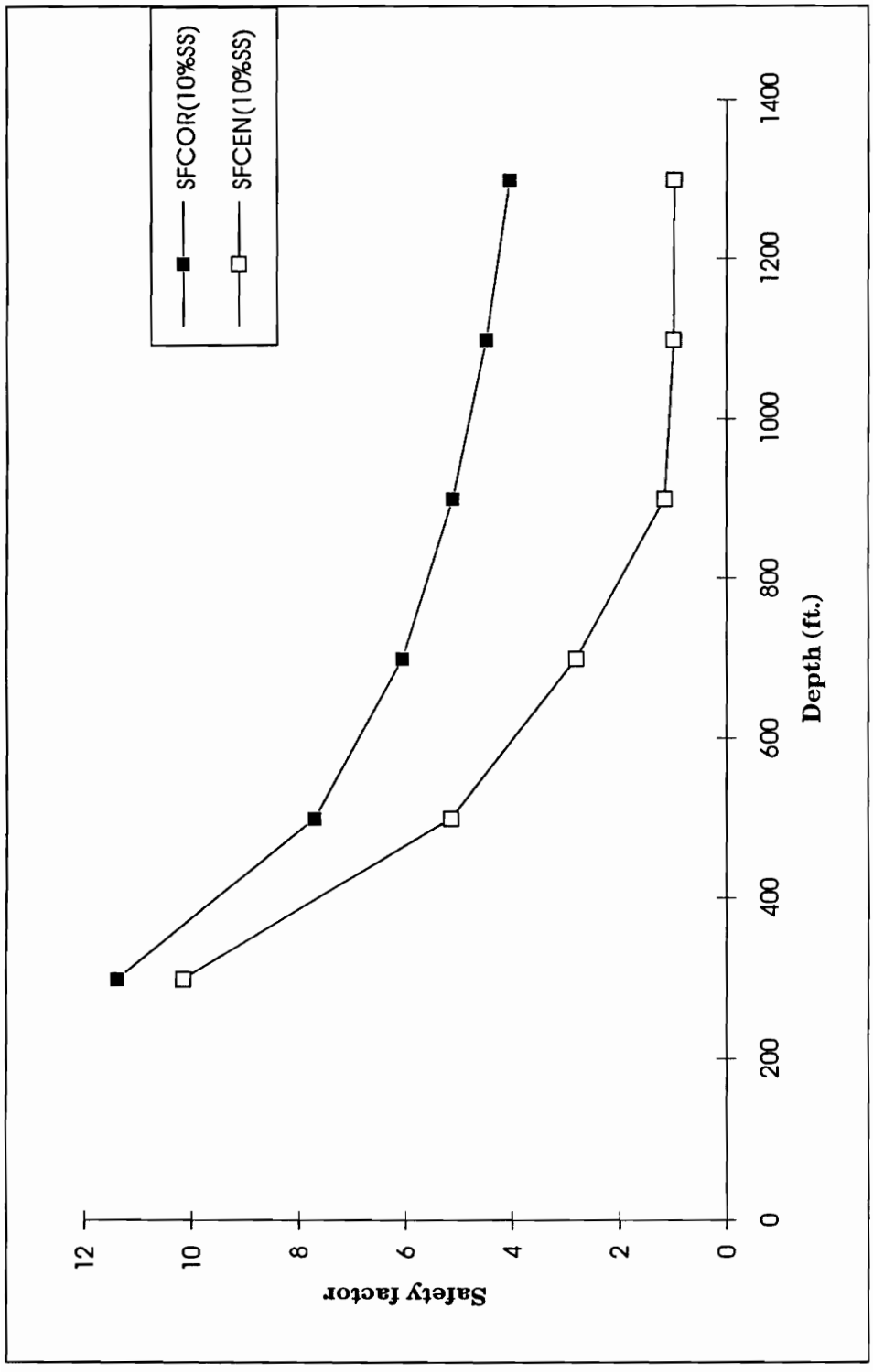

Figure 5.6 Effect of depth on entry stability for 10 percent sandstone in the bottom of innerburden

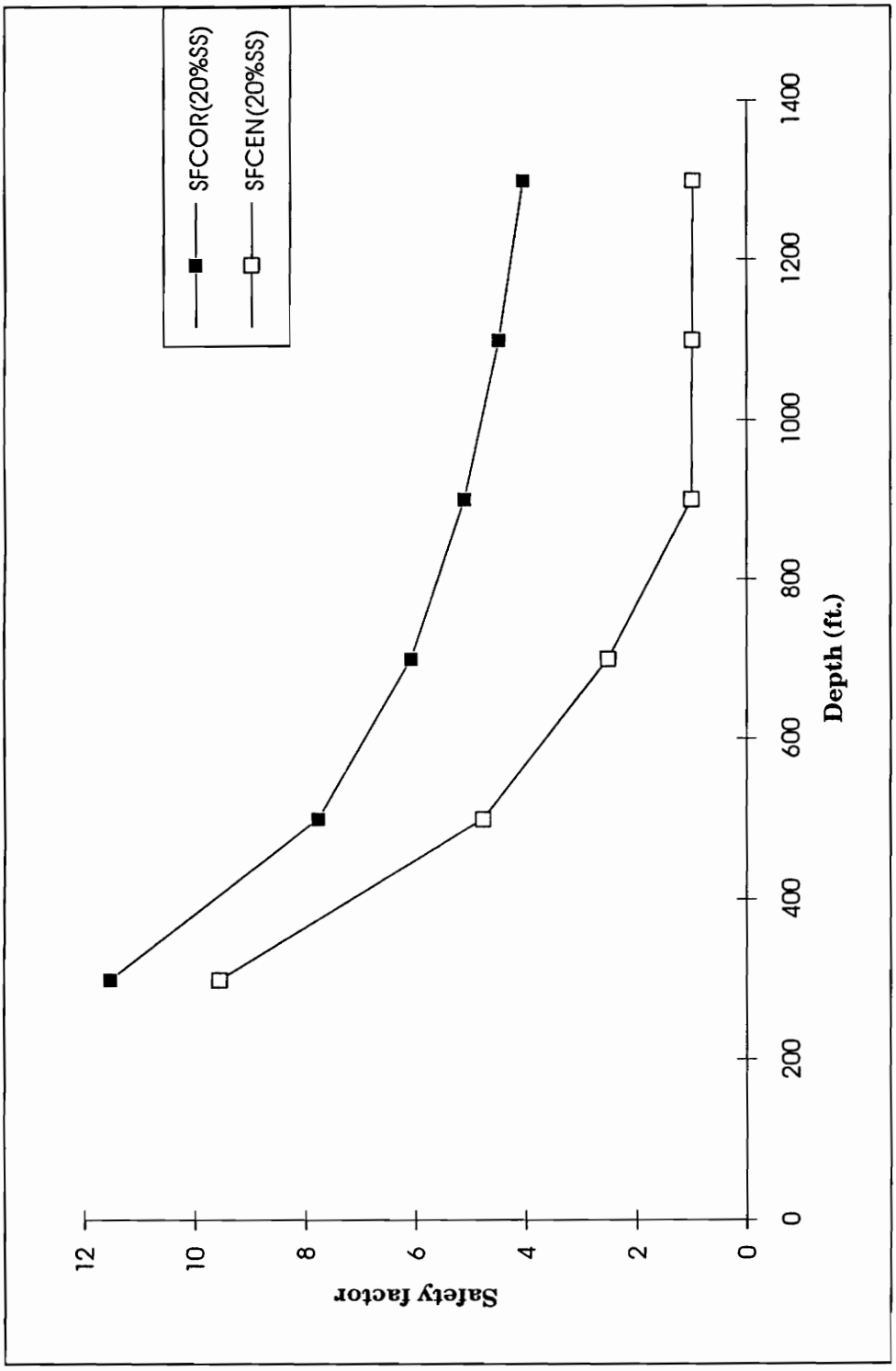

Figure 5.7 Effect of depth on entry stability for 20 percent sandstone in the bottom of innerburden

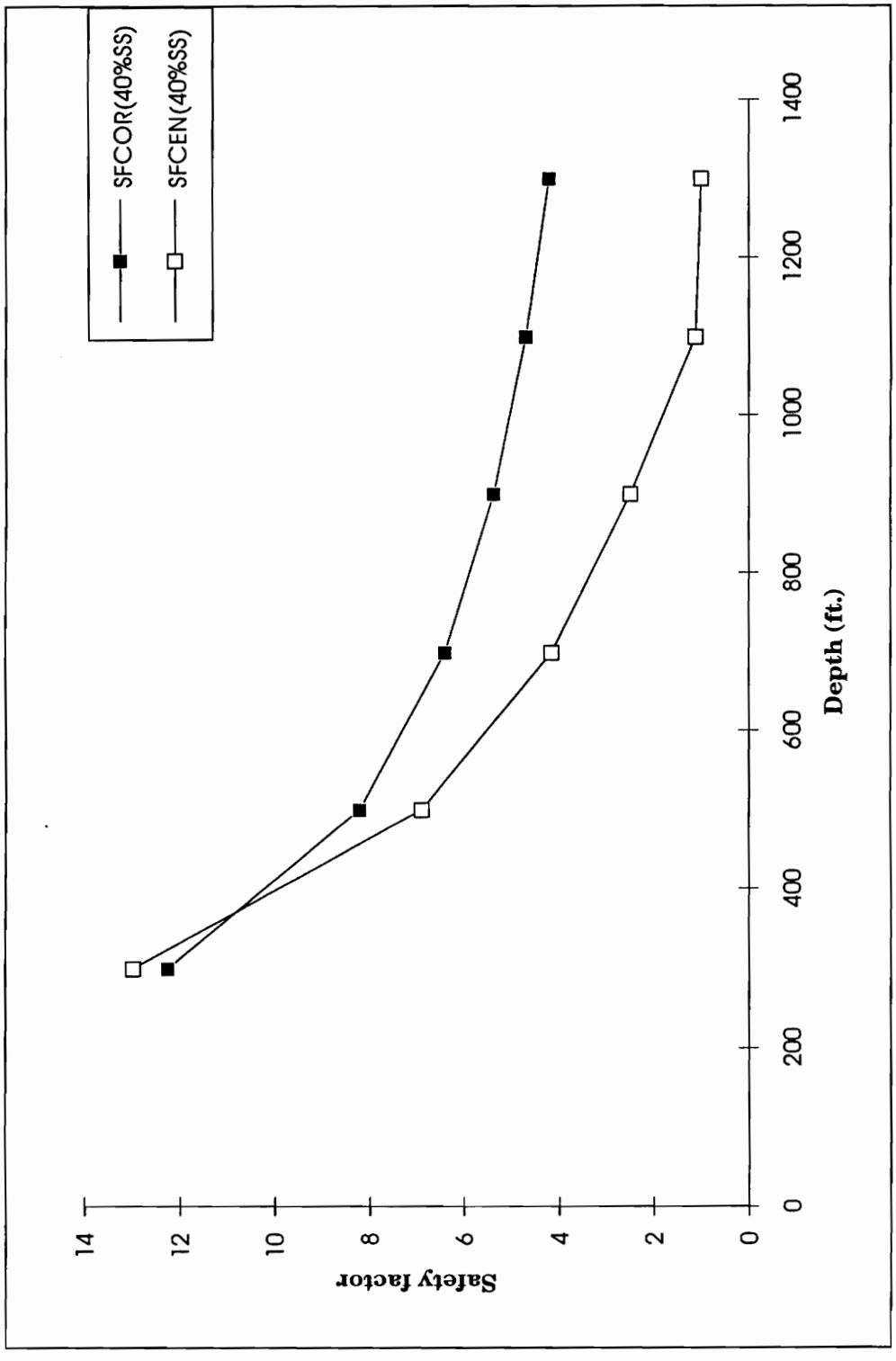

Figure 5.8 Effect of depth on entry stability for 40 percent sandstone in the bottom portion of innerburden

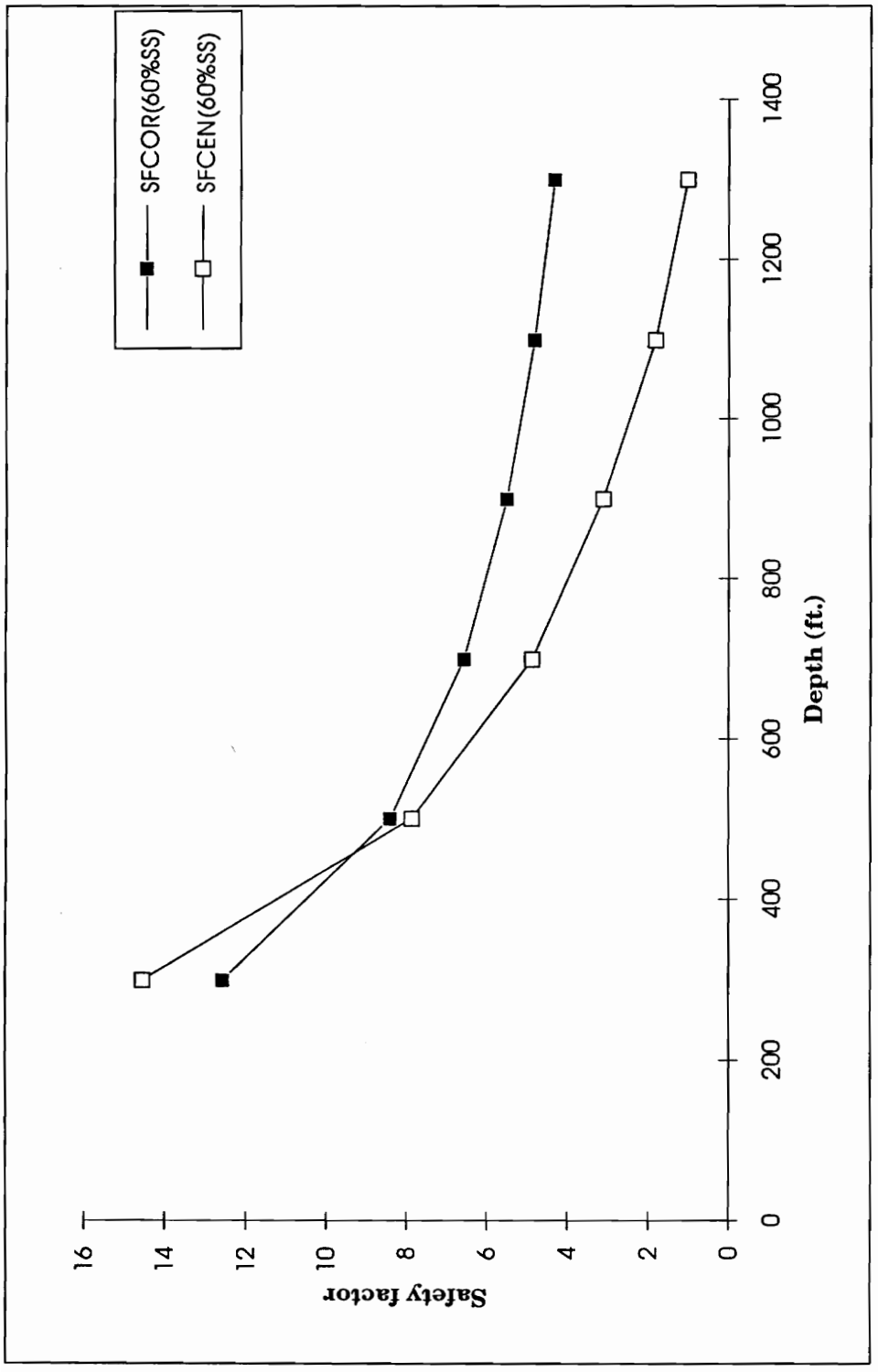

Figure 5.9 Effect of depth on entry stability for 60 percent sandstone in the bottom portion of innerburden

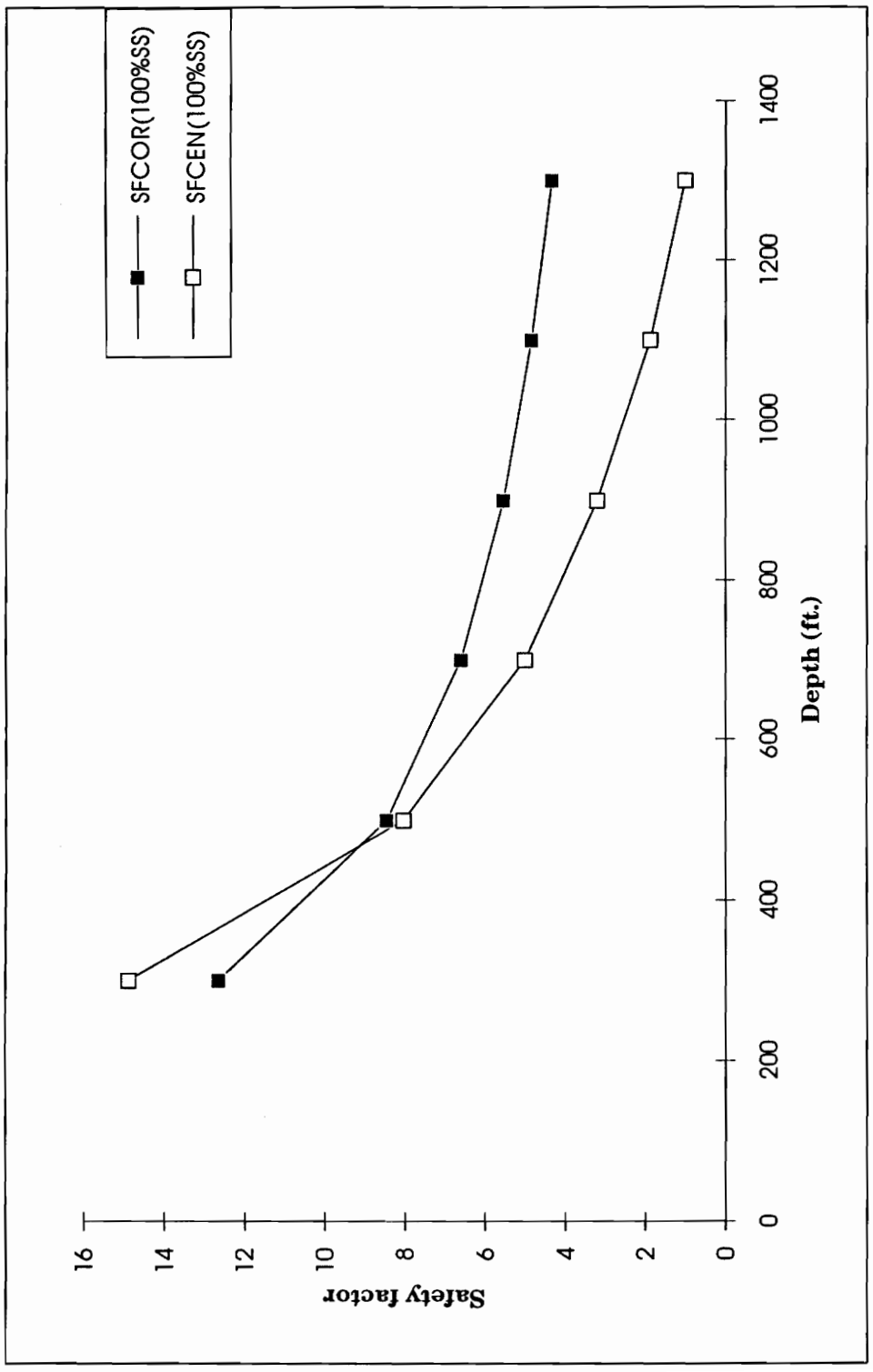

Figure 5.10 Effect of depth on entry stability for sandstone roof

60 percent) greatly improves the stability. The depth at which yielding of the roof rock can occur is increased from 900 to 1100 to 1300 feet with increasing sandstone percentage. To quantify the changes in safety factors observed for various lithologies and overburden depths, empirical equations were obtained for each of the plots shown in Figures 5.5 through 5.10. The following set of five equations gives roof corner safety factors for five different innerburden lithologies.

$$f(x) = 628.1300\ [x^{-0.7061}] \qquad 5.11$$

$$f(x) = 673.7060\ [x^{-0.7162}] \qquad 5.12$$

$$f(x) = 768.4770\ [x^{-0.7285}] \qquad 5.13$$

$$f(x) = 789\ 8660[x^{-0.7289}] \qquad 5.14$$

$$f(x) = 803.5670\ [x^{-0.7307}] \qquad 5.15$$

The equations 5.11 through 5.15 give roof corner safety factors for 10%, 20%, 40%, 60%, and 100 % innerburden sandstone, this sandstone being in the immediate roof. The next set of five equations computes safety factors at the entry roof midspan.

$$f(x) = 17.3380\ [e^{-0.002504}] \qquad 5.16$$

$$f(x) = 15.3340\ [e^{-0.002430}] \qquad 5.17$$

$$f(x) = 27.3260\ [e^{-0.002691}] \qquad 5.18$$

$$f(x) = 30.7780\ [e^{-0.002608}] \qquad 5.19$$

$$f(x) = 31.6727\ [e^{-0.002615}] \qquad 5.20$$

The above equations correspond to 10%, 20%, 40%, 60% and 90 % innerburden sandstone in the immediate roof.

To compare all the cases covered above, the results were divided into two separate groups each containing two subgroups:

1) roof center safety factors
    a) shale in the immediate roof
    b) sandstone in the immediate roof
2) roof corner safety factors
    a) shale in the immediate roof
    b) sandstone in the immediate roof.

The plots for these four categories of results are shown in Figures 5.11 through 5.14. Figure 5.11 summarizes the safety factor plots at the entry midspan for all the cases in which the immediate roof is of shale. For the other sequence (where the immediate roof is of sandstone), results are summarized in Figure 5.12. The safety factor plots for the entry corners in these two sequences are shown in Figures 5.13 and 5.14. Figures 5.15 and 5.16 give a three-dimensional representation of the results for the two sequences using different sandstone percentages and overburden depths.

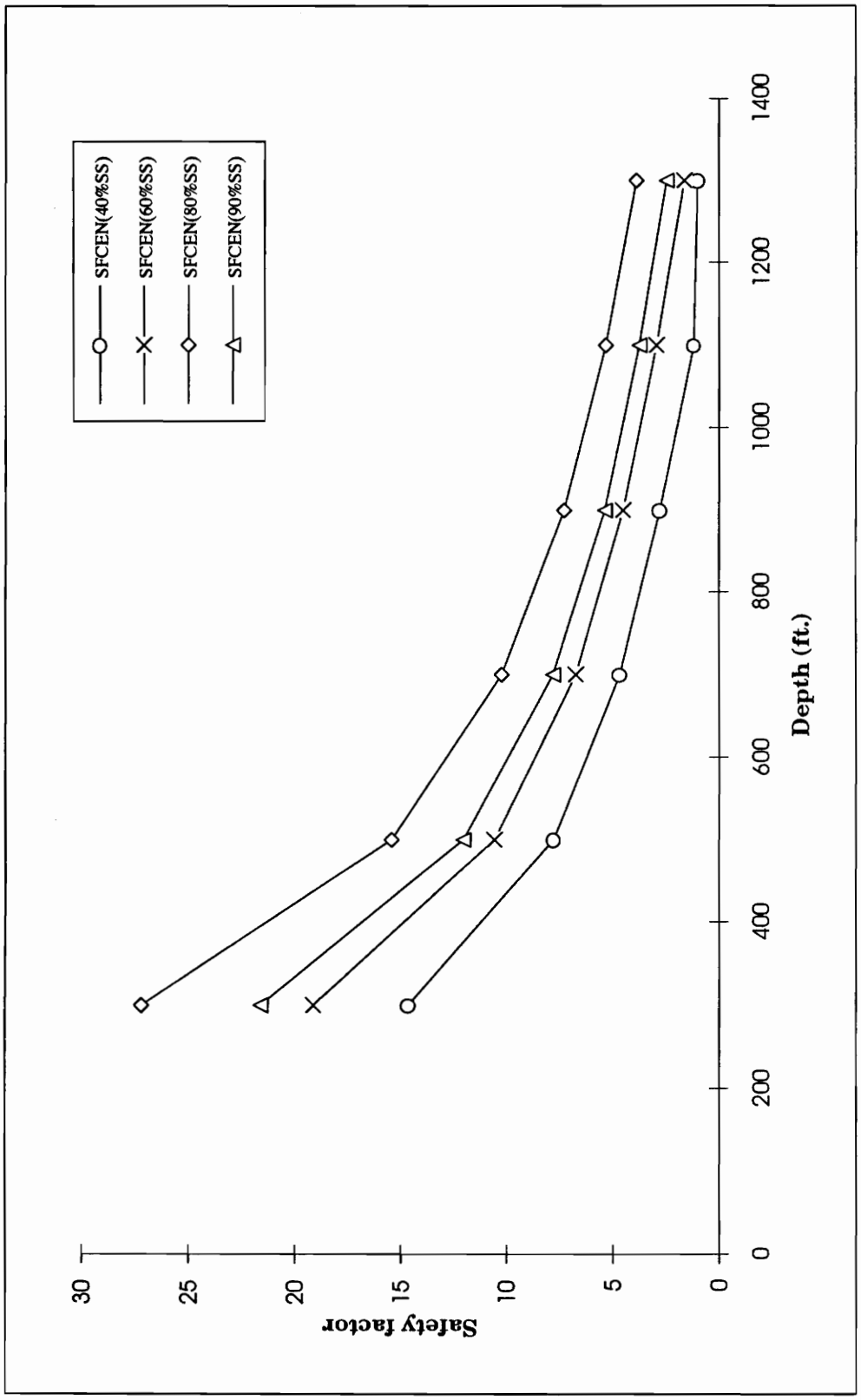

Figure 5.11 Effect of hardrock increase on the entry center stability (top to bottom increase)

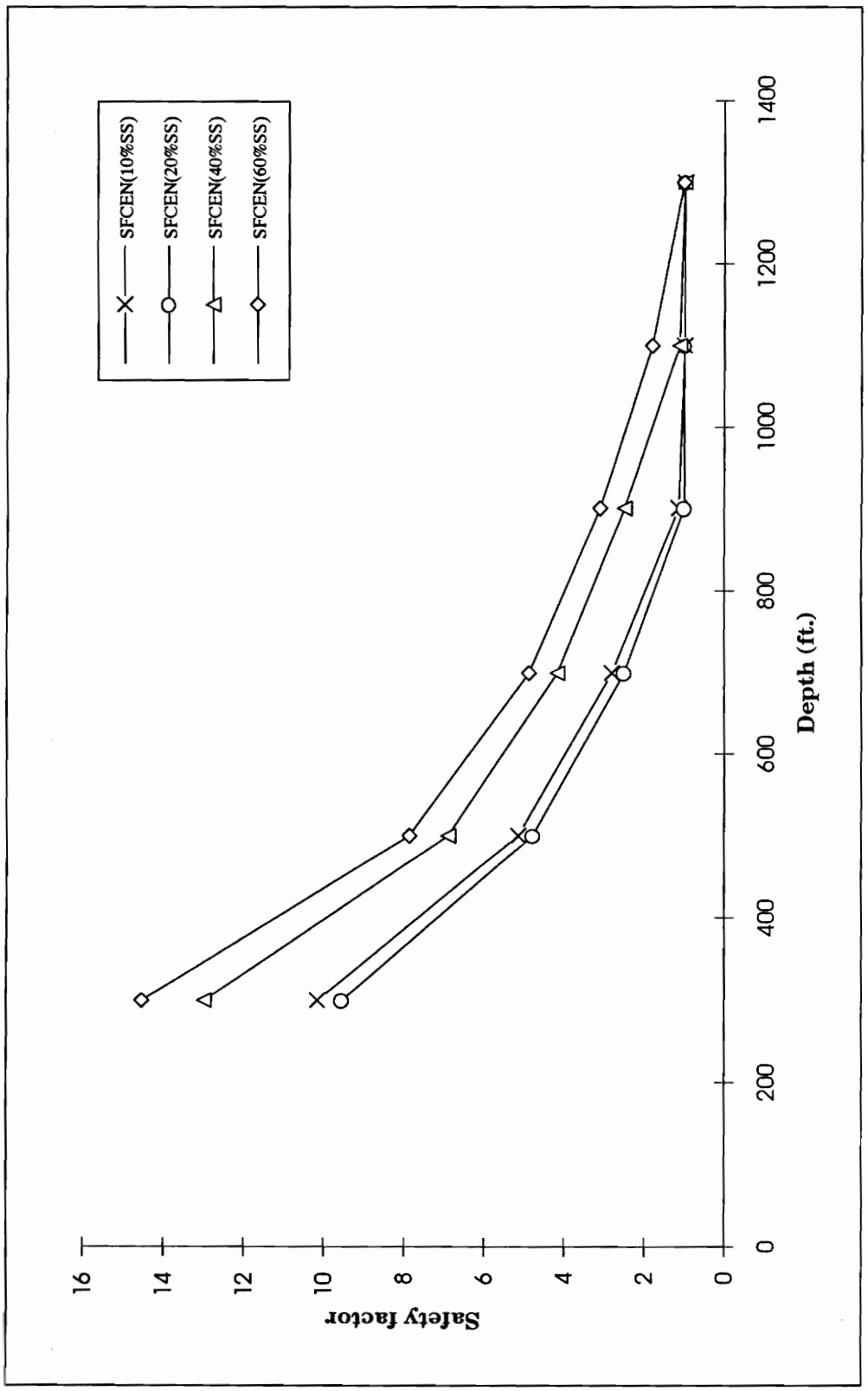

Figure 5.12 Effect of hardrock increase on the entry center stability (bottom to top increase)

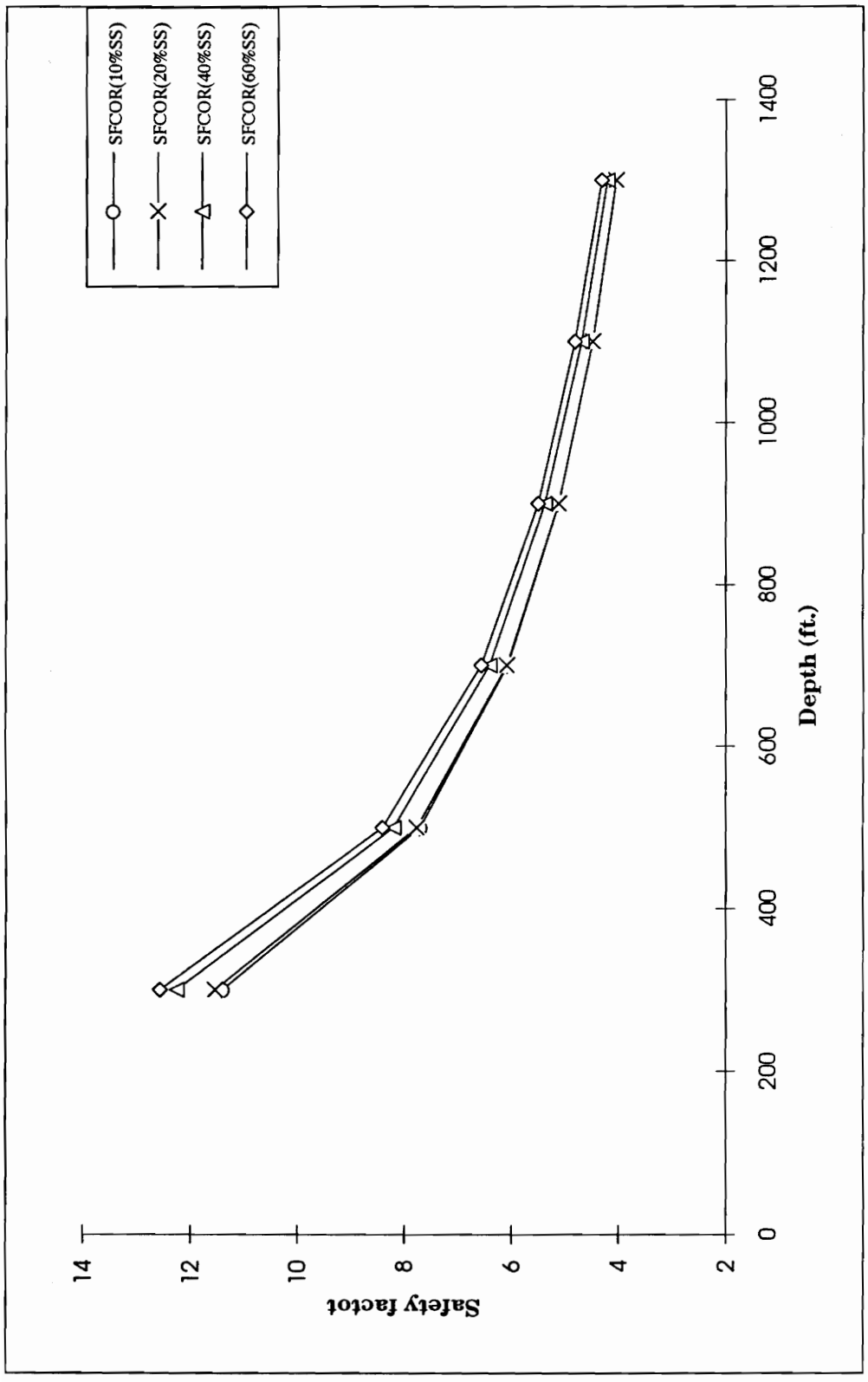

Figure 5.13 Effect of hardrock increase on the entry corner stability (bottom to top increase)

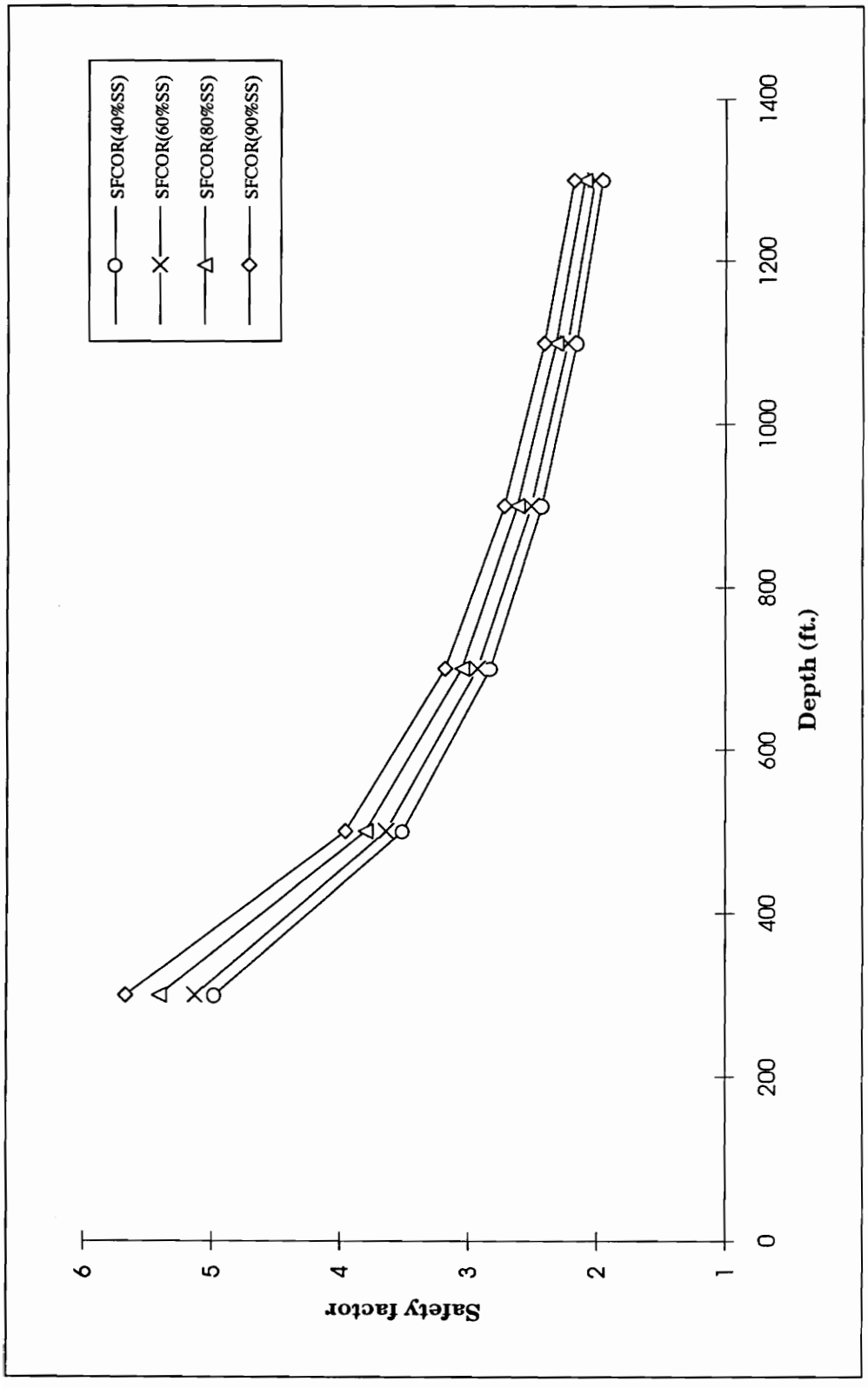

Figure 5.14 Effect of hardrock increase on the entry corner stability (top to bottom increase)

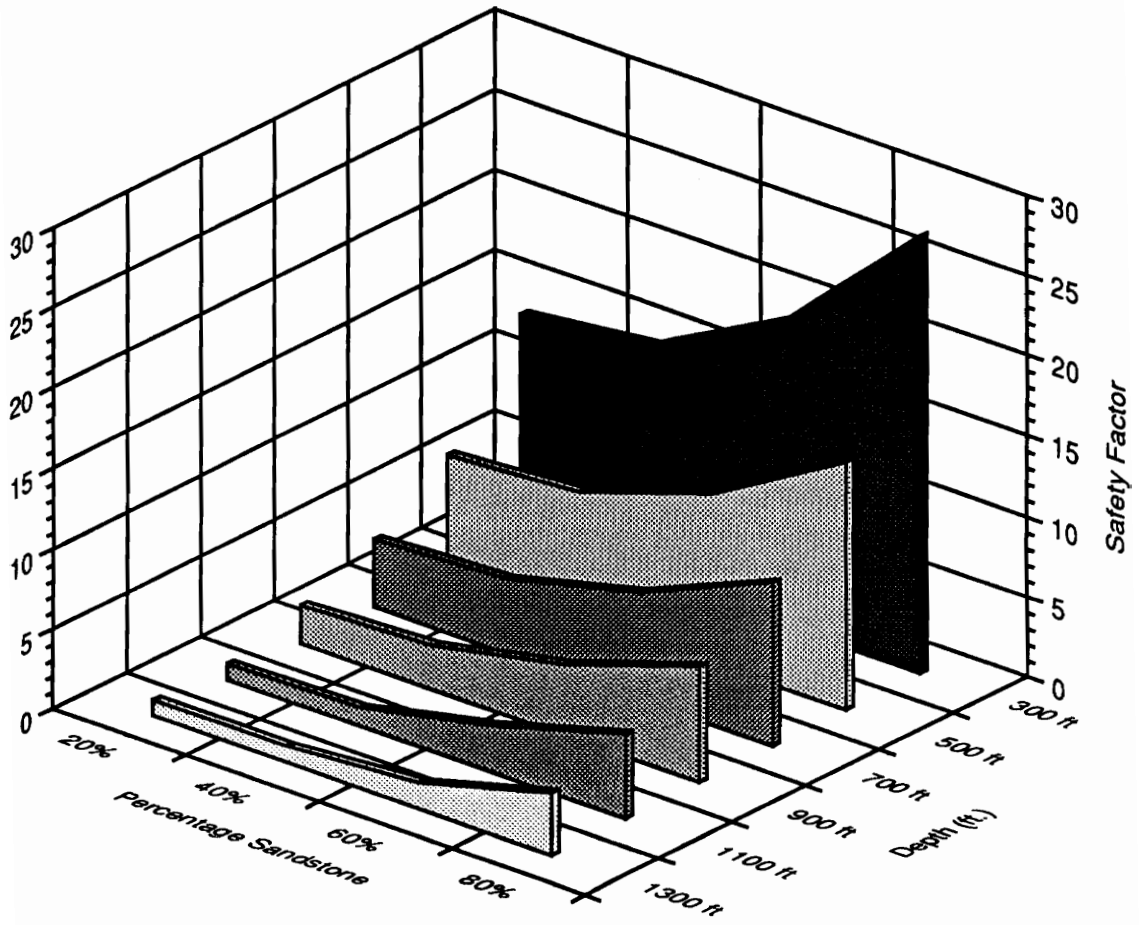

Figure 5.15 Variation of safety factor due to increasing percentage of sandstone from the top to the bottom

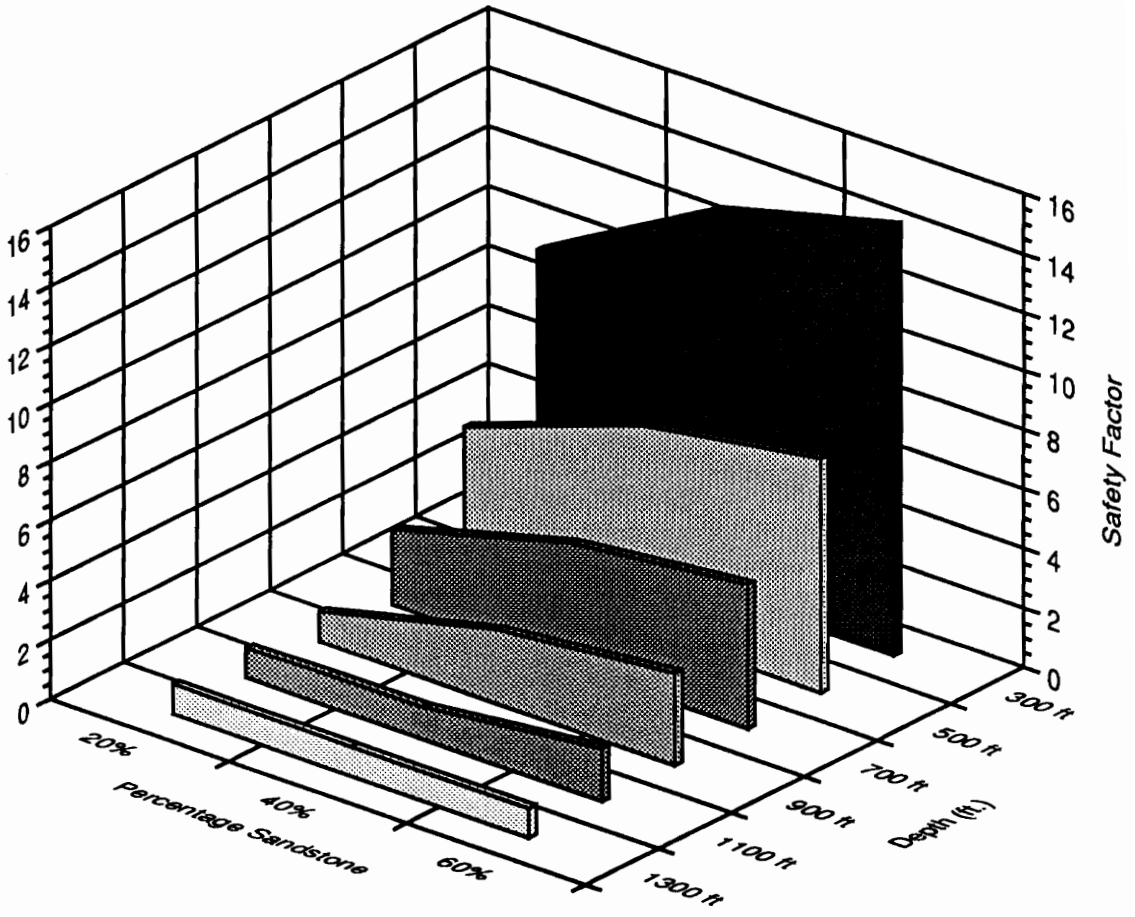

Figure 5.16 Variation of safety factor due to increasing percentage of sandstone from the bottom to the top

The finite element results confirmed that the amount of hard rock in the innerburden as well as its location within the innerburden is critical to the stress transfer mechanisms. It also showed that the rock type in the immediate roof had a direct influence on the type and location of failure. The critical location can change from the edge of the opening suffering shear failure to the center of the opening where tensile failure is critical. These observations confirm what was derived from analysis of field data involving undermining (Haycocks and Karmis, 1983; Matetic and Chekan, 1988).

5.3 Loading Conditions

Previous research has identified factors that affect stress interaction in a multi-seam environment (Haycocks and Karmis, 1983; Grenoble and Haycocks, 1985; Peng and Chandra, 1980). Analysis of field data allowed identification of significant factors affecting stress interaction and assessment of their importance (Chekan et al., 1986). The overburden depth, innerburden thickness, the types of rock present in the innerburden, and distribution of the hardrock in the immediate roof are some of the factors which govern the type of loading that lower seam structures will experience.

To facilitate analysis, three basic external loading conditions of the innerburden were identified (Zhou and Haycocks, 1990). These loading conditions are controlled by relative positions of the upper and lower seam pillars. Gradations between these conditions may be observed underground depending on precise spatial relationships between upper and lower seam structures. Loading conditions may change radically if there is failure in any

component of the system such as pillar or floor (Hsiung and Peng, 1985). Stress field is also expected to change due to such factors as progressive pillar edge softening and non-elastic deformations (Wang et al., 1974). The three loading conditions analyzed in this study are:

1) columnized pillars
2) partial offset pillars
3) total offset pillars.

5.3.1 Columnized Pillars

Self loading of the innerburden governs the failure of lower seam entries in this case. Therefore innerburden thickness is critical in determining the possibility and type of failure. To evaluate this parameter, four models with different innerburden thicknesses were analyzed. The innerburden thickness was varied from 50 to 40 to 30 to 20 feet. The innerburden lithology in all these cases was kept constant (shale in the immediate roof overlain by sandstone comprising 80 percent of the innerburden). Overburden depth was 900 feet. A comparison of the lower seam safety factors for these cases shows more than a two-fold increase in center safety factors when innerburden is decreased from 50 to 40 to 30 feet. Further decrease in the innerburden thickness, however, shows a decline in roof safety factors. The probable cause of this trend is the less transverse loading experienced by roof beds for relatively thin innerburden. The effect of reduced self loading will be valid only up to a certain minimum innerburden thickness beyond which high interaction stresses will offset the effect of less transverse loading. Taking the safety factor for 50 feet of innerburden as a

base, a correction for the safety factor was calculated for other innerburden thicknesses. The plot of this calculated correction factor versus innerburden thickness for entry corner and center is shown in Figures 5.17 and 5.18. The empirical equations obtained by curve fitting for entry corner and center are given below.

$$f(x) = -0.008473x + 1.403435 \quad 5.21$$

$$f(x) = -0.002665x^2 + 0.130395x + 1.030467 \quad 5.22$$

In these equations x is the innerburden thickness and f(x) is the multiplication factor for the correction of safety factors obtained for 50 feet innerburden thickness.

The innerburden thickness, lithology, and overburden depth will determine the type of failure. The critical combination of overburden depth and roof lithology can create a high stress gradient which can contribute to shear failure at the lower rib edge. At a relatively short distance from the lower seam, the upper pillar can transfer highly concentrated pressure to the rib edge of the lower pillar thus causing shear failure. This type of failure was reported by Holland (1951). Tensile failure of the lower seam entry roof is also possible with the innerburden failure under its own weight for thin innerburdens (Zhou and Haycocks, 1990).

5.3.2 Partially Offset Pillars

This condition is most frequently observed underground and is usually due to surveying errors in mines designed for columnization or when operating a

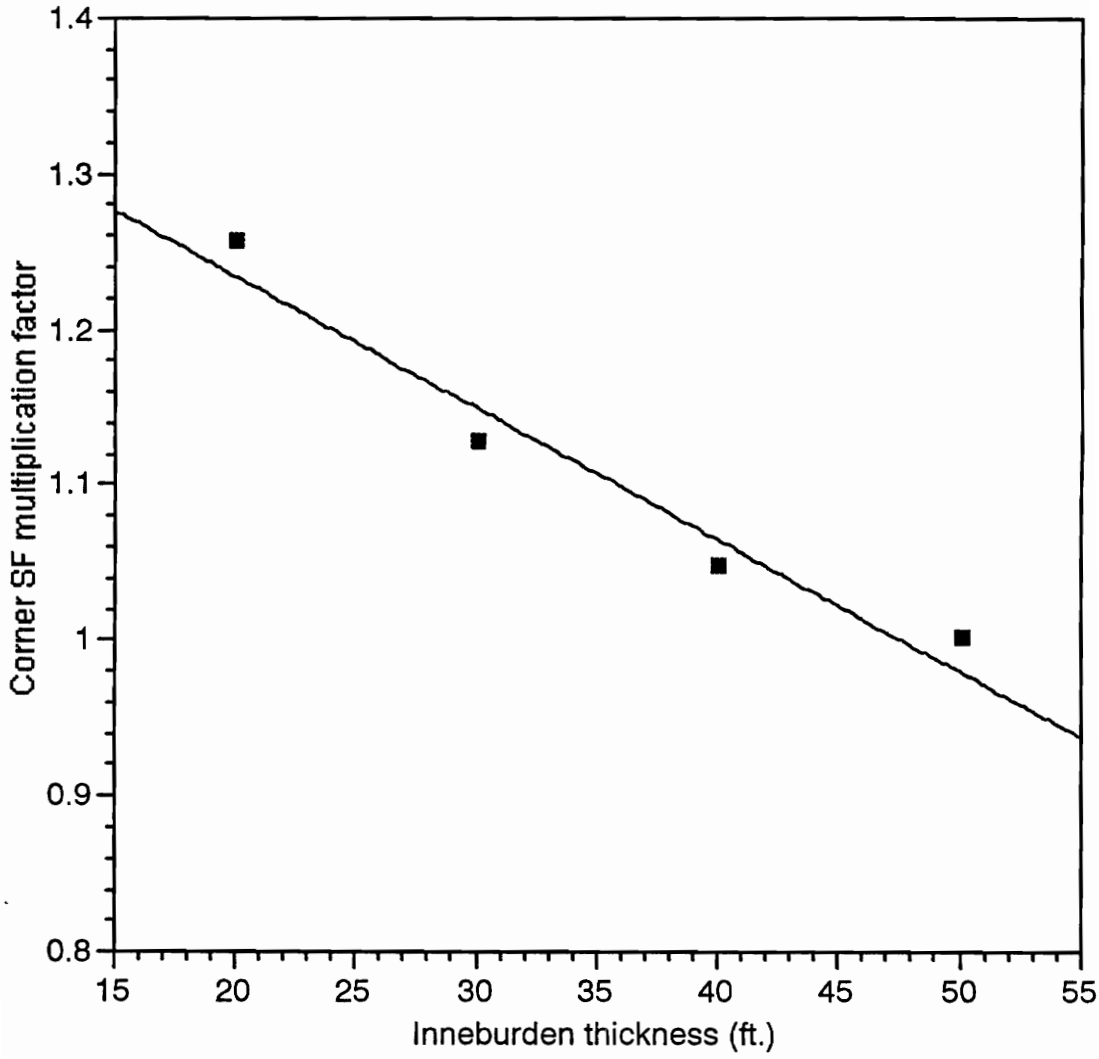

Figure 5.17 Influence of innerburden thickness on entry corner safety factor for columnized pillars

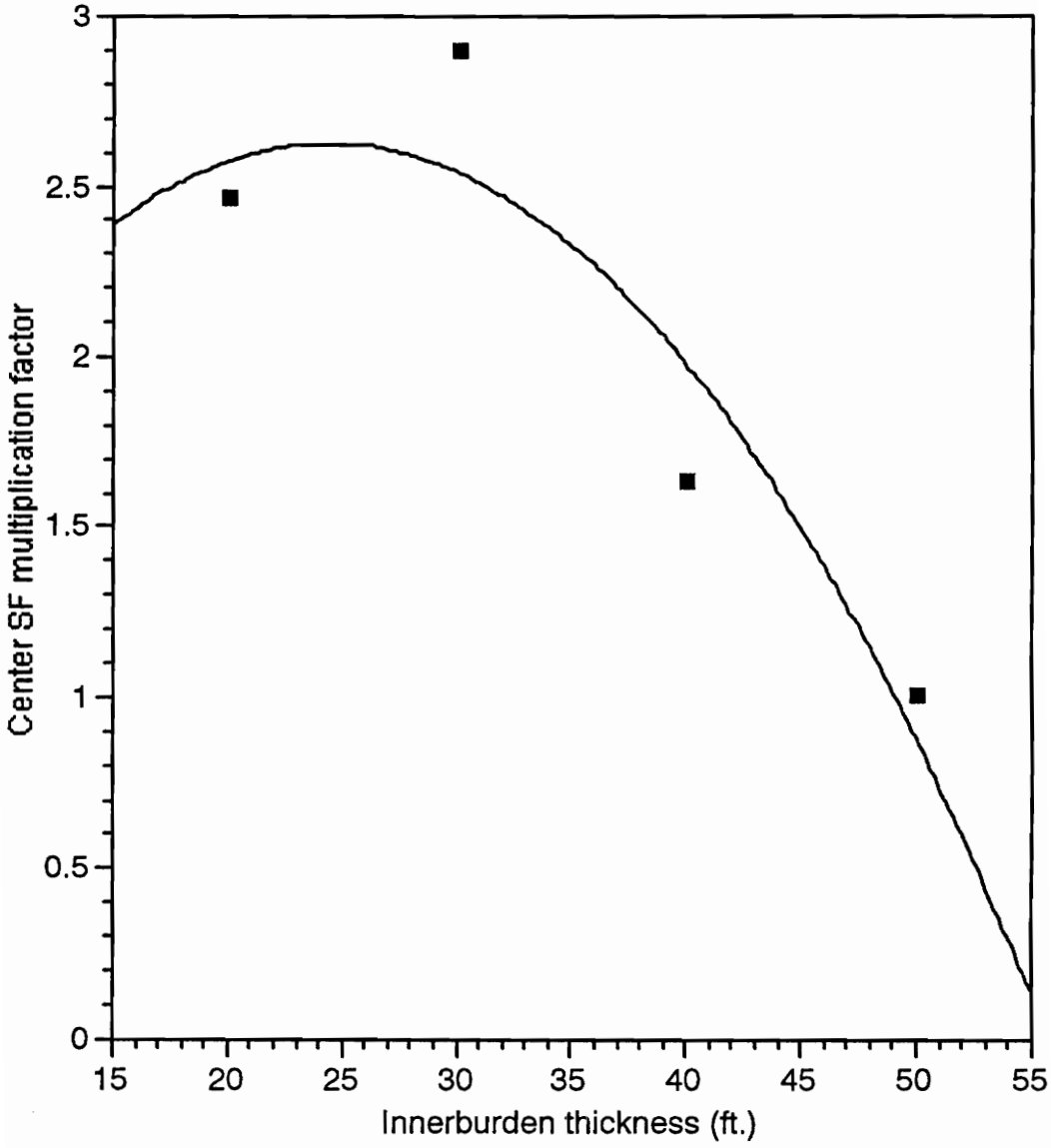

Figure 5.18 Influence of innerburden thickness on entry center safety factor for columnized pillars

mine of unknown layouts (Matetic and Chekan, 1988). To quantify the effect of offset pillars on lower seam entry roofs, four models with innerburden thicknesses of 50, 40, 30 and 20 feet were analyzed. The entries in the lower seam were placed in such a way that the upper seam pillar edge was in line with center of lower seam entries. The high stresses developed in such cases generate shear failure in the lower seam entry corner which, during collapse, produces tensile failure at the opposite rib line. This type of failure is reported as cutter failure which is a high angle shear failure in the entry corner (Zhou and Haycocks, 1989).

The correction factors due to offsetting the pillars were calculated for various innerburden thicknesses. These correction factors were plotted against innerburden thickness for offset pillars (Figure 5.19 and 5.20). The corresponding equations obtained by curve-fitting are given below.

$$f(x) = .000016539x^3 - .00204197x^2 + 0.08059772x - .007632 \qquad 5.23$$

$$f(x) = -.00167469x^2 - .127063x - 1.272695 \qquad 5.24$$

To compute the safety factors for entry roof corner or center for any innerburden thickness with offset pillars, the correction factor obtained from one of the above equations is multiplied by the safety factor computed for 50 feet of innerburden with columnized pillars.

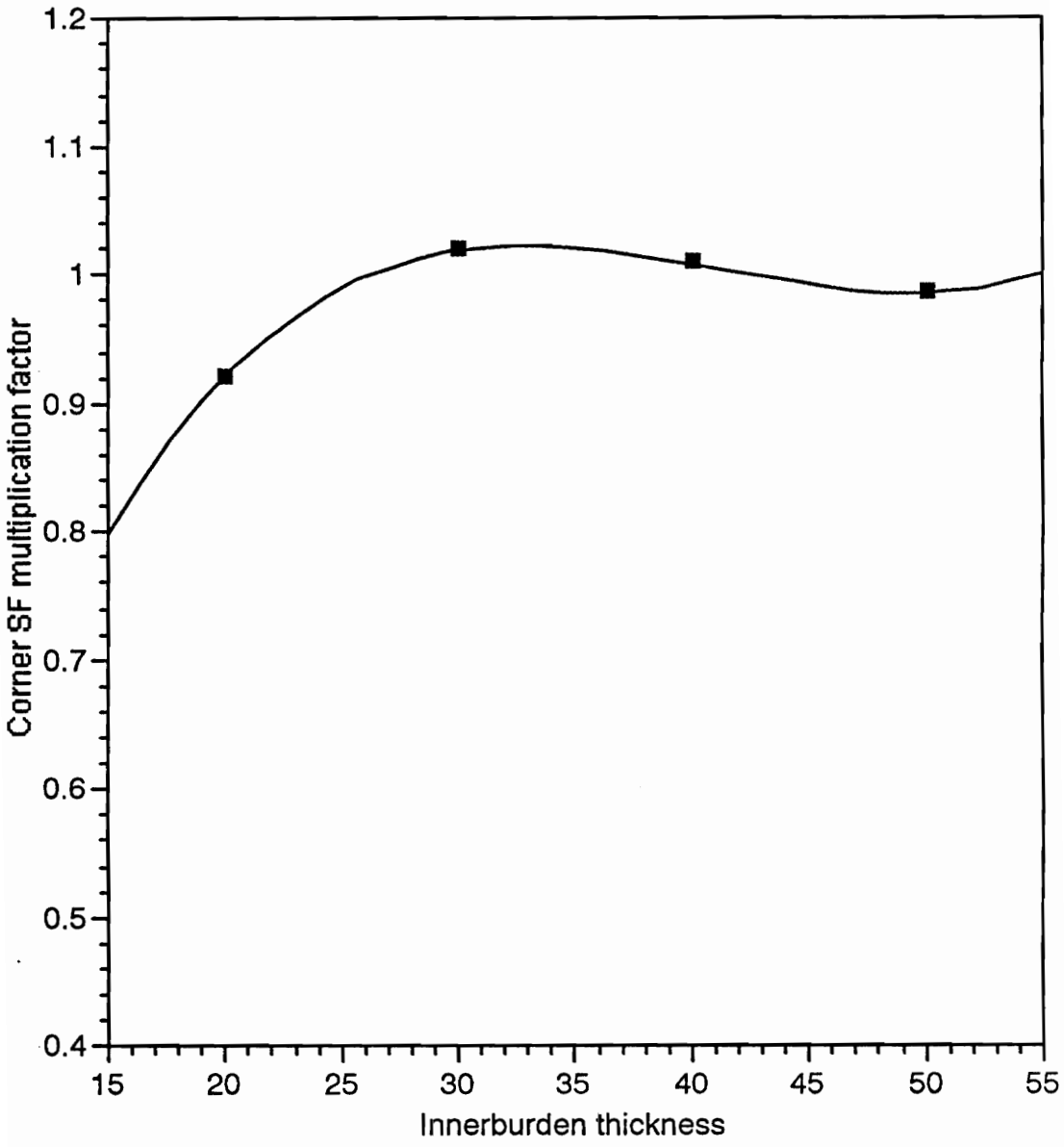

Figure 5.19 Influence of innerburden thickness on entry corner safety factor for partial offset pillars

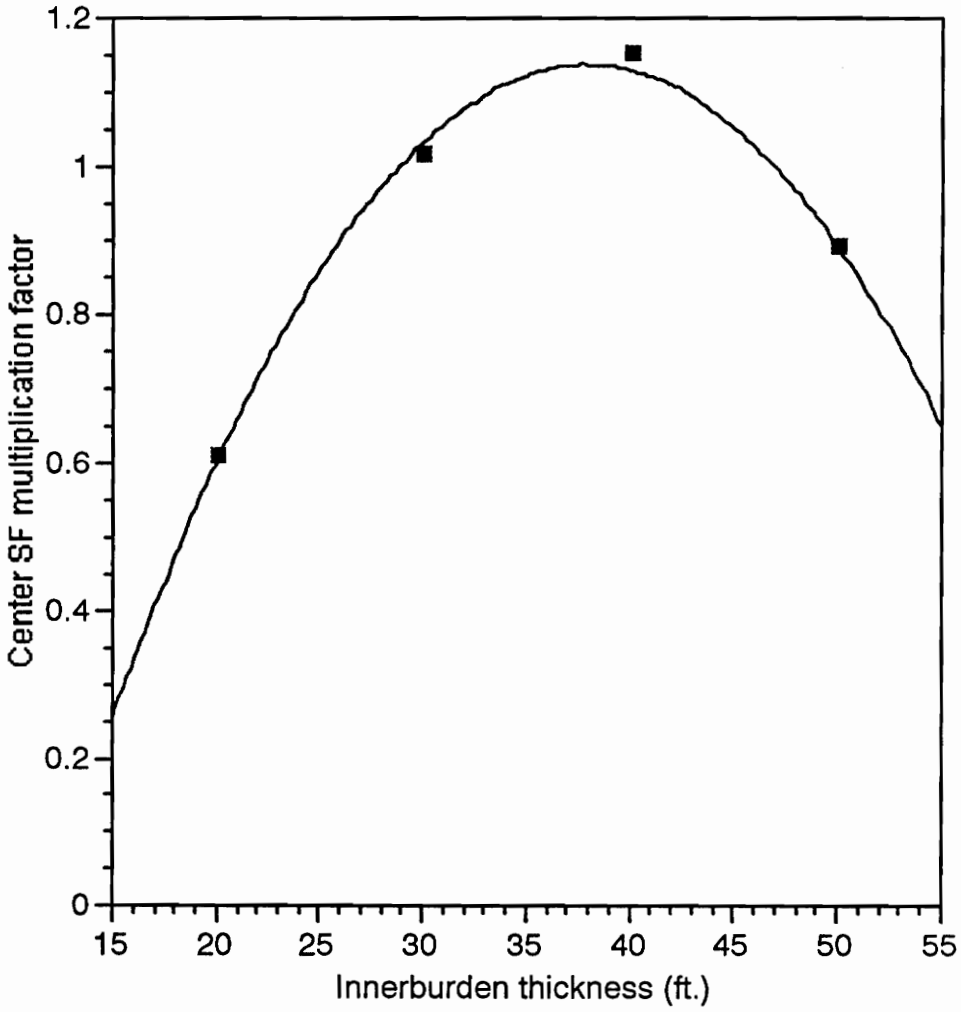

Figure 5.20 Influence of innerburden thickness on entry center safety factor for partial offset pillars

5.3.3 Total Offset Pillars

To evaluate the effect of offset pillars, mesh similar to the one described above was analyzed, but the entries in the lower seam were placed completely under the upper seam pillars. The results showed that this arrangement was the most disastrous as far as the lower seam entry roof was concerned. The safety plot across the entry shows an impending failure in the entry center. Structurally this is the most undesirable of the relative positions between the upper and lower seam pillars. To quantify this effect, a number of models with changing innerburden thicknesses but the same total offset pillar arrangement were analyzed. As in the partial offset case a correction factor for each case was calculated and plotted against the innerburden thickness (Figure 5.21 and 5.22). The equations obtained from these curves are given below.

$$f(x) = .0000012725x^3 - .00036262x^2 + 0.025255x + .45037 \qquad 5.25$$

$$f(x) = 0001856975x^2 + .00650598x - .1008219 \qquad 5.26$$

The factors obtained from these equations are used to calculate the final safety factor for any given innerburden thickness for the totally offset cases.

Three types of failures can be generated in the lower seam entry roofs due to this arrangement, depending upon the relative size of the upper pillar with respect to the opening width of the lower seam:

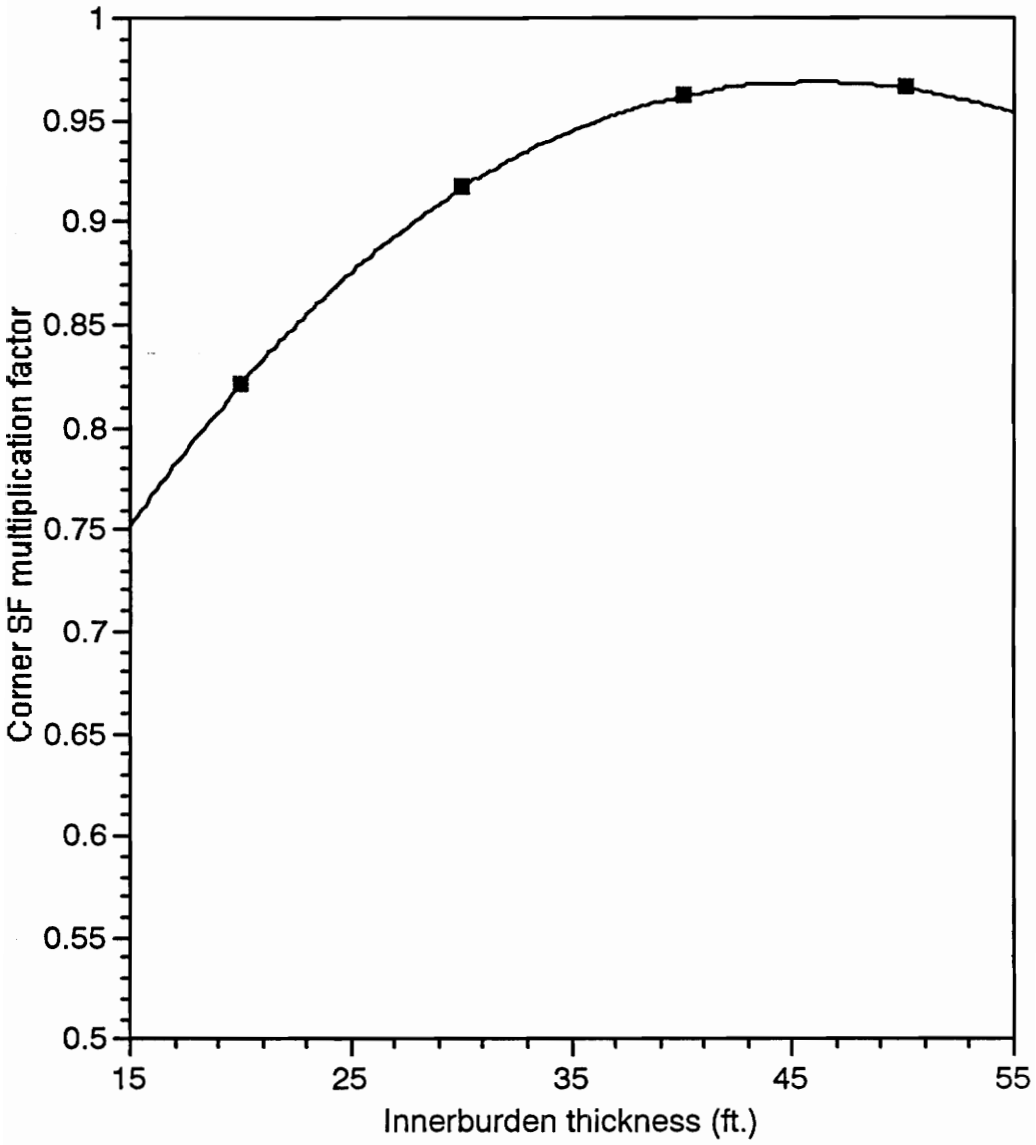

Figure 5.21 Influence of innerburden thickness on entry corner safety factor for total offset pillars

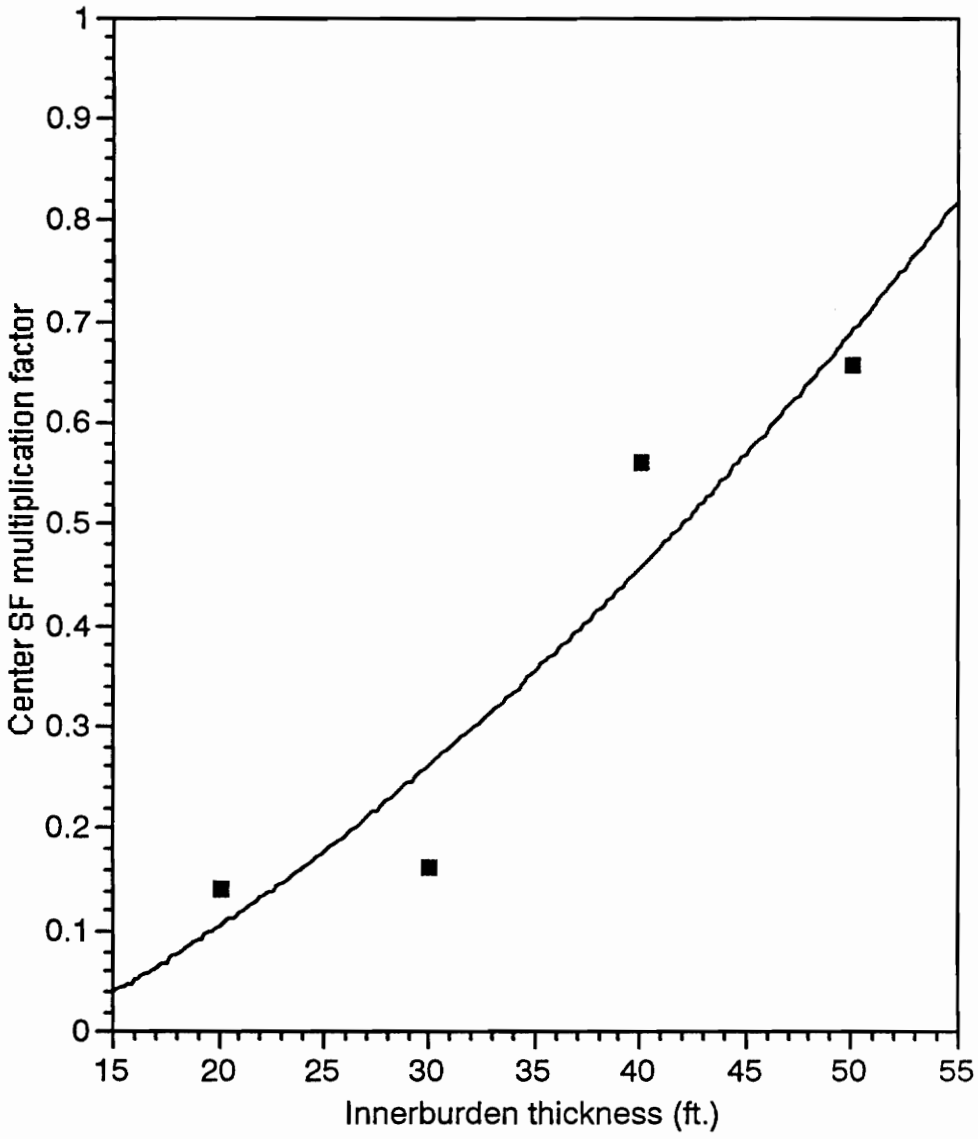

Figure 5. 22 Influence of innerburden thickness on entry center safety factor for total offset pillars

1) Small upper seam pillars whose width is less than the opening width. Under these conditions tensile failure in the lower seam entry is expected (Zhou and Haycocks, 1989).
2) Medium-sized upper seam pillars whose width is equal to the opening widths. These will usually cause the innerburden to fail in shear or near the lower rib edge (Akram et al., 1991).
3) Large upper pillars whose width exceeds the opening width are most common. This type of offset pillars results in shear failure. (Haycocks, 1976).

With other conditions being equal, the stability of the innerburden increases from case 1 to case 3 due to the more evenly distributed lower seam stress concentration and the protective action provided by larger pillars.

The comparative effect of the three types of pillar arrangements (columnized, partial offset and total offset) is shown in Figure 5.23. The decrease in safety factors from the columnized to partially offset to complete offset case is evident. The entry is stable even for a relatively thin innerburden (20 feet) if the pillars are columnized. The offset pillars, however, transfer overburden stresses to the entry roof making it susceptible to failure.

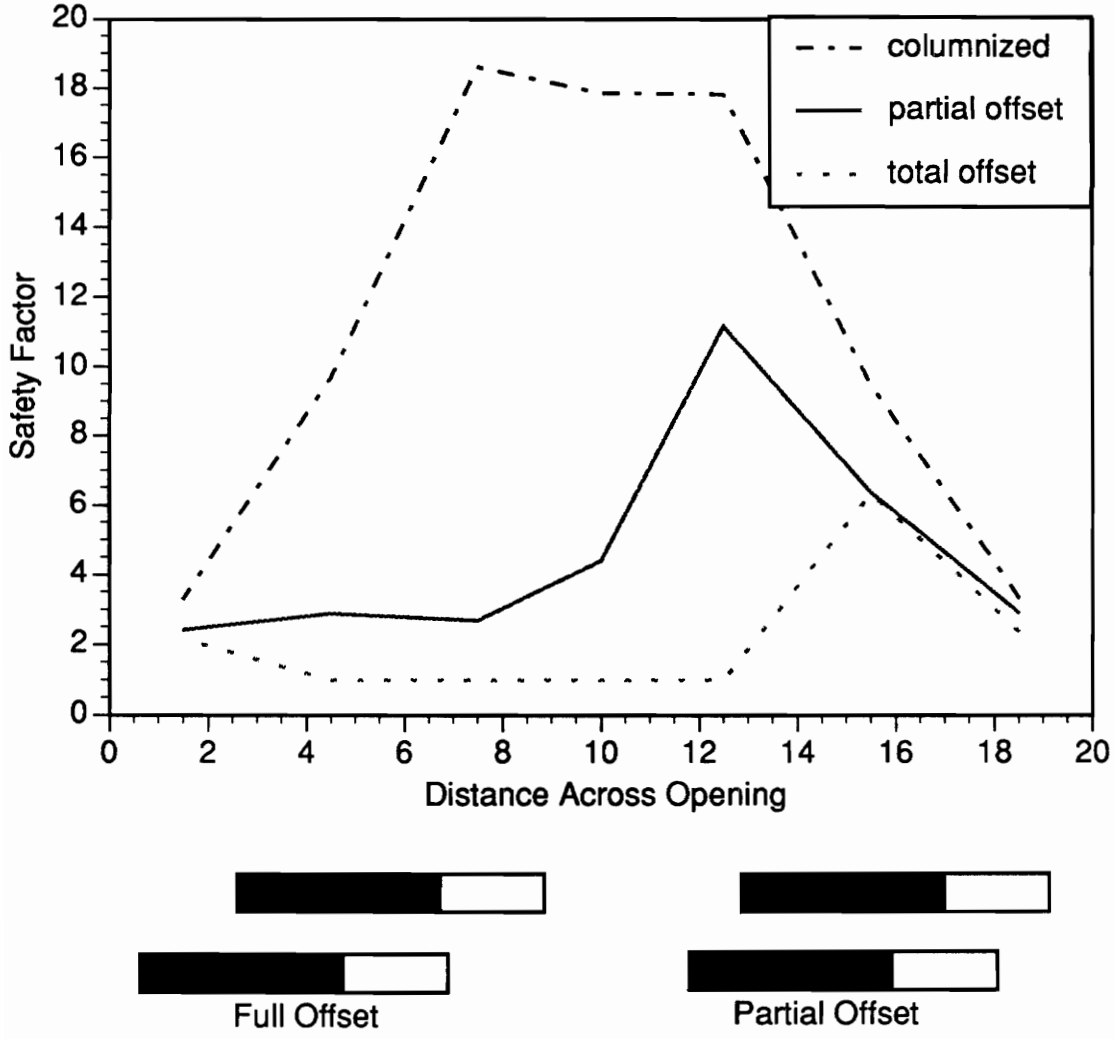

Figure 5.23 Effect of unsymmetric loading due to offset pillars on lower seam entry stability

Chapter 6

Field Verification and Model Development

6.1 Introduction

To verify predicted failures, the modeling technique was used to investigate roof instability under a variety of geologic and loading conditions. The versatility of the approach was demonstrated through its successful application to longwall as well as to multi-seam conditions.

6.2 Unsymmetric Loading of Gate Entries

The effect of unsymmetric loading similar to that experienced with longwall gate entries was modeled by simulating a ramp load. The results of this modeling are shown in Figure 6.1. This plot suggests an impending offset failure about two feet away from the rib line under the influence of differential loading. The tensile stresses induced by the offset loading cause this type of failure. It begins as a tensile failure, but ultimately propagates

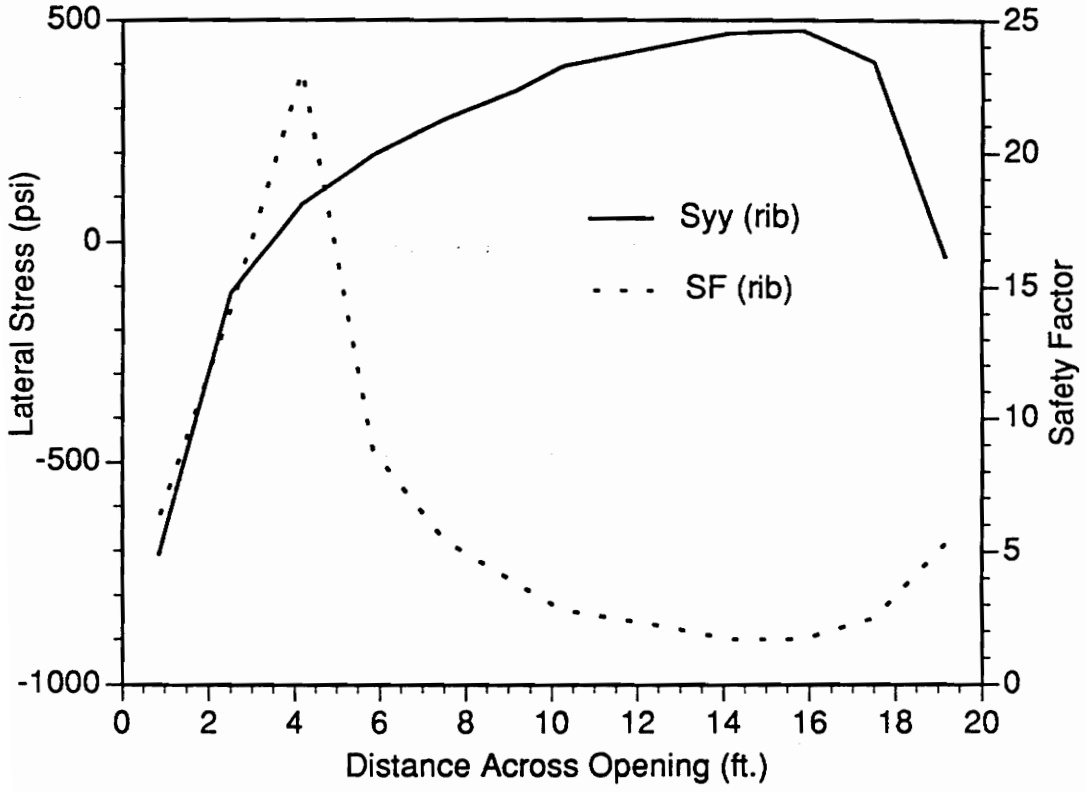

Figure 6.1 The effect of unsymmetric loading on a longwall gate entry

as a shear failure, as has been reported in many longwall gate entries.

Such a case of offset failure in longwall gate entries was studied for a West Virginia mine (Lightfoot #1 mine). This mine is located in No. 2 Gas Coalbed under a cover varying from 400 feet to about 1000 feet. The entries experiencing roof problems have competent shales in the immediate roof, overlaid by sandy shales with some interbedded sandstone. The floor is of laminated and fractured shales.

Roof problems mainly occurred in tailgates where the overburden was 1000 feet or more. Crib deterioration appeared closely associated with rib spalling and roof failure just inside the rib line (Plates 6.1 and 6.2). This type of roof failure, under the influence of differential loading, leads to rib spalling which in turn increases roof and pillar instability due to increased entry span and reduced pillar size.

Where the roof had fallen out around the resin bolts, the bolts exhibited considerable lateral distortion indicating differential loading (Plate 6.3). Sheet spalling of the ribs observed in many places indicated excessive lateral movement of the pillars under the influence of unsymmetric load (Plate 6.4). This type of excessive unsymmetric loading on gate entries can be tackled by providing improved crib placement. Location of cribs is crucial for improving roof conditions under this type of loading. Optimum location should coincide with the location associated with the lowest safety factor obtained before the placement of the crib. Prestressing cribs during installation also could yield

6.1 Photograph showing roof failure just inside the rib line

6.2 Photograph showing crib deterioration due to differential loading of the roof

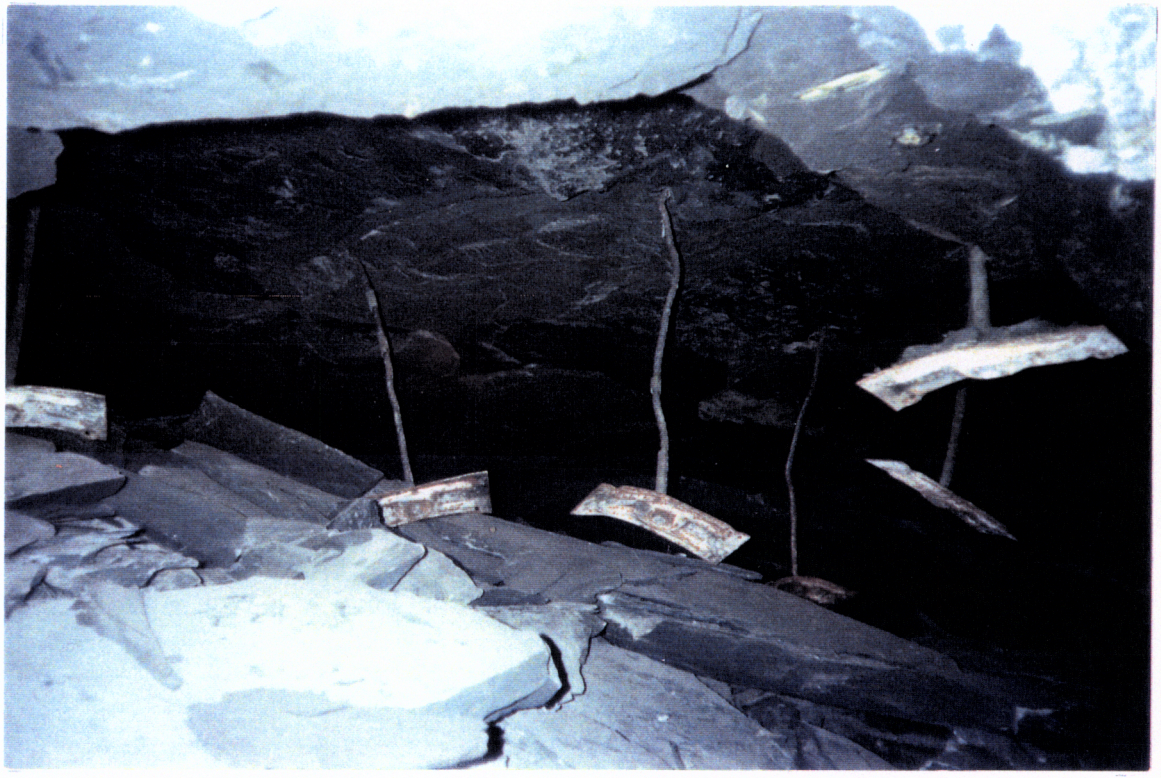

6.3 Photograph showing lateral distortion of roof bolts under the influence of unsymmetric loading

6.4 Photograph showing excessive rib spalling

significant benefits by turning the crib into an active form of support.

6.3 Influence of Horizontal Stress on Entry Stability

The influence of high horizontal stress on the lower seam entry roof was studied by simulating excessive horizontal stress in the range of 200 to 2000 psi for an overburden depth of 1000 feet. The safety factors for two critical entry roof locations are plotted and are shown in Figure 6.2. The corner safety factor, which governs the shear failure, indicates an improvement for an initial increase in the horizontal stress, then it declines with further increase in the horizontal stress. This trend confirms the speculation that excessively high horizontal stresses are the cause of shear failure reported in many Appalachian coal mines. The possibility of cutter failure under the influence of high horizontal stresses is further increased by the certain combinations of geology and overburden depth. As discussed in the previous sections, varying the immediate roof conditions using differing sandstone combinations showed that shale roofs are vulnerable to shear failure. The analysis confirms that the combination of roof lithology and stress field is responsible for the high angle shear failures reported in many mines.

The effect of horizontal stress on tensile failure, however, is different. The safety factors for the midspan rise dramatically as the horizontal stress is increased. A six-fold increase in safety factors is achieved corresponding to 800 psi of excess horizontal stress. After that peak, the safety factors again start to decline with the increasing stress. Initial increase in the excess

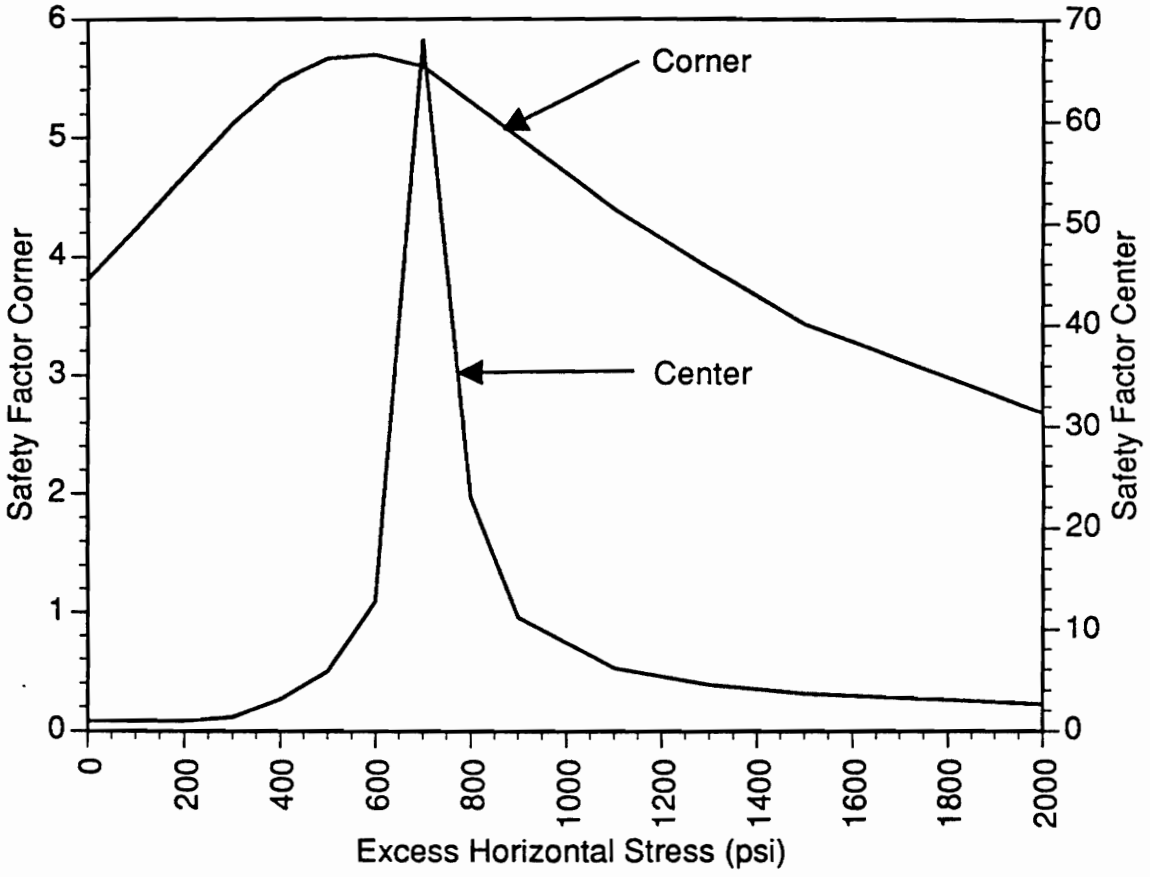

Figure 6.2 Influence of excess horizontal stress on the safety factor in the corner and center of mine opening

horizontal stress relieves the tensile stresses at the entry center, thus improving stability, but further increase can cause buckling failure of the immediate roof layers.

6.4 Case Study Data

Numerous case studies exist of lower seam roof conditions subject to high stresses arising from multi-seam interaction. Eighteen such cases were selected from the literature representing a wide range of conditions for the undermining sequence. The data for these cases is given in Appendix B. To evaluate the effects of interaction on lower seam entries, stress levels at the lower seam level were calculated using USEAM which is a multi-seam interaction evaluation package developed at VPI & SU as a consequence of previous research (Grenoble and Haycocks, 1985). The procedure followed to calculate stresses is briefly described in section 2.2. The details of the stress calculation procedure can be seen in the relevant reference. A correlation between these stresses and the percentage of sandstone in the innerburden was obtained. This correlation is expressed in the following equation:

$$f(x) = 340 + 26.57x \qquad 6.1$$

In the above equation x is the percentage of sandstone in the innerburden and f(x) is vertical stress at the lower seam horizon. The results of this correlation are shown in Figure 6.3. The separation line between the failed and stable conditions demonstrates the effects of increasing stress on

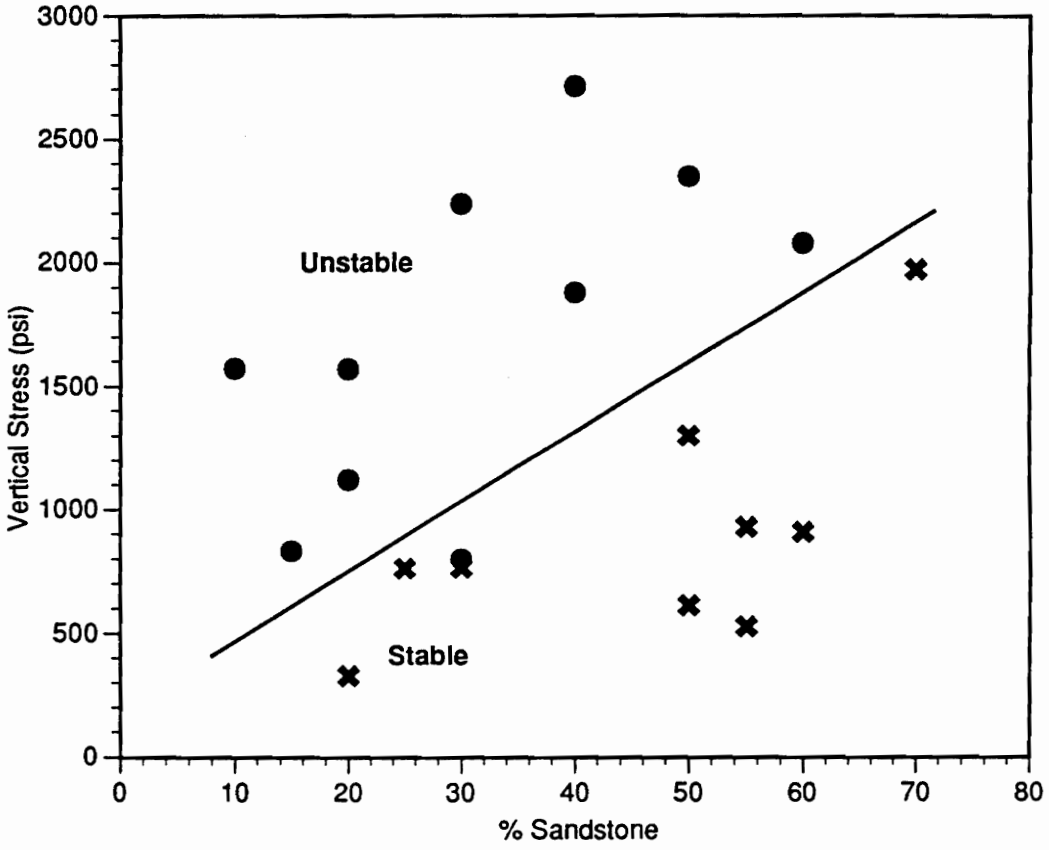

Figure 6.3 Entry stability as a function of percent hardrock in the innerburden and vertical stress based on case studies

stability with varying roof lithologies. This correlation was compared with the finite element results (Figure 6.4) The similarity in results, as predicted by numerical modeling and plots of raw field data, reinforces the value of numerical analysis for this type of investigation.

6.5 Stability Assessment Model

To analyze the often complex response of entry roofs to increasing stress, a mine roof stability assessment model was developed utilizing the FEM results and case study data discussed in the previous sections. This is an essential first step in relating the possible instability in underlying entry roofs to stress field changes occurring due to stress transfer. The basic steps in the model **SESAME** (**S**tability **E**valuation of **S**tress **A**pplied to **M**ine **E**ntries) are shown in Figures 6.5 and 6.6

The model has two options for the analysis of an underlying multi-seam case. In the approximate analysis option, the vertical stress at the lower seam horizon for a given innerburden sandstone percentage is compared with the predicted stress capable of causing instability in the roof. The approximate analysis utilizes the relationship derived from the analysis of field data (Equation 5.27). This field equation relates the computed or measured vertical stress at the lower seam horizon with the observed roof condition.

For the approximate analysis, the vertical stress at the lower seam horizon for the case to be analyzed is computed either by ALPS or USEAM, and

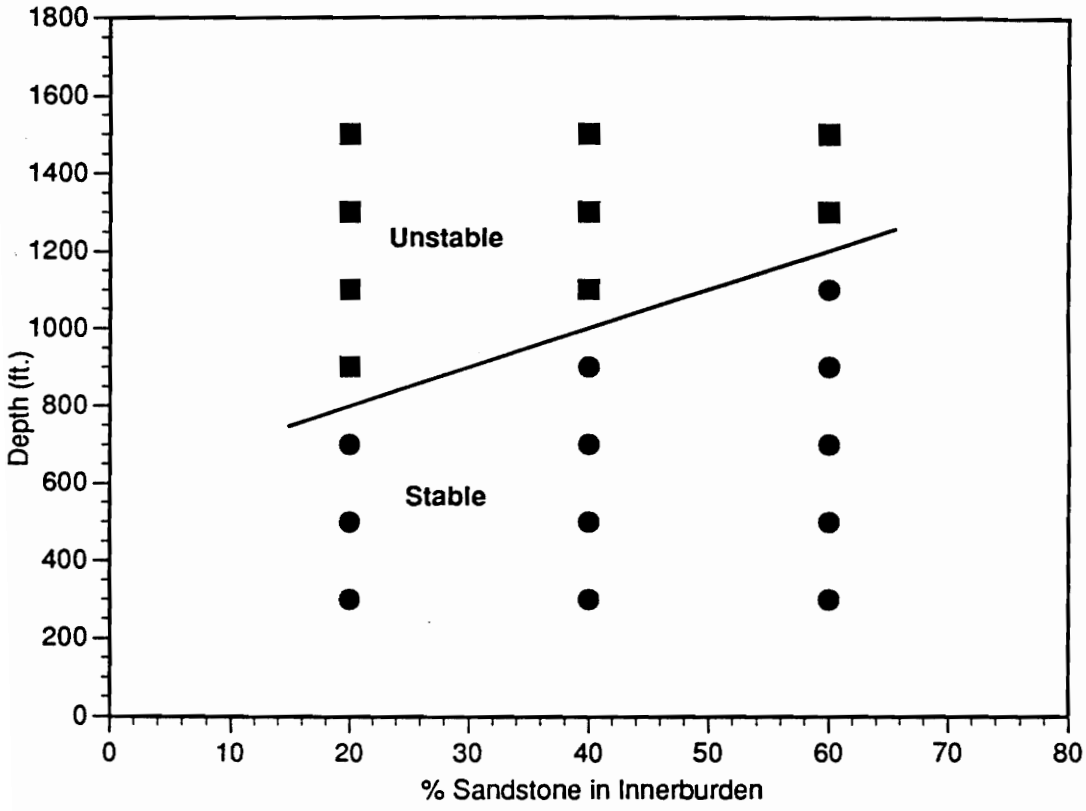

Figure 6.4 Lower seam entry stability as a function of depth and percent sandstone in the innerburden based on finite element study

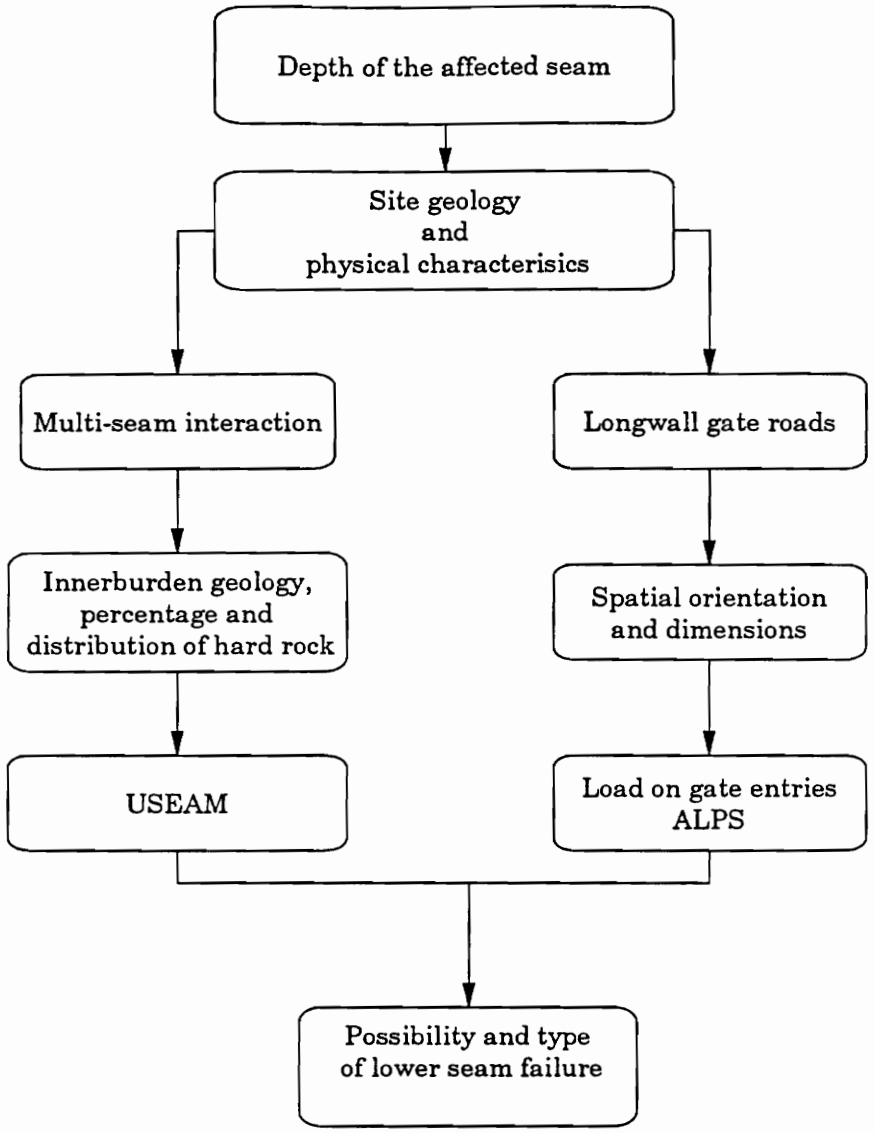

Figure 6.5 Outline of the procedure used to calculate vertical stresses using USEAM and ALPS

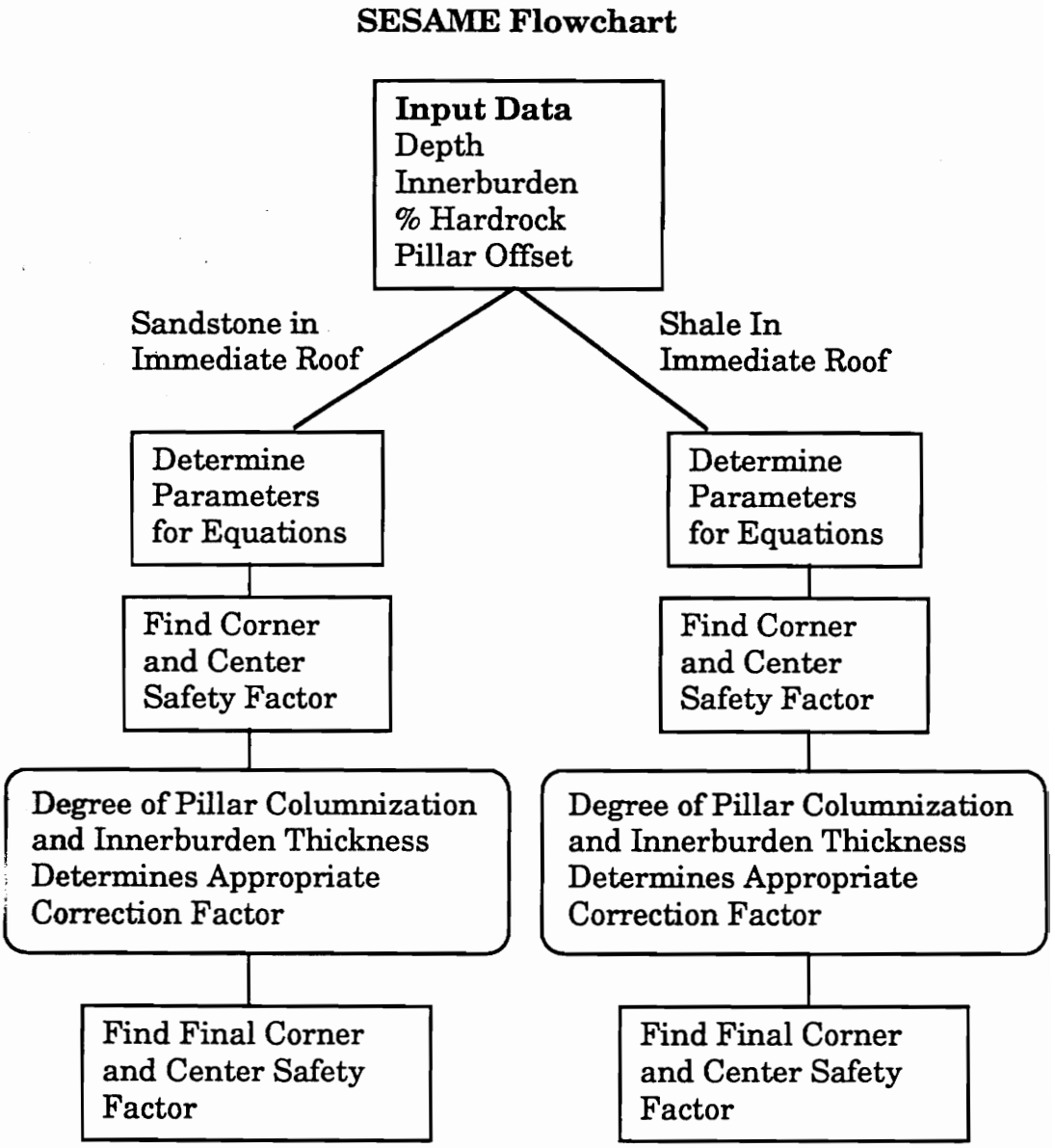

Figure 6.6 SESAME flowchart showing basic steps involved in the interaction analysis

compared to the predicted stress level capable of causing instability. For room and pillar mines USEAM is used, which requires overburden depth, lower and upper seam thicknesses, innerburden thickness, pillar size, entry size and sandstone percentage in the innerburden as the input parameters. For longwall gate entries, the load is estimated using the procedure outlined in section 2.2 (ALPS).

For the detailed analysis, the model utilizes the set of equations obtained by curve fitting of the numerical modeling results of this research (Equations 5.1 through 5.26). These equations calculate entry roof safety factors for the given value of sandstone percentage, its location, overburden depth and the relative location of pillars in the two seams. Two sets of equations are used, one for computing safety factors in the entry roof corner and the other in the entry midspan.

The model **SESAME** is implemented as a spreadsheet template in EXCEL, a WINDOWS application program. For a given set of values of innerburden sandstone percentage, its location in the innerburden, and overburden depth, the program first computes entry corner and center safety factors for 50 foot thick innerburden with columnized pillars, and then corrects these values for the input value of innerburden and pillar offsetting. The correction for innerburden thickness for the specified pillar offsetting is obtained by using the curve fitted correction equations (Equations 5.21 to 5.26).

The model output includes safety factors against failure for the given set of

conditions. It can later be modified to use data ranges instead of single values. In that case, it will utilize Monte Carlo sampling to produce the probabilities of failure or reliability estimates.

6.6 Mining Under Room and Pillar Workings--A Case Study

To demonstrate the application of **SESAME** for use in underground mine design, the model was used to evaluate the possibility of roof instability in a coal mining situation. Mining had been attempted in the lower seam but had to be abandoned due to massive innerburden failures. The challenge was to determine whether any of the remaining coal seams could be mined without encountering further massive roof failures.

The investigation commenced with the acquisition of the relevant information viz-a-viz surface elevation data, borehole logs and mine plans for the upper and lower seam. From this data, contour plots were prepared for the overburden depth and innerburden thickness which are shown in Figures 6.7 and 6.8 respectively. Mine workings in the upper and lower seam were overlaid on these plots. The resulting plots showed that the roof failures occurred in an area where sandstone innerburden were approximately 15 feet or less and overburden depth was 800 feet.

Since the precise location of the upper seam pillars were unknown and access to the upper mine was not possible, pillar columnization in any future mining could not be practiced. The case was therefore analyzed for offset

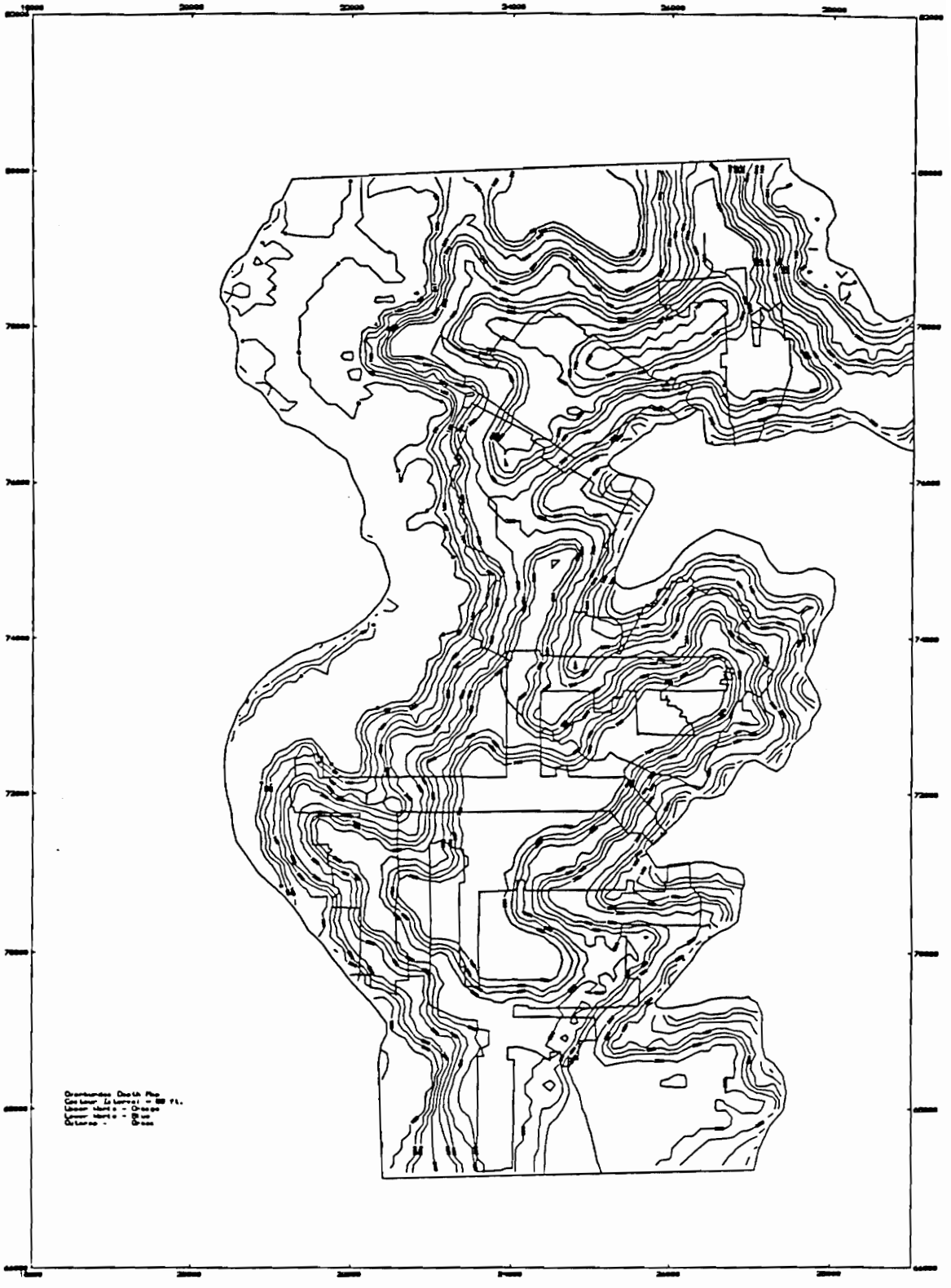

Figure 6.7 Overburden isopach map of the upper seam

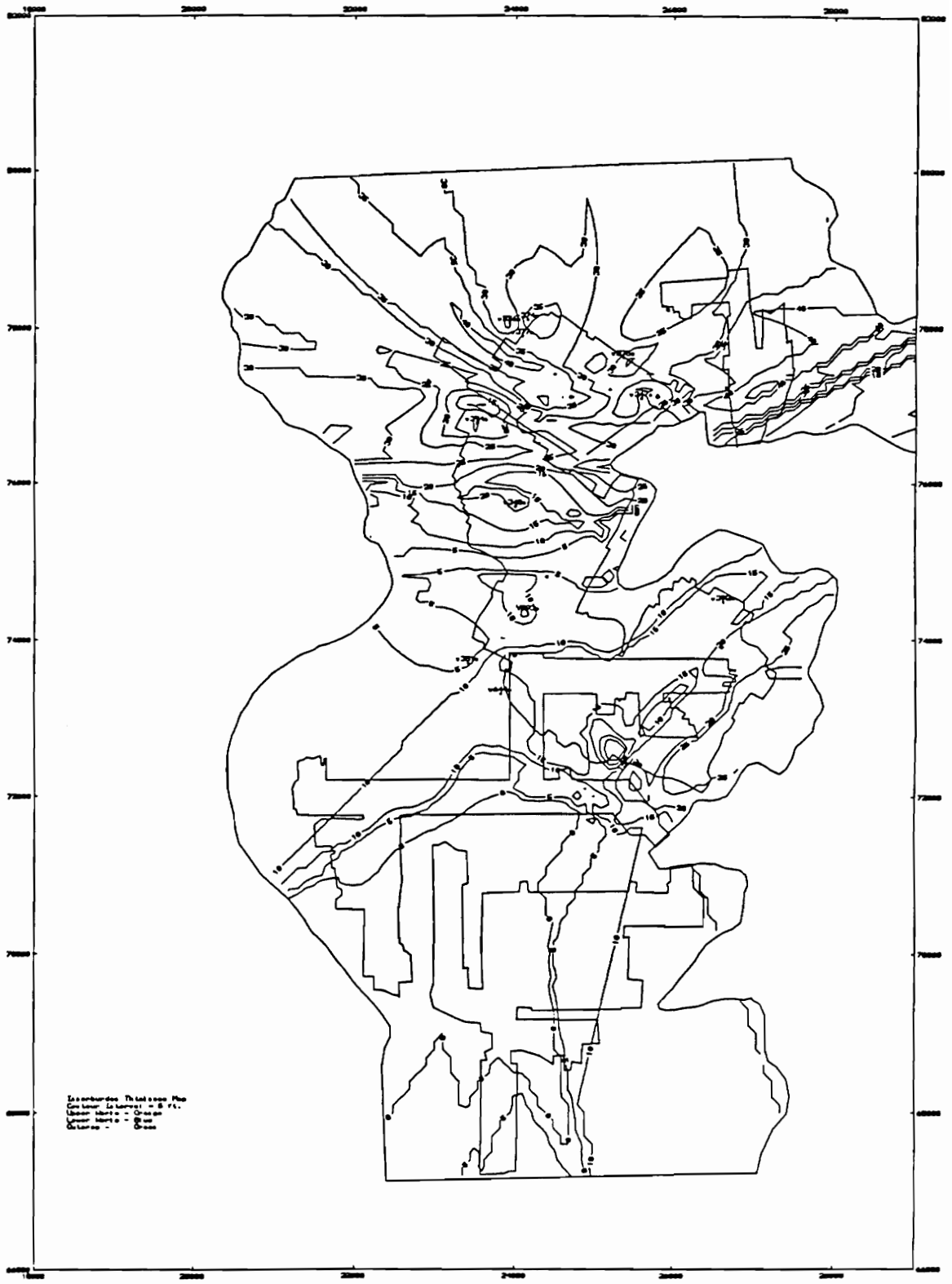

Figure 6.8 Innerburden isopach map for the lower seam

pillars using **SESAME**. Results clearly showed the innerburden to be unstable at 15 feet, as was experienced in actual mining. Various innerburden thicknesses were tried to determine their effect on lower seam entry safety factors. As shown in Figure 6.9, the entry would be stable when the innerburden thickness was greater than 25 feet. The effect of overburden depth on entry stability, as predicted by **SESAME**, is shown in Figure 6.10. Further analysis showed that mining operations in the lower seam could be safely carried out in areas where the innerburden is 25 feet or more, and the depth less than 800 feet.

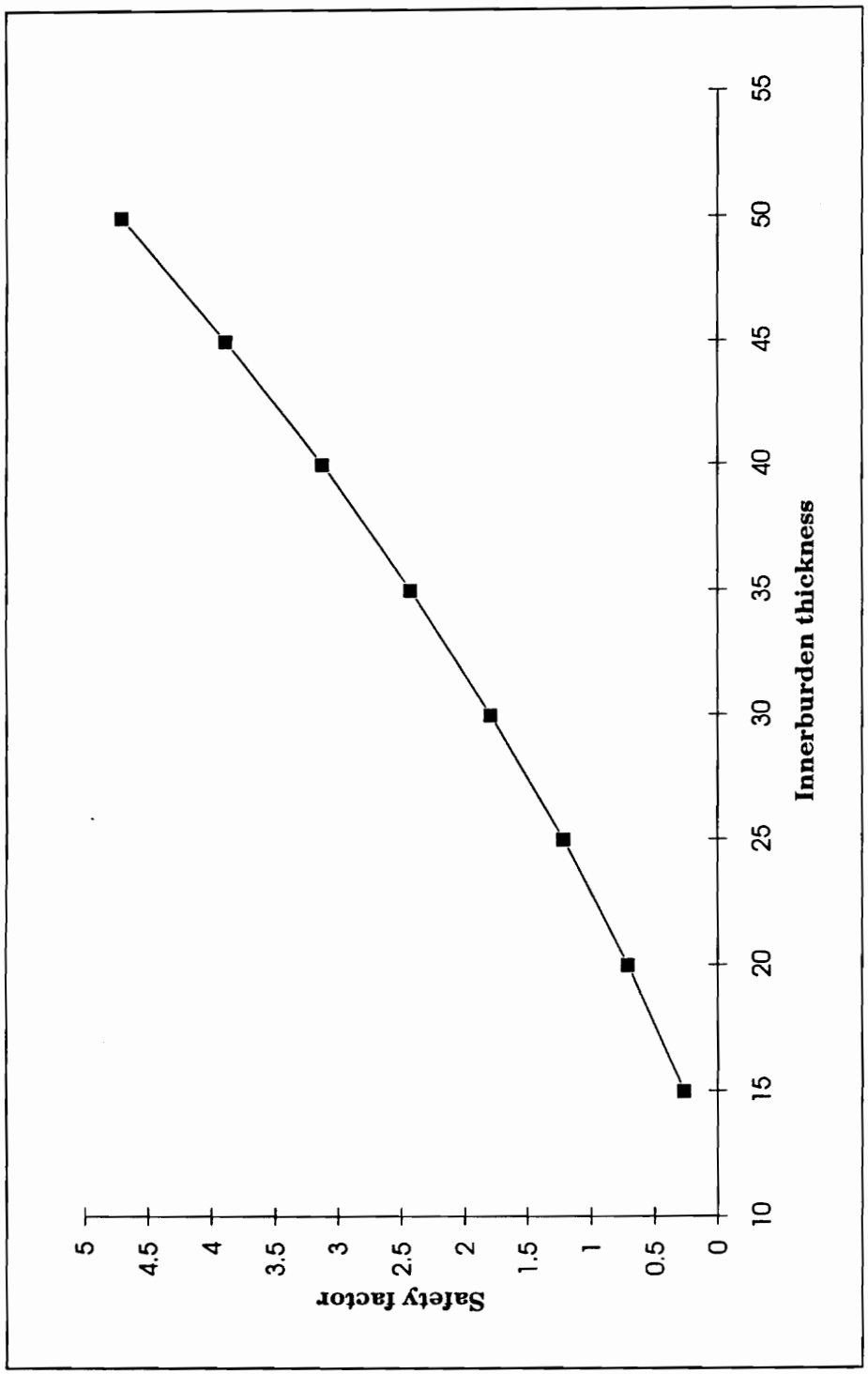

Figure 6.9 Effect of innerburden thickness on entry roof stability for 800 feet of depth

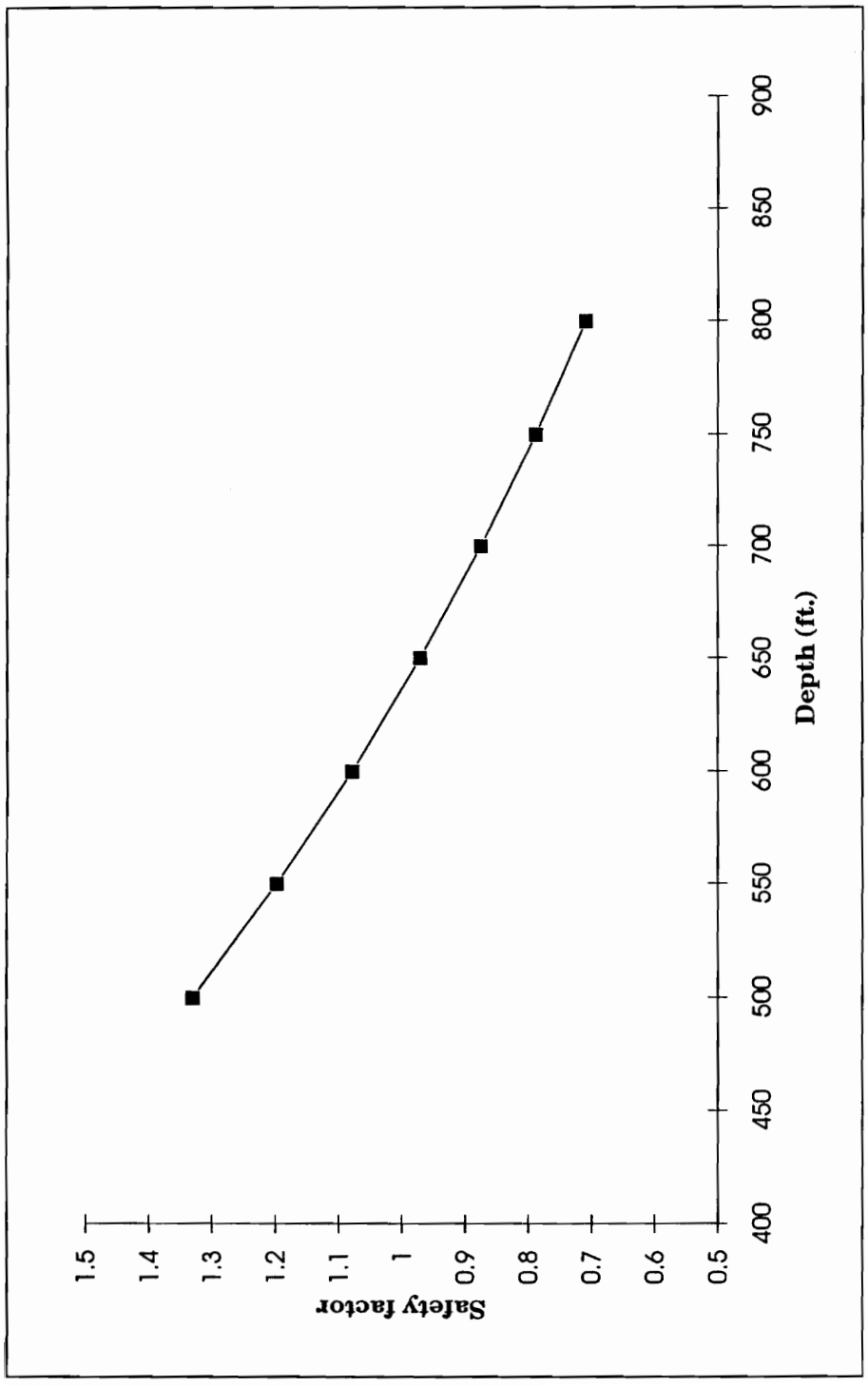

Figure 6.10 Effect of depth on entry roof stability for 20 feet of innerburden thickness

Chapter 7

Conclusions and Recommendations

7.1 Conclusions

Lower seam entry roofs were analyzed for possible instability due to increased stress levels under upper seam structures. The role of geology and loading conditions in causing instability in the lower seam entries was investigated. The findings of this research are summarized in the following conclusions.

The percentage of hard rock in the innerburden is a major factor in the roof stability for underlying multiple-seam mines. The presence of sandstone in the innerburden has a stabilizing effect on the entry roofs. Although entry stability increases with increasing percentage of sandstone, the increase is more pronounced at the midspan than at the entry rib.

The location of hard rock in the innerburden is an important factor as far as

type and location of failure is concerned. The critical location can change from shear failure near the rib to tensile failure at the center. An entry with shale in the immediate roof overlain by sandstone in the upper part of the innerburden is more susceptible to shear failure in the corner than tensile failure at the midspan. Entries having sandstone in the immediate roof loaded by shale are much likely to fail in tension in the center than in shear at the corner. The critical failure location is also affected by overburden.

Innerburden thickness and columnization of pillars are the two most important factors in creating instability in the lower seam entries especially in close seam cases where the innerburden thickness is under 50 feet. Stable lower seam conditions can be maintained for innerburdens as thin as 20 feet if the precise columnization of pillars is ensured.

The unsymmetrical loading of room and pillar entries in a lower seam or longwall gate entries, can result in an offset failure of the roof. Such failures commence as tensile failure under the influence of high bending moments then propagate as shear failures.

Excess horizontal stress up to a certain value can enhance the entry stability against both shear and tensile failure. Further increase, however, makes the entry susceptible to shear failure. The chances of shear failure under the influence of high horizontal stress are further increased if the immediate roof is of shale.

The entry roof stability analysis model, SESAME, developed as a result of this research, furnishes a quick and reproducible means of determining the effect of innerburden thickness, pillar layouts, overburden depth, and the amount and distribution of hard rock in the innerburden on the lower seam entry roofs.

7.2 Recommendations

The study provides a means of determining the type and location of possible failure in lower seam entry roofs under given conditions of geology and innerburden loading. The next step is to determine an optimum support plan for the predicted conditions in a given situation. The effect of different types of supports and their placement should be investigated to devise a comprehensive ground control plan compatible with geology and loading conditions.

The finite element results formed the basis of the stability assessment model developed in this study. Although these results were found to be consistent with the observed field conditions, they need to be further verified by an extensive back analysis. It is proposed that a data bank of case studies should be compiled based on detailed evaluations of localized site damage in areas subject to interaction. Each case study should contain details of specific failure modes, mechanisms, roof and floor lithology, sequence, structure, spatial, support and mining method.

References

Akram, M., Haycocks, C., Haycocks, S. G. and Karmis, M., 1991, "Ultra-Close Seam Failure Mechanisms," *Proceedings*, 9th Annual Workshop, Generic Mineral Technology Center, Mine Systems Design and Ground Control, Nov., Lexington, Kentucky, pp. 73-79.

Adler, L., and Sun, M., 1976, "Ground Control in Bedded Formations," *Bulletin 28*, Research Division, VPI & SU, Dec., 266 pp.

Agapito, J. F. T., Mitchell, S. J., and Hardy, M. P., 1980, "A Study of Ground Control Problems in Coal Mines with High Horizontal Stresses," *Proceedings*, 21st US Symposium on Rock Mechanics, Missouri-Rolla, pp. 820-825.

Aggson, J. R., 1978, "Coal Mine Floor Heave in Beckley Coalbed, an Analysis," *RI 8274*, US Bureau of Mines, 32 pp.

Aggson, J. R., and Curran, J., 1978, "Coal Mine Ground Control Problems Associated with a High Horizontal Stress Field," *Preprint*, SME-AIME, Denver, CO, 12 pp.

Aggson, J. R., and Mouyard, D. P., 1988, "Geomechanical Evaluation of a Coal Mine Arched Entry," *International Journal of Mining and Geological Engineering*, Vol. 6, pp. 185-193.

Ahola, M. P., Donato, D. A., and Kripakov, N. P., 1991, "Application of Numerical Modeling Techniques to Analysis of Cutter Roof Failure," *IC 9287*, US Bureau of Mines, 28 pp.

Barton, N., 1976, "Recent Experiences with the Q-System of Tunnel Support Design. *Proceedings*, Symposium on Exploration for Rock Engineering, Johannesburg, Vol. 1, 1976, pp. 107-117.

Bauer, E. R., 1989, "Tips on Controlling Cutter Roof Failure," *Coal Magazine*, May, pp. 80-80D.

Bauer, E. R., 1990, "Cutter Roof Failure: Six Case Studies in the Northern Appalachian Coal Basin," *IC 9266*, US Bureau of Mines, 18 pp.

Bieniawski, Z. T., 1974, "Geomechanics Classification of Rock Masses and its Application in Tunneling," *Proceedings*, 3rd International Congress on Rock Mechanics, ISRM, Denver, CO, Vol. 11A, 1974, pages 27-32.

Bieniawski, Z. T., 1976, "Rock Mass Classification in Rock Engineering," *Proceedings*, Symposium on Exploration for Rock Engineering, Johannesburg, Vol. 1, pp. 97-106.

Bieniawski, Z. T., 1989, *Engineering Rock Mass Classification*, John Wiley & Sons, New York, 251 pp.

Blevins, C. T., 1982, "Coping With High Lateral Stresses in an Underground Illinois Coal Mine," *Preprint 82-156*, SME - AIME, Feb., Dallas Meeting.

Blevins, C. T., and Dopp, D., 1985, "Ground Control Experiences in High Horizontal Stress Field at Inland Steel Coal Mine No. 2," *Proceedings*, 4th Conference on Ground Control in Mining, July 22-24, Morgantown, WV, pp. 227-233.

Brady, B. H., and Brown, E. T., 1985, *Rock Mechanics for Underground Mining*, George Allen & Unwin Ltd., London, U. K.

Chase, F. E., and Sames, G. P., 1983, "Kettlebottoms: Their Relation to Mine Roof and Support," *RI 8785*, US Bureau of Mines, 13 pp.

Chekan, G. R., and Matetic, R. J., 1990, "Interactions Between Multiple Seam Longwall and Room-and-Pillar Operations -- A Case Study in Boone County, WV," *RI 9299*, US Bureau of Mines, 14 pp.

Chekan, G. R., and Matetic, R. J., 1992, "Analysis and Design Considerations for Superimposed Longwall Gate Roads," *RI 9305*, US Bureau of Mines, 14 pp.

Chekan, G. R., Matetic, R. J., and Galek, J. A., 1986, "Strata Interactions in Multi-Seam Mining--Two Case Studies in Pennsylvania," *RI 9056*, US.Bureau of Mines, 17 pp.

Choi, D. S., and McCain, D. L., 1980, "Design of Longwall Systems," *Transactions*, SME-AIME, Vol. 268, pp. 1761-1764.

Dahl, H. D., 1969, "A Finite Element Model for Anisotropic Yielding in Gravity Loaded Rock," *Ph. D. Dissertation*, The Pennsylvania State University, 155 pp.

Deere, D. U., 1964, "Technical Description of Rock Cores for Engineer-Purposes," *Rock Mechanics and Engineering Geology*, Vol. 1, Number 1, pp. 17-22.

Denkhaus, H. G., 1964, "Critical Review of Strata Movement Theories and Their Applications to Practical Problems," *Journal of South African Institute of Mining & Metallurgy*, Vol. 64, pp. 310-332.

Desai, C. S. and Abel, J. F., 1972, *Introduction to the Finite Element Method*, Von Nostrand Reinhold Co., New York.

Dinsdale, J. R., 1935, "Ground Pressure and Pressure Profiles Around Mining Excavations," *Colliery Engineer*, U. K., Vol. 12, pp. 406-409.

Ehgartner, B. L., 1982, "Pillar Load Transfer Mechanisms in Multi-Seam Mining," *M. S. Thesis*, VPI & SU, Blacksburg, VA, 164 pp.

Fraher, R., Sellami, M., Haycocks, C., and Karmis, M., 1992, "A Hazard Approach to Multi-Seam Reserve Determination," *Proceedings*, 9th Annual Workshop, Generic Mineral Technology Center, Mine Systems Design and Ground Control, Nov., Lexington, Kentucky, pp. 81-89.

Grenoble, B. A., 1985, "Microcomputer Simulation of Near Seam Interaction," *M. S. Thesis*, VPI & SU, Blacksburg, VA, 128 pp.

Grenoble, B. A., and Haycocks, C., 1985, "Design Factors in Near Seam Interaction," *Proceedings*, 4th Conference on Ground Control in Mining, Morgantown, WV, pp. 166-177.

Hanna, K., 1988, "Design of Coal Mine Entry Intersection," *Preprint 88-39*, SME-AIME, 11 pp.

Hanna, K., and Haramy, K., 1985, "Field Investigation of Roof and Pillar Stability in Coal Mine Intersections," *Proceedings*, 2nd Conference on Ground Control Problems in the Illinois Basin, pp. 76-83.

Hanna, K., Haramy, K., and Conover, D., 1986, "Effect of High Horizontal Stress on Coal Mine Entry Intersection Stability," *Proceedings*, 5th Conference on Ground Control in Mining, Morgantown, WV, pp. 167-182.

Haycocks, C., 1976, "Ameliorating Coal Mine Roof Condition," *Proceedings*, 7th Annual Institute on Coal Mining Health, Safety and Research, Blacksburg, VA, pp. 269-284.

Haycocks, C., 1991, "Ground Control in Multi-Seam Mining," *Proceedings*, 22nd Annual Institute on Coal Mining Health, Safety and Research, Blacksburg, VA, pp. 123-131.

Haycocks, C., Ehgartner, B., Karmis, M., and Topuz, E., 1982, "Pillar Load Transfer Mechanisms in Multi-Seam Mining," *Preprint 82-69*, SME-AIME, 7 pp.

Haycocks, C., and Karmis, M., 1979, "An Overview of Roof Control with Regard to Coal Mine Layout and Design," *Proceedings*, 10th Annual Inst. on Coal Mining Health, Safety and Research, VPI&SU, Blacksburg, VA, pp. 159-173.

Haycocks, C. and Karmis, M., 1983, "Ground Control Mechanisms in Multi-Seam Mining," *Final Report, for the Office of Mineral Institute*, US Bureau of Mines, Oct., 328 pp.

Haycocks, C., Wu, W., and Zhou, Y., 1987, "Integrated Design for Stability in Multiple-Seam Mining," *IC 9173*, US Bureau of Mines, pp. 44-56.

Haycocks, C., and Zhou, Y. X., 1990, "Multi-Seam Mining -- A State-of-the-Art Review," *Proceedings*, 9th International Conference on Ground Control in Mining, June, pp. 1-11.

Hill, J. L., 1986, "Cutter Roof Failure: An Overview of the Causes and Methods for Control," *IC 9094*, US Bureau of Mines, 27 pp.

Hladysz, Z., 1985, " Analysis of Risk in Multiple Seam Mines," *Preprint 85-357*, SME-AIM 8 pp.

Hoek, E., and Brown, E. T., 1982, *Underground Excavations in Rock*, Institute of Mining and Metallurgy, London, pp. 100-101.

Hoek, E., Grabinsky, M. W., and Diederichs, M. S., 1991, "Numerical Modeling for Underground Excavation Design," *Transactions*, Institute of Mining and Metallurgy, Vol. 100, pp. A22-A30.

Holland, C. T., 1951, "Multiple-seam Mining," *Coal Age*, August, pp. 89-93.

Hsiung, S. M., and Peng, S. S., 1985, "Chain Pillar Design for U. S. Longwall Panels," *Mining Science and Technology*, Vol. 2, pp. 279-305.

Ingram, D. K. and Molinda, G. M., 1988, "Relationship Between Horizontal Stresses and Geological Anomalies in two Coal Mines in Southern Illinois," *RI 9189*, US Bureau of Mines, 18 pp.

Jaeger, J. C. and Cook, N. G. W., 1969, *Fundamentals of Rock Mechanics*, Methuen, London, pp. 184-194.

Jeremic, M.L., 1981, "Coal Mine Roadway Stability in Relation to Lateral Tectonic Stress - Western Canada," *Mining Engineer*, pp. 704-709.

Jeremic, M. L., 1985, *Strata Mechanics in Coal Mining*, A. A. Balkema, Rotterdam, pp. 148.

Johnson, G., 1973, "Rock Mechanics, a Nomogram for the Assessment of Roadway Conditions," *Colliery Guardian*, Vol. 221, pp. 16-20.

Jones, R. E. and Pariseau, W. G., 1990, "Sandstone Escarpment Stability in Vicinity of Longwall Mining," *Proceedings*, 31st US Symposium on Rock Mechanics, Balkema, pp. 555-562.

Karabin, G. J., Cybulski J. A., and Kramer, J. M., 1982, "The Formation and Effects of Transient Abutment Stress During Non-uniform Face Advance," *Proceedings*, 2nd Conference on Ground Control in Mining, Morgantown, WV, pp. 233-240.

King, H. G., and Whittaker, B. N., 1971, "A Review of Current Knowledge on Roadway Behavior," *Proceedings*, Symposium on Roadway Strata Control, Institute of Mining and Metallurgy, pp. 73-87.

King, H. G. and Whittaker, B. N., 1972, "The Effects of Interaction in Mine Layouts," *Proceedings*, 5th International Conference on Strata Control, London, Paper No. 17, 11 pp.

Kripakov, N. P., 1991, "Application of Numerical Modeling Techniques to the Analysis of Cutter Roof Failure," *IC 9287*, US Bureau of Mines, 28 pp.

Kripakov, N. P., Beckett, L. A., Donato, D. A., and Durr, J. S., 1988, "Computer-Assisted Mine Design for Longwall Mining," *RI 9172*, US Bureau of Mines, 38 pp.

Mark, C., 1989, "Longwall Pillar Design -- Some Recent Developments," *Preprint 89-103*, SME-AIME, 9 pp.

Mark, C., 1990, "Pillar Design Methods for Longwall Mining," *IC 9247*, US.Bureau of Mines, 50 pp.

Mark, C., 1991, "Horizontal Stress and its Effects on Longwall Ground Control," *Mining Engineering*, Nov., pp. 1356-1360.

Mark, C, and Bieniawski, Z. T., 1986, "An Empirical Method For The Design of Chain Pillars for Longwall Mining," *Proceedings*, 27th US Symposium on Rock Mechanics, pp. 415-422.

McCabe, K. W., and Pascoe, W., 1978, "Sandstone Channels: Their Influence on Roof Control in Coal Mines," *MSHA Report No. 096*, 24 pp.

Matetic, R. J., Chekan, G. J., 1988, "Comparative Study of Pillar Load Transfer Associated with Multiple-Seam Mining," *RI 9176*, US Bureau of Mines, 20 pp.

Matetic, R. J., Chekan, G. J., Galek, J. A., 1987, "Pillar Load Transfer Associated with Multi-Seam Mining," *RI 9066*, US Bureau of Mines, 23 pp.

McMahon, T. J., and Pariseau, W. G., 1989, "A Comparison Between Two and Three-Dimensional Numerical Models of a Coeur d'Alene Mine," *Proceedings*, 30th US Symposium on Rock Mechanics, Balkema, pp. 963-970.

Merritt, A. H., 1972, "Geologic Prediction for Underground Excavations," *Proceedings*, First North American Rapid Excavation and Tunneling Conference, AIME, New York, pp. 115-132.

Milici, R. C., Gathright, T. M., Miller, B. W., and Gwin, M. R., 1982, "Geological Factors Related to Coal Mine Roof Falls in Wise County, Virginia, " *Appalachian Regional Commission Report No. CO-7232-80-1-302-0206*, 103 pp.

Moebs, N. N., 1984, "Geologic Factors in Coal Mine Roof Stability - A Progress Report," *IC 8976*, U. S. Bureau of Mines.

Moebs, N. N., 1986, "Coal Mine Roof Instability: Categories and Causes," *IC 9076*, US Bureau of Mines, 15 pp.

Moebs, N. N., and Bauer, E. R., 1989, "Appalachian Roof Instability," *Coal Magazine*.

Moebs, N. N., and Ellenberger, J. L., 1982, "Hazardous Roof Structures in Appalachian Coal Mines," *Proceedings*, Ground Control in Room and Pillar Mining, ed. Chug, Y. P., SME - AIME, NY. pp. 9-16

Moebs, N. N., and Stateham, R. M., 1986, "Coal Mine Roof Instability: Categories and Causes," *IC 9076*, US Bureau of Mines, 15 pp.

National Coal Board, 1954, "Divisional Stress Control Research Committee, National Coal Board Durham and Northern Divisions Report of the Effects of Working in Adjacent Seams upon New Developments," *Transactions*, IME Vol. 113, U. K.

National Coal Board, 1972, "Design of Mine Layout," *Working Party Report*, London, U. K., 41 pp.

Pariseau, W. G., 1969, "Plasticity Theory for Anisotropic Rocks and Soils," *Proceedings*, 10th Symposium on Rock Mechanics, University of Texas, Austin, pp. 267-295.

Pariseau, W. G., 1978, "A Two Dimensional Finite Element Approach to the Evaluation of Underground Coal Mine Stability," *Final Report for US Bureau of Mines under Contract No. H0220077*, 172 pp.

Pariseau, W. G., 1992, *SME Mining Engineering Handbook*, ed. Hartman, pp. 829-847.

Pariseau, W. G., 1993, *Personal Communications*.

Pariseau, W. G., McDonald, M. M., Johnson, J. C., and Poad, M. E., 1992, "Personal Computer Finite Element Modeling for Ground Control and Mine Design," *Workshop*, US Bureau of Mines, Denver, CO, pp. 43.

Park, D. W., 1991, "Stability Analysis of a Room-and-Pillar Mine with Thinly Laminated Roof, Strong Pillar and Weak Floor," SME.

Park, D. W., Jiang, Y. M., Morley, L. A. and Keeton, W., 1992, "Stability Analysis of a Room-and-Pillar Mine with Thinly Laminated Roof, Strong Pillars, and Weak Floor," *Mining Engineering*, Vol. 44, No. 11, ,Nov., pp. 1355-1360.

Peng, S. S. and Chandra, U., 1980, "Getting the Most from Multiple-Seam Reserves," *Coal Mining and Processing*, Nov., pp. 78-84.

Peng, S. S., and Chiang, H. S., 1982, "Roof Stability in Longwall Faces," *Proceedings*, 1st. Int. Conference. on Stability in Underground Mining," Vancouver, Canada, Aug., pp. 295-339.

Peng, S. S. and Chiang, H. S., 1984, *Longwall Mining*, John Wiley & Sons, NY, p. 51.

Plumb, R. A., and Cox, J. W., 1987, "Stress Directions in Eastern North America Determined to 4.5 km from Borehole Elongation Measurements," *Journal of Geophysical Research*, Vol. 92, No. B6, May, pp. 4905 - 4916.

Reddy, J. N., 1984, *An Introduction to the Finite Element Method*, Mcgraw Hill Book Company, NY, 495 pp.

Serata, S., 1984, "Stress Control Method Applied to Stabilization of Underground Coal Mine Openings," *Proceedings*, 25th US Symposium on Rock Mechanics, SME-AIME, pp. 583-590.

Spedding, M., 1976, "Multiple-Seam Mining," *Proceedings*, 17th US.Symposium on Rock Mechanics, pp. 22-28.

Stassen, P., and Van Duyse, H., 1972, "Harmful Influence on Face on the Roadways in a Colliery Layout," *Proceedings*, 5th International Conference on Strata Control, p. 125.

Stefanko, R., 1983, *Coal Mine Technology Theory and Practice*, SME-AIME, p. 84.

Stemple, D. T., 1956, "A Study of Problems Encountered in Multiple Seam Mining in the Eastern United States," *Bulletin 5*, Virginia Polytechnic Institute, Vol. XLIX, March, 64 pp.

Su, W. H., and Peng, S. S., 1984, "An Investigation of the Causes of Roof Falls in a Deep Underground Coal Mine," *Preprint 84-433*, SME-AIME, 4 pp.

Su, W. H., and Peng, S. S., 1987, "Cutter Roof and its Causes," *Mining Science and Technology*, vol. 4, pp. 113-132.

Szwilski, T., 1979, "Evaluation of Structural Properties of Coal Seams," *Proceedings*, 20th US Symposium on Rock Mechanics, pp. 59-65.

Tandanand, S., and Thill, R. E., 1987, "Mechanical Behavior of Coal Measure Rocks: Elastic-Inelastic Behavior," *RI 9109*, US Bureau of Mines, 28 pp.

Terzaghi, K., 1946, "Rock Defects and Loads on Tunnel Supports," Rock Tunnelling with Steel Supports, Youngstown, OH, pp. 15-99.

Timoshenko, S. P., and Goodier, J. N., 1970, *Theory of Elasticity*, 3rd ed., McGraw-Hill Inc., NY.

Wang, F. D., Panek, L. A., and Sun, M. C., 1971, "Stability Analysis of Underground Openings Using a Coulomb Failure Criteria," *Transactions*, SME-AIME, Vol. 250, pp. 317-21.

Wang, F. D., Ropchan, D. M., and Sun, M. C., 1974, "Structural Analysis of a Coal Mine Opening in Elastic, Multilayered Material," *RI 7845*, US Bureau of Mines.

Wen, H., and Peng, S. S., 1986, "Cutter Roof and its Causes," *Mining Science and Technology*, pp. 113-132.

Whittaker, B. N., 1974, "An Appraisal of Strata Control Practice," *Mining Engineer*, London, U. K.,pp. 9-24.

Whittaker, B. N., and Hodgkinson, D. R., 1971, "Design and Layout of Longwall Workings," *Mining Engineering*, London, U. K., Vol. 131, No. 134, pp. 79-96.

Whittaker, B. N., and Pye, J. H., 1975, "Design and Layout Aspects of Longwall Methods of Coal Mining," *Proceedings*, 16th US Symposium on Rock Mechanics, pp. 303-330.

Wickham, G. E., Tiedemann, H. R., and Skinner, E. H., 1972, "Support Determination Based on Geological Predictions," *Proceedings*, 1st North American Rapid Excavation and Tunnelling Conference, AIME, NY, pp. 43-64.

Wilson, A. H., 1982, "Pillar Stability in Longwall Mining," *Proceedings*, Symposium on State-of-the-Art of Ground Control in Longwall Mining and Subsidence, SME, Sept., pp. 85-95.

Wilson, J. W., Singh, B. D., and Nekajima, S., 1982, "Design Considerations for Mining Thick Seams and Seams Lying in the Close Proximity to Another Seam," Monogram on Rock Mechanics Applications in Mining, SME - AIME, NY.

Wu, W., 1987, "An Analysis of Close Interaction Problems in the Appalachian Coal Fields," *Ph. D. Dissertation*, VPI & SU, Blacksburg, VA, 220 pp.

Zienkiewicz, O. C., 1971, *The Finite Element Method*, 2nd Ed., McGraw Hill, London, U. K., 521 pp.

Zhou, Y., and Haycocks, C., 1990, "Ultra-Close Multiple-Seam Mining," *Proceedings*, 8th Annual Workshop, Generic Mineral Technology Center, Mine Systems Design and Ground Control, Nov., Nevada, pp. 67-74.

Zhou, Y., and Haycocks, C., 1989, "Failure Mechanisms in Ultra-Close Seam Mining," *Proceedings*, 30th US Symposium on Rock Mechanics, 8 pp.

Appendix A Preprocessing Code

```
************************************************************************
************************************************************************
************** MESH GENERATION PROGRAM ***************
************************************************************************
************************************************************************

c  this program takes the segment dimensions of the mesh in the x and y
c  directions and generates  coordinates of each node and information about
c  the connectivity of each element.

      DIMENSION XC(10000),YC(10000),KEL(10000),NDO(10000,5)
      DIMENSION X(100), Y(100), M(100), NC(10000)

c  data is read from INPUT.DAT file. the first two elements of this input
c  file are the number of nodes in the x and y directions respectively.
c  after this the values of x segments and their material codes are given
c  in order and it is followed by y segments in order.
c  NUMX is the number of nodes in the x direction and NUMY is the number of
c  number of nodes in the y direction.

      OPEN(1, FILE='INPUT.DAT')
      READ(1,*)NUMX
      READ(1,*)NUMY

c  the values of x segments and their material codes are read into the X
c  and the M arrays respectively in a formatted manner.

      DO 10 I=1,NUMX
      READ(1,70)X(I),M(I)
 10   CONTINUE
 70   FORMAT(F3.1,I1)

c  the values of y segments are read into Y array.

      DO 20 I=1,NUMY
      READ(1,*)Y(I)
 20   CONTINUE

************************************************************************
************** NODE COORDINATE GENERATION *************
************************************************************************

c  the NCD.DAT file will get the values of the node coordinates for each
c  node.

      OPEN(2,FILE='NCD.DAT')
      YCORD=0.
      NODE=0

c  YCORD will add different y-segment values on each iteration of the
c  following loop. to get the node numbers for each node the counter node
```

```
c  is set. XCORD will add the x-segment values.

      DO 30 I=1,NUMY
      XCORD=0.
      YCORD=YCORD+Y(I)
      DO 40 J=1,NUMX
      NODE=NODE+1

c  NC array contains the node number of each node.
c  XC array contains the x coordinates of nodes and YC array contains the
c  y coordinates.

      NC(NODE)=NODE
      XCORD=XCORD+X(J)
      XC(NODE)=XCORD
      YC(NODE)=YCORD
 40   CONTINUE
 30   CONTINUE

c  in order to get the output in the required format the following program
c  segment is used.

      IC=0
 110  IC=IC+1
      WRITE(2,60)NC(IC),XC(IC),YC(IC),NC(IC+1),XC(IC+1),YC(IC+1),
     +NC(IC+2),XC(IC+2),YC(IC+2)
      IC=IC+2
      IF ((NODE-2).GT.IC) THEN
      GOTO 110
      ELSE
      IF ((NODE-IC).EQ.2) THEN
      WRITE(2,61)NC(IC+1),XC(IC+1),YC(IC+1),NC(IC+2),XC(IC+2),YC(IC+2)
      ELSE
      IF ((NODE-IC).EQ.1) WRITE(2,62)NC(IC+1),XC(IC+1),YC(IC+1)
      ENDIF
      ENDIF
 60   FORMAT(3(I5,2F10.3))
 61   FORMAT(2(I5,2F10.3))
 62   FORMAT(I5,2F10.3)

*************************************************************************
********** ELEMENT CONNECTIVITY GENERATION **********
*************************************************************************

c  the ELEM.DAT file contains the node connectivity information. KEL array
c  contains the element number.
c  NDO is a two dimensional array; the size being number of elements
c  multipied by 5.
c  each fist dimension gives the element number.
c  the first four second dimensions will give the four node numbers forming
c  the element and the fifth second dimension gives the material code of
```

```
c  the element.

      OPEN(3,FILE='ELEM.DAT')
      K=0
      DO 90 I=1,NUMY-1
      DO 80 JN=1,NUMX-1
      K=K+1
      J=JN+(I-1)*NUMX
      KEL(K)=K
      NDO(K,1)=NC(J)
      NDO(K,2)=NC(J+1)
      NDO(K,3)=NC(J+NUMX+1)
      NDO(K,4)=NC(J+NUMX)
      NDO(K,5)=M(JN+1)
 80   CONTINUE
 90   CONTINUE

c  NE is the total number of elements.

      NE=(NUMY-1)*(NUMX-1)

c  the follwing program segment is used to write the output in the desired
c  format.

      I=0
 120  I=I+1
     WRITE(3,100)KEL(I),NDO(I,1),NDO(I,2),NDO(I,3),NDO(I,4),NDO(I,5),
     +KEL(I+1),NDO(I+1,1),NDO(I+1,2),NDO(I+1,3),NDO(I+1,4),NDO(I+1,5)
      I=I+1
      IF ((NE-1).GT.I) GOTO 120
      IF (I.EQ.NE) GOTO 130
     WRITE(3,101)KEL(I+1),NDO(I+1,1),NDO(I+1,2),NDO(I+1,3),
     + NDO(I+1,4),NDO(I+1,5)

 100  FORMAT(2(6I5))
 101  FORMAT(6I5)

 130  STOP
      END
```

```
**************************************************************************
**************************************************************************
************ BOUNDARY CONDITIONS PROGRAM **************
**************************************************************************
**************************************************************************

c  this program is used to find the force and displacement values
c  of the individual boundary nodes of the mesh under different loading and
c  displacement conditions.

      DIMENSION XC(10000),YC(10000),FADD(100),FNCLD(100)
      DIMENSION FYOUT(100),FXOUT(100)
      DIMENSION X(100), Y(100), M(100), NC(10000)

c  data is read from INPUT.DAT file. the first two elements of this input
c  file are the number of nodes in the x and y directions respectively.
c  after this the values of x segments and their material codes are given
c  in order and it is followed by y segments in order.
c  NUMX is the number of nodes in the x direction and NUMY is the number of
c  number of nodes in the y direction.

      OPEN(1, FILE='INPUT.DAT')
      READ(1,*)NUMX
      READ(1,*)NUMY

c  the values of x segments and their material codes are read into the X
c  and the M arrays respectively in a formatted manner.
c  the values of y segments are read into Y array.

      DO 10 I=1,NUMX
      READ(1,70)X(I),M(I)
 10   CONTINUE
 70   FORMAT(F3.1,I1)

      DO 20 I=1,NUMY
      READ(1,*)Y(I)
 20   CONTINUE

      YCORD=0.
      NODE=0

c  this program segment genrates the node coordinates and puts them into
c  the arrays XC and YC

      DO 30 I=1,NUMY
      XCORD=0.
      YCORD=YCORD+Y(I)
      DO 40 J=1,NUMX
      NODE=NODE+1
      NC(NODE)=NODE
      XCORD=XCORD+X(J)
```

```
      XC(NODE)=XCORD
      YC(NODE)=YCORD
 40   CONTINUE
 30   CONTINUE

c  the input file BOUND.DAT contains the input information to the program
c  regarding the general loading and displacement conditions at the
c  boundary of the mesh.
c  the values to the variables IDEN, VSTR, HSTR, KT, KS are read in order
c  IDEN is the identifier whose value tells the program if there is any
c  additional load on top of the mesh.
c  the IDEN=0 implies that there is no additional load
c  the value of 1 signifies an additional uniform load and a value of 2
c  tells the program that there is an additional ramp load and a value 3
c  tells the program that there is a uniform load upto a certain point and
c  after that the load is a ramp function.
c  the value of VSTR is the vertical stress and the value of HSTR is the
c  horizontal stress.
c  KT is the code value for the top nodes and KS is the code vlaue for the
c  side nodes. these code vlaues are required by UTAH-2 program and their
c  significance is documented with UTAH-2 literature.

      OPEN(5,FILE='BOUND.DAT')
      READ(5,*)IDEN
      READ(5,*)VSTR
      READ(5,*)HSTR
      READ(5,*)KT
      READ(5,*)KS

      IF (IDEN.EQ.0) GOTO 80
      IF (IDEN.EQ.1.OR.IDEN.EQ.2) THEN

c  this option is reached if there is additional load on top of the mesh.
c  FLOADVAL takes the vlaue of the load and NEND1 takes the value of the
c  node upto which the uniform load is applied.  NEND2 is read as the
c  second node upto which a linearly increasing load will apply if such
c  is the case.

      READ(5,*)FLOADVAL
      READ(5,*)NSTRT
      READ(5,*)NEND1
      ELSE
      READ(5,*)FLOADVAL
      READ(5,*)NSTRT
      READ(5,*)NEND1
      READ(5,*)NEND2
      ENDIF

 80   CLOSE(5)

c  the x and y displacement values of each node are given by DX and DY and
```

```
c  the force values by FX and FY respectively. KN gives the code of the
c  node as given by KT or KS and as a value of 0 is taken for two extreme
c  bottom nodes.

*************************************************************************
***************** BOTTOM NODE CONDITIONS ******************
*************************************************************************

      OPEN(4,FILE='LOAD.DAT')
      DX=0.
      DY=0.
      FX=0.
      FY=0.
      KN=0

c  the two extreme bottom nodes are written first with the node code 0.
c  all the load values are taken 0 for all the bottom nodes

      WRITE(4,200)NC(NUMX),KN,DX,DY,FX,FY
      WRITE(4,200)NC(NUMX*NUMY),KN,DX,DY,FX,FY
      KN=1

c  a node code of 1 is specified for the rest of the bottom nodes and
c  are written next to the file LOAD.DAT

      DO 300 II=2,NUMY-1
      WRITE(4,200)NC(NUMX*II),KN,DX,DY,FX,FY
 300  CONTINUE

*************************************************************************
****************** SIDE NODE CONDITIONS ********************
*************************************************************************

      KN=KS

c  KN takes the side node code and the value of force on each side node
c  is calculated using simple mathematics.  FYOUT array contains the
c  magnitude of that force for each side node. note that the FX values
c  for each side node are 0. these FYOUT values are same for either side
c  of the mesh.

      H=HSTR*6
      DO 210 I=3,NUMX-2
      FYOUT(I)=(X(I)+X(I+1))*H
 210  CONTINUE
      FYOUT(2)=(2*X(2)+X(3))*H
      FYOUT(NUMX-1)=(2*X(NUMX)+X(NUMX-1))*H

      DO 310 J=2,NUMX-1
      WRITE(4,200)NC(J),KN,DX,DY,FX,FYOUT(J)
      WRITE(4,200)NC(J+NUMX*(NUMY-1)),KN,DX,DY,FX,-1.*FYOUT(J)
```

```
310  CONTINUE

*************************************************************************
******************** TOP NODE CONDITIONS ********************
*************************************************************************

c  FXOUT contains the FX values for the top nodes without considering any
c  additional load.

      KN=KT
      V=VSTR*6
      DO 220 I=2,NUMY-1
      FXOUT(I)=(Y(I)+Y(I+1))*V
220   CONTINUE
      FXOUT(1)=Y(2)*V
      FXOUT(NUMY)=Y(NUMY)*V

      DO 335 I=1,NUMY
      FNCLD(I)=0.
      FADD(I)=0.
335   CONTINUE

c  this segment of the program takes control to specific program segments
c  so that different loading conditions are taken care of.

      IF (IDEN.EQ.0) GOTO 330
      IF (IDEN.EQ.2) GOTO 350
      IF (IDEN.EQ.3) GOTO 360

c  this program segment is executed for the condition that there is a
c  uniform load only, starting at NSTRT and ending at NEND1.
c  FNCLD is an array giving the load function so that the values of the
c  additional loads are calculated with ease.
c  FADD gives these additional load values at each node.

      D=0.
      DO 340 I=NSTRT,NEND1-1
      D=D+Y(I+1)
340   CONTINUE
      S=FLOADVAL/D
      DS=0.
      DO 345 I=NSTRT,NEND1-1
      DS=DS+Y(I+1)
      FNCLD(I+1)=S*DS*12
345   CONTINUE
      DO 347 I=NSTRT,NEND1-1
      FADD(I)=(FNCLD(I)/6+FNCLD(I+1)/3)*Y(I+1)+(FNCLD(I-1)/3
     + + FNCLD(I)/6)*Y(I)
347   CONTINUE
      FADD(NEND1)=(FNCLD(NEND1-1)/3+FNCLD(NEND1)/6)*Y(NEND1)
```

```
      GOTO 330

c  this program segment is used to calculate the additional load values
c  because of a triangular load (ramp) only.

 350  VADD=FLOADVAL*6
      DO 352 I=NSTRT+1,NEND1-1
      FADD(I)=(Y(I)+Y(I+1))*VADD
 352  CONTINUE
      FADD(NSTRT)=Y(NSTRT+1)*VADD
      FADD(NEND1)=Y(NEND1)*VADD
      GOTO 330

c  if there is a combination of uniform and ramp load, the program control
c  goes to this segment.

 360  D=0.
      DO 361 I=NSTRT,NEND1-1
      D=D+Y(I+1)
 361  CONTINUE
      S=FLOADVAL/D
      DS=0.
      DO 362 I=NSTRT,NEND1-1
      DS=DS+Y(I+1)
      FNCLD(I+1)=S*DS*12
 362  CONTINUE
      DO 363 I=NSTRT,NEND1-1
      FADD(I)=(FNCLD(I)/6+FNCLD(I+1)/3)*Y(I+1)+(FNCLD(I-1)/3
     + + FNCLD(I)/6)*Y(I)
 363  CONTINUE
      FENDIM1=(FNCLD(NEND1-1)/3+FNCLD(NEND1)/6)*Y(NEND1)

c  the load values are calculated from NEND1 to NEND2 as the ramp.

      VADD=FLOADVAL*6
      DO 364 I=NEND1+1,NEND2-1
      FADD(I)=(Y(I)+Y(I+1))*VADD
 364  CONTINUE
      FENDIM2=Y(NEND1+1)*VADD
      FADD(NEND2)=Y(NEND2)*VADD
      FADD(NEND1)=FENDIM1+FENDIM2

c  the eventual values of the load are put in the FXOUT and written to
c  the output file.

 330  DO 370 I=1,NUMY
      FXOUT(I)=FXOUT(I)+FADD(I)
 370  CONTINUE

      DO 320 J=0,NUMY-1
      WRITE(4,200)NC(J*NUMX+1),KN,DX,DY,FXOUT(J+1),FY
```

```
320  CONTINUE

200  FORMAT(2I5,4F10.0)

     STOP
     END
```

```
*************************************************************************
*************************************************************************
****************** CUTELEMENT PROGRAM ***********************************
*************************************************************************
*************************************************************************

c this program is used to find the elements in a cut sequence. only the
c starting element number, the number of rows of the opening, and the
c the number of columns of the opening are given.  this program was
c developed to facilitate the formation of the list of elements for
c different openings in the same mesh.

      DIMENSION NOUT(10000)

c the input file INCUT.DAT gives the number of nodes in the x direction,
c the number of nodes in the y direction and the total number of the
c openings NOPEN.

      OPEN(1,FILE='INCUT.DAT')
      READ(1,*)NUMX
      READ(1,*)NUMY
      READ(1,*)NOPEN

c an outer I loop makes the program to compute the elements in an opening
c as many times as there are the openings.

      ICNT=0
      DO 10 I=1,NOPEN
      READ(1,*)NSE
      READ(1,*)NROW
      READ(1,*)NCLM

c the element numbers are written to NOUT array so that only the elements
c belonging to the opening are written.

      DO 20 M=1,NCLM
      DO 30 K=1,NROW
      ICNT=ICNT+1
      NOUT(ICNT)=NSE+(M-1)*(NUMX-1)+K-1
30    CONTINUE
20    CONTINUE
10    CONTINUE

c UTAH-2 requires that the cut element file has a -1 at the begining.

      OPEN(2,FILE='OUTCUT.DAT')
      INTEGE=-1
      WRITE(2,51)INTEGE
51    FORMAT(I5)

c the following program segment puts the output data in the required
```

```
c  format.

      INTICNT= INT(ICNT/10)
      IREMAIN= ICNT-10*INTICNT
      DO 40 I=1,INTICNT
      WRITE(2,50)(NOUT(K+(I-1)*10),K=1,10)
 40   CONTINUE
      IF (IREMAIN.EQ.0) GOTO 60
      WRITE(2,50)(NOUT(K+INTICNT*10),K=1,IREMAIN)
 50   FORMAT(10(I5))

 60   STOP
      END
```

Appendix B Case Studies Data Sheets

CASE #:1

SOURCE OF INFORMATION:	Chekan, 1990
NAME/LOCATION OF MINE:	Boone County, WV
LOWER SEAM:	
Bed Name:	Eagle
Thickness:	72 inches
Method of Extraction:	Longwall
Extraction Ratio:	
Immediate Roof:	Dark gray and black shale overelain by sandstone
Immediate Floor:	Dark gray shale
INNERBURDEN:	
Thickness:	800 feet
Nature of Strata:	Interbedded sandstone and shale
Percent of Hardrock:	40 to 50 %
UPPER SEAM:	
Bed Name:	Dorothy
Thickness:	72 inches
Method of Extraction:	Room and Pillar
Extraction Ratio:	
Immediate Roof:	gray shale
Immediate Floor:	Medium grained sandstone
OVERBURDEN:	
Cover thickness:	300 to 500 feet
Nature of Strata:	Shale and Sandstone

CASE #:2

SOURCE OF INFORMATION:	Stemple, 1956
NAME/LOCATION OF MINE:	McDowell County, WV
LOWER SEAM:	
Bed Name:	Pocahontas No.3
Thickness:	44 inches
Method of Extraction:	Room and Pillar
Extraction Ratio:	75%
Immediate Roof:	20-60 inches clod slate overlain by a fairly firm shale; sandstone about 10 feet above the coal.
Immediate Floor:	"Slate", fairly firm.
INNERBURDEN:	
Thickness:	60-70 feet
Nature of Strata:	Shales and some fairly thick sandstones.
Percent of Hardrock:	45%
UPPER SEAM:	
Bed Name:	Pocahontas No.4
Thickness:	Faulty. Average 60 inches where good.
Method of Extraction:	Room and Pillar
Extraction Ratio:	
Immediate Roof:	Soft "slate" and rash, about 29 inches thick.
Immediate Floor:	6-8 inches soft "slate" underlain by hard shale.
OVERBURDEN:	
Cover thickness:	500 feet.
Nature of Strata:	Shales, etc.; 5-6 feet sandstone beds, 25-40 feet thick at varying intervals.

CASE #: 3

SOURCE OF INFORMATION:	Stemple, 1956
NAME/LOCATION OF MINE:	Raleigh County, WV
LOWER SEAM:	
Bed Name:	Pocahontas No. 4
Thickness:	Avg. 36 inches, plus a parting midway in the seam 1-18 inches thick.
Method of Extraction:	Room and Pillar
Extraction Ratio:	90%
Immediate Roof:	Hard gray shale 3 feet or more thick, overlain in places by a rider coal, then sandstone. Generally good.
Immediate Floor:	Soft "slate", tears up easily.
INNERBURDEN:	
Thickness:	270-300 feet
Nature of Strata:	Several sandstone beds up to 25 feet thick; balance is shales and sandy shales.
Percent of Hardrock:	15%
UPPER SEAM:	
Bed Name:	Beckley
Thickness:	One bench: 20-56 inches. Two benches: Top 30-72 inches. Parting 10-42 inches. Bottom 6-42 inches.
Method of Extraction:	Room and Pillar
Extraction Ratio:	87-90%
Immediate Roof:	Slate 2 inches to several feet; some sandstone top, from excellent to very poor.
Immediate Floor:	"Slate" or sandy shale, generally firm.
OVERBURDEN:	
Cover thickness:	450 feet
Nature of Strata:	Predominantly shale, with a sandstone bed up to 50 feet thick about 100 feet over the upper seam.

CASE #: 4

SOURCE OF INFORMATION:	Stemple, 1956
NAME/LOCATION OF MINE:	Floyd County, VA
LOWER SEAM:	
Bed Name:	Elkhorn No. 1
Thickness:	42-48 inches
Method of Extraction:	Room and Pillar
Extraction Ratio:	75%
Immediate Roof:	6-12 inches drawslate, overlain by 5 or 6 feet blue shale; in some cases this is overlain with sandstone. Poor top.
Immediate Floor:	Slate (shale), firm.
INNERBURDEN:	
Thickness:	20-35 feet
Nature of Strata:	Mostly "slate"; where interval is maximum, sandstone appears.
Percent of Hardrock:	30%
UPPER SEAM:	
Bed Name:	Elkhorn No. 2
Thickness:	34-38 inches plus 4-6 inches of bone.
Method of Extraction:	Room and Pillar
Extraction Ratio:	75% approx.
Immediate Roof:	Hard sandy shale or sandstone. Good top.
Immediate Floor:	Hard "slate"
OVERBURDEN:	
Cover thickness:	Avg. 500 feet
Nature of Strata:	Mostly sandstones, some from 30-120 feet thick; shales, 20-60 feet thick; thin coal seams and fireclays.

CASE #: 5

SOURCE OF INFORMATION:	Stemple, 1956
NAME/LOCATION OF MINE:	Cambria County, PA
LOWER SEAM:	
Bed Name:	Lower Kittanning
Thickness:	42-48 inches
Method of Extraction:	Room and Pillar
Extraction Ratio:	85%
Immediate Roof:	1-8 inches bone (comes with coal) overlain usually by black laminated "slate", which falls often up to the Middle Kittanning seam, 20-25 feet above.
Immediate Floor:	Fireclay, fairly firm.
INNERBURDEN:	
Thickness:	115-125 feet
Nature of Strata:	Mostly shales; the unmined dirty Middle Kittanning seam is about 80 feet below upper seam, underlain by fireclay and with a 20 feet to 40 feet thick sandstone bed directly over it.
Percent of Hardrock:	20%
UPPER SEAM:	
Bed Name:	Upper Kittanning
Thickness:	54-60 inches
Method of Extraction:	Room and Pillar
Extraction Ratio:	85%
Immediate Roof:	Sandy shale, generally good top.
Immediate Floor:	Smooth, medium hard fireclay.
OVERBURDEN:	
Cover thickness:	450 feet
Nature of Strata:	Predominantly shales, with several sandstone beds 15-40 feet thick, lying mostly 200-300 feet above the upper seam.

CASE #: 6

SOURCE OF INFORMATION:	Stemple, 1956
NAME/LOCATION OF MINE:	McDowell County, WV
LOWER SEAM:	
Bed Name:	Pocahontas No. 3
Thickness:	Avg. 60 inches
Method of Extraction:	Room and Pillar
Extraction Ratio:	80-85%
Immediate Roof:	About 24 inches drawslate, overlain by a 2 inches rooster clay, then black shale.
Immediate Floor:	Sandy fireclay, firm.
INNERBURDEN:	
Thickness:	Avg. 67 feet
Nature of Strata:	Sandstone is in three beds, 10-20 feet thick; balance is shale and fireclay.
Percent of Hardrock:	60%
UPPER SEAM:	
Bed Name:	Pocahontas No. 4
Thickness:	Avg. 48 inches
Method of Extraction:	Room and Pillar
Extraction Ratio:	85-90%
Immediate Roof:	Normally sandstone; grey shale in some locations.
Immediate Floor:	Fireclay, fairly hard.
OVERBURDEN:	
Cover thickness:	800 feet
Nature of Strata:	Sandstones, shales and thin coals; 200 feet or so of hard sandstones show persistently above the upper seam.

CASE #: 7

SOURCE OF INFORMATION:	Stemple, 1956
NAME/LOCATION OF MINE:	Floyd County, KY
LOWER SEAM:	
Bed Name:	Elkhorn No. 1
Thickness:	Avg. 36 inches
Method of Extraction:	Room and Pillar
Extraction Ratio:	65% to 70% planned
Immediate Roof:	Mostly "slate" and some sandstone. All very good top.
Immediate Floor:	Fireclay, soft.
INNERBURDEN:	
Thickness:	24 feet
Nature of Strata:	Mostly shale or "slate".
Percent of Hardrock:	10%
UPPER SEAM:	
Bed Name:	Elkhorn No. 2
Thickness:	Avg. 38 inches
Method of Extraction:	Room and Pillar
Extraction Ratio:	65-70% Planned
Immediate Roof:	"Slate", 6-8 feet thick, overlain by sandstone. Fairly good top.
Immediate Floor:	Shale, hard.
OVERBURDEN:	
Cover thickness:	300 feet
Nature of Strata:	Predominantly "slate" (shale) No drill logs available.

CASE #: 8

SOURCE OF INFORMATION:	Stemple, 1956
NAME/LOCATION OF MINE:	Mingo County, WV
LOWER SEAM:	
Bed Name:	Lower Thacker
Thickness:	70 inches
Method of Extraction:	Room and Pillar
Extraction Ratio:	85%
Immediate Roof:	Brittle, laminated shale up to 20 feet(?) thick; sometimes sandstone.
Immediate Floor:	Firm fireclay or grey shale
INNERBURDEN:	
Thickness:	68 feet
Nature of Strata:	Sandy laminated shales, and an undulating, non-persistent sandstone up to 20 feet thick, often less.
Percent of Hardrock:	30%
UPPER SEAM:	
Bed Name:	Upper Thacker
Thickness:	50 inches
Method of Extraction:	Room and Pillar
Extraction Ratio:	80%
Immediate Roof:	Laminated shale or drawslate, 2-3 feet thick.
Immediate Floor:	Firm shale or fireclay; deteriorates when wet.
OVERBURDEN:	
Cover thickness:	Avg. 300 feet
Nature of Strata:	Shales, sandy shales, sandstone, etc., with a 35-50 feet thick sandstone bed, 2-3 feet above the upper seam.

CASE #: 9

SOURCE OF INFORMATION:	Chekan et al., 1986
NAME/LOCATION OF MINE:	Indiana County, PA
LOWER SEAM:	
Bed Name:	Lower Freeport
Thickness:	55 inches
Method of Extraction:	Room and Pillar
Extraction Ratio:	50-55%
Immediate Roof:	5-10 feet of black shale overlain by dark gray shale.
Immediate Floor:	5-6 feet of light gray fireclay underlain by gray sandy shale.
INNERBURDEN:	
Thickness:	65 feet
Nature of Strata:	Shale interbedded with sandstone
Percent of Hardrock:	40%
UPPER SEAM:	
Bed Name:	Upper Freeport
Thickness:	42 inches
Method of Extraction:	Room and Pillar
Extraction Ratio:	55-60%
Immediate Roof:	Dark gray shale 10-20 feet thick.
Immediate Floor:	5-10 feet of dark gray fireclay underlain by gray sandy shale.
OVERBURDEN:	
Cover thickness:	400 feet
Nature of Strata:	Interbedded shale and sandstone.

CASE #: 10

SOURCE OF INFORMATION:	Matetic et al., 1988
NAME/LOCATION OF MINE:	Rakeigh County, WV
LOWER SEAM:	
Bed Name:	No. 2 Gas Coalbed
Thickness:	48 inches
Method of Extraction:	Room and Pillar
Extraction Ratio:	
Immediate Roof:	
Immediate Floor:	
INNERBURDEN:	
Thickness:	40 feet
Nature of Strata:	Sandstone with innerbedded shale units.
Percent of Hardrock:	70%
UPPER SEAM:	
Bed Name:	Peerless Coalbed
Thickness:	72 inches
Method of Extraction:	Room and Pillar
Extraction Ratio:	
Immediate Roof:	
Immediate Floor:	
OVERBURDEN:	
Cover thickness:	960 feet
Nature of Strata:	Predominantly sandstone with innerbedded shale units of varying thickness.

CASE #: 11

SOURCE OF INFORMATION:	Stemple, 1956
NAME/LOCATION OF MINE:	Kanawha County, WV
LOWER SEAM:	
Bed Name:	Cedar Grove
Thickness:	34 inches
Method of Extraction:	Room and Pillar
Extraction Ratio:	80%
Immediate Roof:	12-18 inches heavy dark shale, overlain by light sandy shale about 20 feet thick.
Immediate Floor:	18 inches fireclay, soft.
INNERBURDEN:	
Thickness:	200 feet
Nature of Strata:	Several strong sandstone beds, 20-40 feet thick; balance mostly shales.
Percent of Hardrock:	55%
UPPER SEAM:	
Bed Name:	Winifrede
Thickness:	56 inches including 6 inches or 8 inches of bone in 2 partings.
Method of Extraction:	Room and Pillar
Extraction Ratio:	70%
Immediate Roof:	35 inches hard shale, overlain by sandstone 40 feet to 75 feet thick. Shale could not be held.
Immediate Floor:	Shale, firm
OVERBURDEN:	
Cover thickness:	500 feet
Nature of Strata:	Shales and sandstones, with a heavy bed of sandstone, up to 75 feet thick, close over the Winifrede seam.

CASE #: 12

SOURCE OF INFORMATION:	Stemple, 1956
NAME/LOCATION OF MINE:	Alabama
LOWER SEAM:	
Bed Name:	Woodstock
Thickness:	Avg. 39 inches
Method of Extraction:	Room and Pillar
Extraction Ratio:	62%
Immediate Roof:	Sandy shale, good top.
Immediate Floor:	Fireclay, fairly hard, underlain by dark shale.
INNERBURDEN:	
Thickness:	380 feet
Nature of Strata:	Shales and sandstone conglomerates.
Percent of Hardrock:	50%
UPPER SEAM:	
Bed Name:	Thompson
Thickness:	54 inches
Method of Extraction:	Room and Pillar
Extraction Ratio:	60% approx.
Immediate Roof:	Slate
Immediate Floor:	Sandy shale.
OVERBURDEN:	
Cover thickness:	400 feet
Nature of Strata:	Shales and sandstones. (No drill logs available.)

CASE #: 13

SOURCE OF INFORMATION:	Stemple, 1956
NAME/LOCATION OF MINE:	Kanawha County, WV
LOWER SEAM:	
Bed Name:	No. 2 Gas
Thickness:	44 inches
Method of Extraction:	Room and Pillar
Extraction Ratio:	75%
Immediate Roof:	Mostly sandstone, excellent roof.
Immediate Floor:	Gray shale, firm
INNERBURDEN:	
Thickness:	Avg. 300
Nature of Strata:	Mostly sandy shales, with sandstones, coal seams, and a 50 feet thick sandstone bed directly beneath the Winifrede.
Percent of Hardrock:	50%
UPPER SEAM:	
Bed Name:	Winifrede (Dorothy)
Thickness:	50 inches
Method of Extraction:	Room and Pillar
Extraction Ratio:	65%
Immediate Roof:	34 inches shale overlain by beds of sandstone up to 75 feet thick.
Immediate Floor:	Shale, fairly firm.
OVERBURDEN:	
Cover thickness:	300 feet
Nature of Strata:	Shales, sandstones etc. No drill log available.

CASE #: 14

SOURCE OF INFORMATION:	Stemple, 1956
NAME/LOCATION OF MINE:	Kanawha County, WV
LOWER SEAM:	
Bed Name:	Eagle
Thickness:	45 inches
Method of Extraction:	Room and Pillar
Extraction Ratio:	Old: 60% New: 75%
Immediate Roof:	Carbonaceous shale, up to 25 feet thick; has never been broken up to the sandstone.
Immediate Floor:	"Slate", fairly firm.
INNERBURDEN:	
Thickness:	100 feet
Nature of Strata:	Close over lower seam is sandstone up to 50 feet thick, then a 30 inch un-mined coal seam overlain by 8-12 feet of sandstone; balance up to upper seam is mostly shale.
Percent of Hardrock:	60%
UPPER SEAM:	
Bed Name:	No. 2 Gas
Thickness:	60 inches
Method of Extraction:	Room and Pillar
Extraction Ratio:	50% approx.
Immediate Roof:	Generally sandstone or sandy shale, thin-bedded, up to 15 feet above coal; about 6 inches of drawslate in some cases.
Immediate Floor:	Gray shale, fairly soft
OVERBURDEN:	
Cover thickness:	400 feet
Nature of Strata:	Shales and sandstones with a sandstone bed up to 28 feet thick immediately over upper coal seam.

CASE #: 15

SOURCE OF INFORMATION:	Stemple, 1956
NAME/LOCATION OF MINE:	Raleigh County, WV
LOWER SEAM:	
Bed Name:	Pocahontas No. 4
Thickness:	Avg. 44 inches , including 2 inches "slate" 24 inches from top.
Method of Extraction:	Panel longwalls, entry chain pillars left between panels.
Extraction Ratio:	80%
Immediate Roof:	Shale, varying up to 50 feet thick, some sandstone roof (or sandy shale), 3 feet or more thick.
Immediate Floor:	Firm shale.
INNERBURDEN:	
Thickness:	Avg. 285 feet
Nature of Strata:	Mostly shales, with one heavy sandstone bed 80 feet thick, about 50 feet above the lower seam.
Percent of Hardrock:	30%
UPPER SEAM:	
Bed Name:	Beckley
Thickness:	Avg. 50 inches, 30-36 inches in low areas.
Method of Extraction:	Room and Pillar
	85% approx.
Immediate Roof:	Shale
Immediate Floor:	Shale
OVERBURDEN:	
Cover thickness:	Avg. 450 feet
Nature of Strata:	Shales and sandstones with a 25 feet thick sandstone bed appearing persistently about 40 feet above the upper bed.

CASE #: 16

SOURCE OF INFORMATION:	Stemple, 1956
NAME/LOCATION OF MINE:	Indiana County, PA
LOWER SEAM:	
Bed Name:	Lower Kittanning
Thickness:	44 inches
Method of Extraction:	Room and Pillar
Extraction Ratio:	60% Approx.
Immediate Roof:	6 inches of bone, comes with coal overlain by dark shale. Only a fair top.
Immediate Floor:	Fireclay, soft.
INNERBURDEN:	
Thickness:	120 feet
Nature of Strata:	Nearly all shales; some non-persistent sandstones and limestones not over 15 feet thick; 2 or 3 coal seams, 6-30 inches thick and fireclays.
Percent of Hardrock:	20%
UPPER SEAM:	
Bed Name:	Upper Freeport
Thickness:	44 inches
Method of Extraction:	Room and Pillar
Extraction Ratio:	75% approx.
Immediate Roof:	Dark shale, 0-10 feet thick, overlain by sandstone. Generally good.
Immediate Floor:	Bone and bottom coal, underlain by fairly firm fireclay.
OVERBURDEN:	
Cover thickness:	Avg. 100 feet
Nature of Strata:	Predominantly shales, with a sandstone bed 15-50 feet thick. Directly over the upper seam.

CASE #: 17

SOURCE OF INFORMATION:	Stemple, 1956
NAME/LOCATION OF MINE:	Tazewell County, VA
LOWER SEAM:	
Bed Name:	Pocahontas No. 3
Thickness:	Avg. 66 inches
Method of Extraction:	Room and Pillar
Extraction Ratio:	80% (Planned)
Immediate Roof:	"Slate" and rotten shale.
Immediate Floor:	"Slate" or shaley fireclay, about 2 feet thick underlain by sandstone.
INNERBURDEN:	
Thickness:	Avg. 95 feet
Nature of Strata:	Mostly slate or shales and the No. 4 Pocahontas coal seam (generally dirty); a persistent sandstone bed, around 15 feet deep, appears directly above the No. 4 seam, about 15 feet below the Pocahontas No. 5 seam.
Percent of Hardrock:	25%
UPPER SEAM:	
Bed Name:	Pocahontas No. 5
Thickness:	Avg. 51 inches
Method of Extraction:	Room and Pillar
Extraction Ratio:	90%
Immediate Roof:	Rash, 2-8 inches thick overlain by about 6 inches drawslate, then 2-3 feet of "slate"; then sandstone.
Immediate Floor:	About 3 inches of rashy coal underlain by sandy fireclay.
OVERBURDEN:	
Cover thickness:	500 feet
Nature of Strata:	Sandstones, shales, coal seams, fireclays; up to 200 feet of sandstone included in the 300 feet directly above the upper seam in several thick beds.

CASE #: 18

SOURCE OF INFORMATION:	Stemple, 1956
NAME/LOCATION OF MINE:	McDowell County WV
LOWER SEAM:	
Bed Name:	Pocahontas No. 3
Thickness:	Avg. 78 inches
Method of Extraction:	Room and Pillar
Extraction Ratio:	80%
Immediate Roof:	Shale, with 2-3 inches drawslate on the coal in some instances.
Immediate Floor:	Shale.
INNERBURDEN:	
Thickness:	86 feet
Nature of Strata:	Sandstone up to 60-70 feet thick in some places; in others almost all shales.
Percent of Hardrock:	70%
UPPER SEAM:	
Bed Name:	Pocahontas No. 4
Thickness:	Avg. 76 inches
Method of Extraction:	Room and Pillar
Extraction Ratio:	60-65%
Immediate Roof:	"Slate", very soft and hard to hold; coal top left in some cases.
Immediate Floor:	"Slate" (shale), fairly firm.
OVERBURDEN:	
Cover thickness:	Avg. 800 feet
Nature of Strata:	Predominantly sandstone, one bed up to 200 feet thick, with shales, coals, etc.

VITA

Muhammad Akram was born on November 27, 1953, in Gujrat, Pakistan. He graduated with a B. S. in Mining Engineering from the University of Engineering and Technology, Lahore, Pakistan in 1978. He joined VPI & SU as a graduate student in the Department of Mining and Minerals Engineering in 1989. He received his M. S. in Mining Engineering in 1991 and is currently pursuing a graduate program leading to the Ph. D. degree. He has worked as an Assistant Director Mineral Development and as an Assistant Professor Mining Engineering in Pakistan.